Piotr Musznicki

The conducted EMI in DC-DC converters

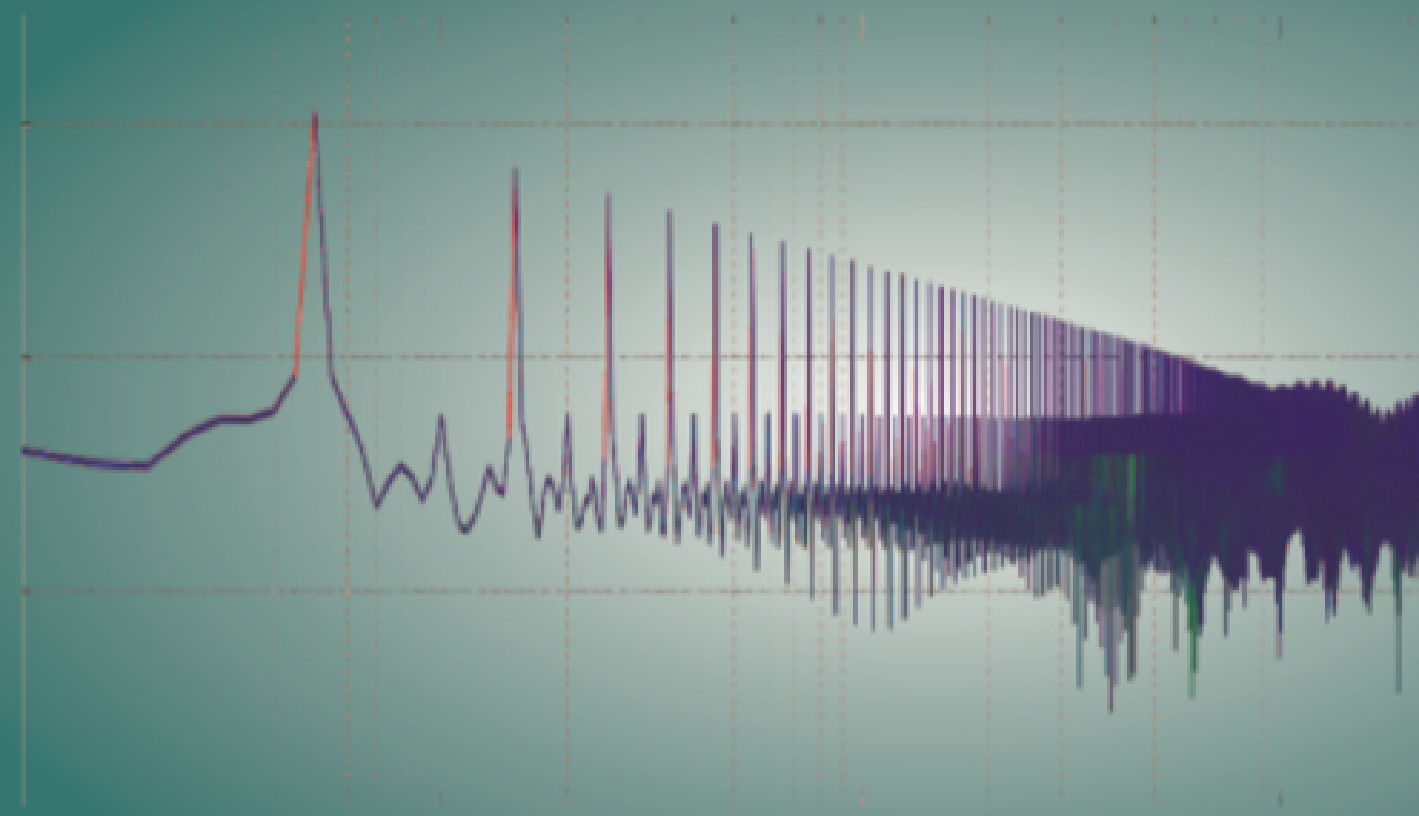

The conducted EMI in DC-DC converters

Piotr Musznicki

II

Contents

Prof Jean-Luc SCHANEN
Head of Power Electronics Group
Grenoble Institute of Technology
May 29th 2018

This letter is written to highly recommend Piotr Musznicki as EMC expert in the field of Power Electronics. I was the PHD co-supervisor of Dr Musznicki between October 2002 and April 07. This PHD was co-supervised with Prof. Chrzan, Gdansk University of Technology, Poland. The topic was about using new signal processing methods to better investigate the origin of EMC disturbances[i]. I really enjoyed working with Dr Musznicki, and was impressed by his skills in both theoretical and experimental aspects.

Since his PHD, I still follow his work. He recently spent a week in Grenoble and we could discuss on several aspects of EMC in Power Electronics. We supervised together a master student.

I had a quick overview of his book proposal, and found this very interesting and well written. It provides a good insight on EMC in Power Electronics using two representative examples of non-insulated and insulated converters

[i] "Méthodologie de traitement du signal pour la maîtrise de l'origine des perturbations CEM", PHD dissertation, co-supervised between Univ Grenoble Alps and Gdansk University of Technology, defended April 24th 2007, Gdansk.

G2Elab - Laboratoire de Génie Electrique de Grenoble
Bâtiment GreEn-ER
21 avenue des Martyrs - CS 90624 - 38031 Grenoble Cedex 1, France
Tél. +33 (0)4 76 82 62 99
www.G2Elab.grenoble-inp.fr

Chapter 1

Introduction

1.1 Motivation

In order to design the DC-DC converters – beyond the basic knowledge about their operation – the understanding the interference generation and propagation is required, considering the significant increase in switching frequency. The limitation of interference can be done in the early design stage taking into account information about components, their placement and printed circuit board (PCB) layout. Of course, the interference should be filtered by a dedicated filter, but the more effective and cheaper method to limit undesirable noise is a correct design, where the interference generation is reduced and naturally filtered inside the converter, by creating internal high frequency current loops.

This book presents the phenomena of conducted electromagnetic interference generation in DC-DC converters. The measurement and simulation are used to analyze impact of most important parameters on the character, level and propagation path of interference. In order to better understand interference generation, the knowledge of converter operation is required, thus the basic theory is described. Next, several basic definitions used in the book is presented.

https://doi.org/10.2478/9783110623925-001

1.2 Basic definition

The definition provided by www.techopedia.com says that ElectroMagnetic Compatibility (EMC) is the ability of different electronic devices and components to work correctly even in the presence of other devices that emit electromagnetic waves. The EMC concerns interaction between devices and the ability to influence one device to another operation.
Electromagnetic interference (EMI) is a phenomenon where one electromagnetic field interferes with another, resulting in the distortion of both fields. It can be propagated in conduction tracks and wires, but also as a magnetic and electrical field coupling. In the standards the conducted EMI is defined as undesirable signal (voltage, current or electromagnetic wave) in the frequency range from 9 kHz to 30 MHz. Depending on the direction the interference can be classified as incoming - interference propagated to a victim - disturbance, outgoing - interference generated by the source - perturbation. Of course, it can be the same signal, but seen from another point of view. The interference generated by source reaches the victim by the coupling. Conducted electromagnetic interference can be propagated by couplings:

- conductive formed by direct electrical connection as wires, cable and conducting PCB tracks
- inductive refers to a magnetic field
- capacitive refers to a electric field

The average (mean – AV) value of function $f(t)$ in interval <a, b> is the integral of this function divided by the length of the interval (b-a). For periodic functions where the averaging interval is equal to T or its multiplicity, is described by equation (1.1)

$$F(t)_{(\mathrm{AV})} = \frac{1}{kT}\int_{a}^{a+kT} f(t)\mathrm{t}x \quad dla \quad k = 1, 2, 3\ldots \tag{1.1}$$

In the case where the periodic function is defined in intervals (for example in three intervals):

$$f(t) = \begin{cases} f_1(t) & dla \quad t \in < a, b) \\ f_2(t) & dla \quad t \in < b, c) \\ f_3(t) & dla \quad t \in < c, a+T), \end{cases} \tag{1.2}$$

the average value is the sum of the integrals of the individual functions in the intervals where they are defined:

$$F(t)_{(AV)} = \frac{1}{T}\left[\int_a^b f_1(t)\mathrm{d}x + \int_b^c f_2(t)\mathrm{d}t + \int_c^{a+T} f_3(t)\mathrm{d}t\right]. \tag{1.3}$$

The root mean square vale (RMS) is defined for periodic function according to the formula:

$$F(t)_{(RMS)} = \sqrt{\frac{1}{T}\int_a^{a+T} f^2(t)\mathrm{d}t}. \tag{1.4}$$

However, for functions defined intervals, as it is defined in (1.2), is equal:

$$F(t)_{(RMS)} = \sqrt{\frac{1}{T}\left[\int_a^b f_1^2(t)\mathrm{d}t + \int_b^c f_2^2(t)\mathrm{d}x + \int_c^{a+T} f_3^2(t)\mathrm{d}t\right]} \tag{1.5}$$

The trapezoidal wave is a waveform in which the amplitude alternates at a steady frequency between fixed minimum and maximum values with rise t_r and fall t_f time defined as in Fig. 1.1. [1]
The trapezoidal and rectangular waveform can be shortly described by the duty cycle γ defined as the ration of pulse width to the total period:

$$\gamma = \frac{\tau}{T} \tag{1.6}$$

It can take values from 0 to 1 (in the percentage for 0 to 100%). In Eq. (1.7) the envelope of the spectrum of the trapezoidal wave is presented, obtained using the fast Fourier transform (FFT), according to formula 1.7. The two characteristic frequencies are distinguish at which the slope changes. The first

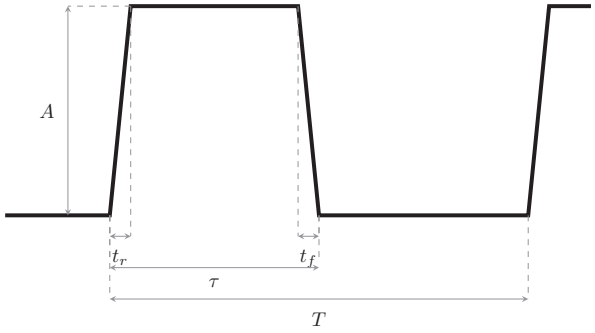

Fig. 1.1: Trapezoidal waveform

one $f_1 = 1/(\pi\tau)$ depends on the pulse width, the second $f_2 = 1/(\pi t_r)$ is linked with rising (falling) time t_r.

$$f(t) = A\frac{\tau}{T} + 2A\frac{\tau}{T}\sum_{n=1}^{\infty}\left[\frac{sin(n\pi f_0\tau)}{n\pi f_0\tau}\right]e^{(-j\pi n f_0\tau)}e^{(2j\pi n f_0 t)} \tag{1.7}$$

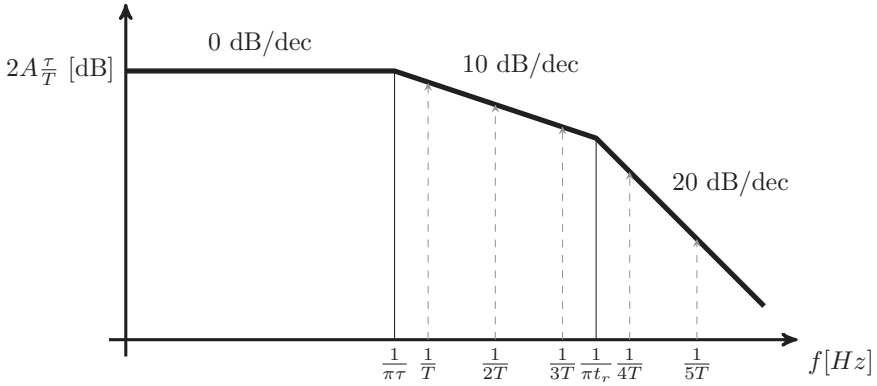

Fig. 1.2: Trapezoidal waveform spectrum

A power switch (ideal) - non-linear element, capable remain in two on and off states. In the ON state, it has a resistance of zero, while the OFF state, it has a resistance equal to infinity. Switching from one state to another occurs in an infinitely short time.

Chapter 2

Components

For understanding the DC-DC converters EMC behavior, it is necessary to know how the particular component influences on perturbation generation and propagation. In every converter passive components can be found (resistors, capacitors, inductors or transformers), semiconductors (transistors, diodes) and connections between them (wires, cables, conducted tracks). In analyses of the converter operation, devices can be represented by functional models which take into account only basic properties and behavior, but for comprehensive analysis what happens in the range of high frequencies, wide band models are required.
In the literature many models can be found. The precision and resolution of models are different for required operation, behavior or physical type. For EMC modeling mainly physical and component models are useful. In this chapter models of components are briefly presented.

2.1 Semiconductor devices

Accurate semiconductor models are necessary for EMI analysis, since they are linked to switching $\mathrm{d}u/\mathrm{d}t$ and $\mathrm{d}i/\mathrm{d}t$, which is the main origin of perturbation. The semiconductors have unipolar and non linear components and therefore are the most difficult power components to be modeled.

https://doi.org/10.2478/9783110623925-002

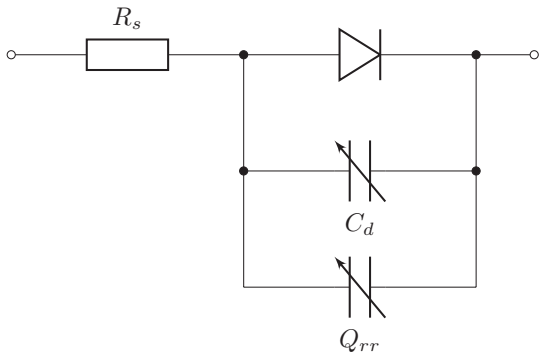

Fig. 2.1: Diode model

2.1.1 Diode

From EMC point of view, in addition to the basic behavior of the diodes, important parameters are related to their the turn on and the turn off times. It results in the switching diode can be the source of disturbance due to fast voltage or current change. It is strongly connected with semiconductor structure and movement of carriers inside the diode. Typically, diode is modeled by nonlinear capacitance (C_d in Fig. 2.1), where the temporary value depends on voltage across the diode. The value of this capacitance is different for a different type of diode – e.q for hte rectifier diode it is much larger than the Schottky or fast diodes.
Another significant phenomena is associated with removing carriers from a junction during turning off [2]. The revers recovery current I_{RM} starts to flow in the opposite direction due to removing the carriers form junction. The number of carriers is proportional to the surface between current waveform and axis (drift region) and is typically presented by revers recovery charge Q_{rr}. The recovery time t_{rr} depends on the diode internal structure and the current value before switching. The limitation of this phenomena can be obtained by applying various doping techniques or using special semiconductor material [3]. The use of diodes with a shorter t_{rr} in DC-DC converters can significantly decrease EMI peaks in reverse recovery frequency range which allows to improve their efficiency and reduce snubber losses.

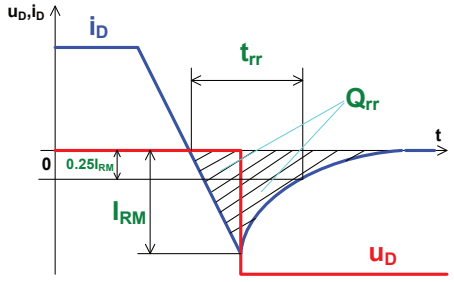

Fig. 2.2: Diode revers recovery

2.1.2 MOSFET transistor

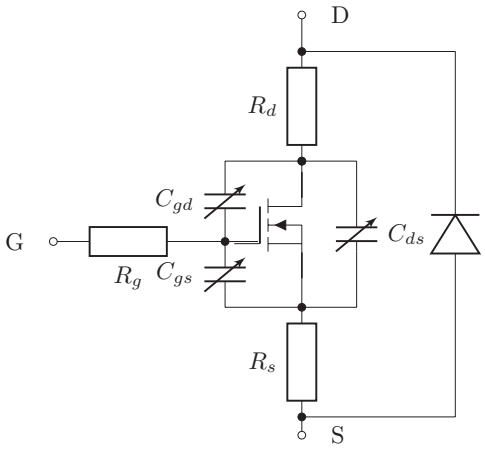

Fig. 2.3: MOSFET model

The MOSFET transistors and other field effect transistors are the most frequently used devices in DC-DC converters as a controlled power electronics switch. The model of MOSFET transistor is presented in Fig. 2.3. The quasi static behavior is typically represented by controlled by a gate-source voltage U_{GS} current source or by a ideal two-state transistor model. The connection resistance is very small compared to other resistances in the converter circuit, but for accurate power dissipation it should be included. Inductive elements can be neglected because this kind of transistors – mainly used for small and middle

power – are negligibly small. However, for high power converters connection and internal inductance can have an impact on oscillation and over-voltages [4].
For EMI point of view, the dynamics behavior of transistor is the most important and it can be modeled by three nonlinear capacitances C_{GS} gate-source, C_{DS} drain-source and C_{GD} gate-drain [5]. The temporary value of these capacitances depends on voltage and it can be obtained using the hyperbolic-tanged-based approximation, where the high and low capacitance levels can be distinguished. The relationship between voltage and capacitance is shown in Fig. 2.4 [6]. The capacitance between gate and drain C_{GD} increases when the transistor is turn on, but C_{DS} decreases and for conducting transistor is negligently small. The voltages ΔU_{CGD} and ΔU_{CGD} define the width of the capacitances characteristic between the extreme's.

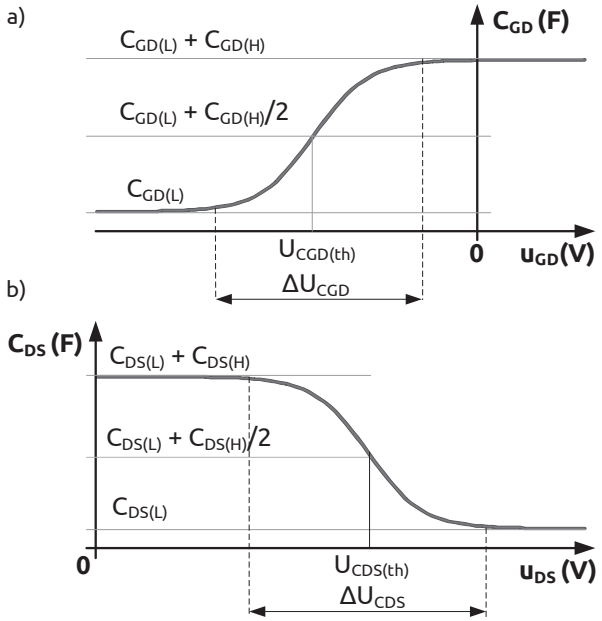

Fig. 2.4: The hyperbolic-tanged-based approximation of nonlinear MOSFET capacitance a) C_{GD} b) C_{DS} (from [6] with authors permission)

The transistor dynamics is strongly connected with capacitances charging and discharging. The rate of carriers supplied to the gate can be controlled by

additional resistor and it has an influence on all voltages and currents slew rates ($\mathrm{d}u/\mathrm{d}t$ $\mathrm{d}i/\mathrm{d}t$). In Fig. 2.5 the transients during the turn on process are presented. In time interval $t \in (t_0, t_1)$, the equivalent input capacitance $C_{ISS(1)}$ is recharged, next in $t \in (t_1, t_3)$ the Miller plateau effect appears and at the end of turn off $t \in (t_3, t_4)$ the capacitance $C_{ISS(2)}$ is recharged. The models parameters can be derived:

$$\begin{cases} C_{GD} & = & C_{RSS(2)} - C_{RSS(1)} \\ C_{GD} & = & C_{RSS(1)} \\ U_{CGD(th)} & = & U_{GS(m)} - U_{DS(m)} \\ C_{GS} & = & C_{ISS(1)} - C_{RSS(1)} \end{cases} \tag{2.1}$$

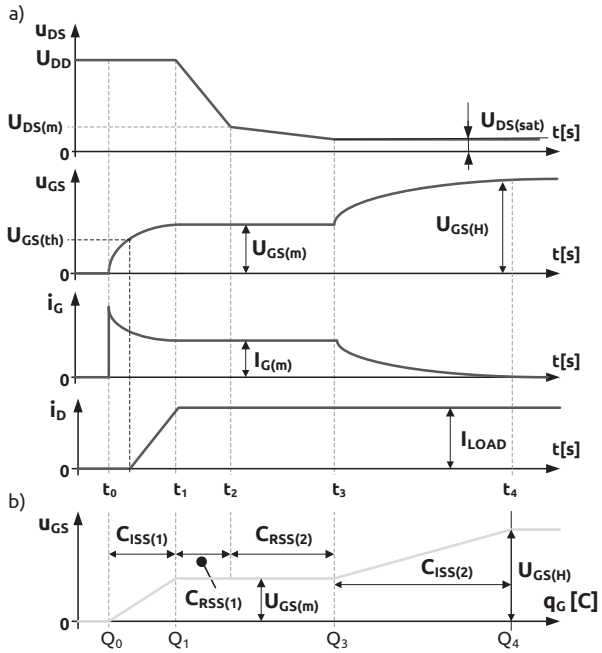

Fig. 2.5: MOSFET turn-on process (from [6] with authors permission)

The models can be constructed using parameters from producer's data sheet, but usually they aren't sufficient for wide band modeling, since manufacturer data are not always match with true values, because of average for series of

products. Furthermore, models attached to simulation software can be applied, but it can be noticed, that models provided with simulator libraries are not very accurate for EMI modeling, especially dependencies in time domain don't agree to real ones. In practice, the libraries don't contain all commercial components, so characteristic values should be extracted from real semiconductor devices. The example of parameters extraction is presented in [7].

2.2 Passive component

For accurate EMI analysis, wide band models of non ideal passive components are needed. Generally, it is sufficient to use models contain inductive, capacitive and resistive elements.

2.2.1 Inductor

The inductor is a two-terminal circuit component, which is able to store energy in the magnetic field. The time varying magnetic field results in a voltage on the terminals according to Faraday's law:

$$U = \frac{\mathrm{d}\varphi}{\mathrm{d}t} = L\frac{\mathrm{d}i}{\mathrm{d}t} \tag{2.2}$$

The ideal inductor contains not only inductance, but the real one consists of resistance which dissipates power and capacitance representing capacitive coupling between the windings and the physical packaging. The parasitic capacitance C_p determines the high frequency performance of the inductor [8]. Depending on the required accuracy and frequency range, the model may have multiple elements - the basic two models of the real inductor are presented in Fig. 2.6. The inductor model can be more complex including core losses, saturation etc, but for conducted EMC analysis of the DC-DC converter, the presented models are sufficient. The example of the inductor impedance spectra is shown in Fig. 2.7, where characteristic resonat peak is visible (here in 2MHz) results from interaction between inductance L and capacitance C_p.

2.2.2 Capacitor

Capacitor is a passive element where the energy is stored in the electrical field. In DC-DC converters, capacitors produced in many technologies are used e.g

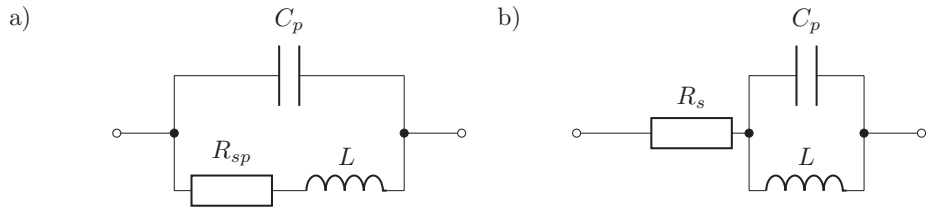

Fig. 2.6: Inductor models

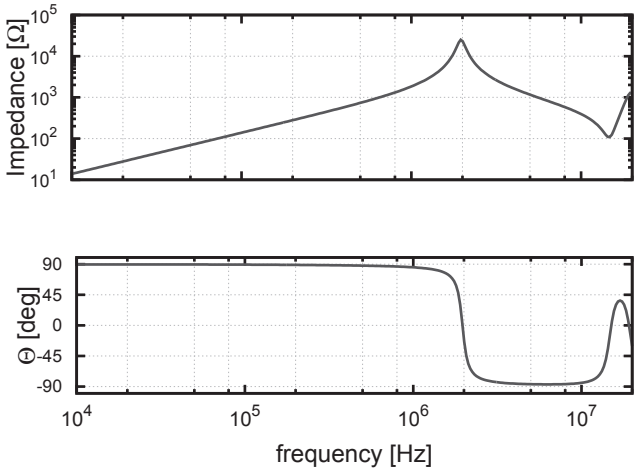

Fig. 2.7: Measured inductor impedance

electrolytic, ceramic or film. They are usually used as filters, ripple attenuator or voltage stabilizers. The capacitor current i depends on the flow passing through and – for constant in time capacitance – current voltage relation can be described by derivation form:

$$i = \frac{\mathrm{d}Q}{\mathrm{d}t} = C\frac{\mathrm{d}u}{\mathrm{d}t} \tag{2.3}$$

From EMC point of view, the most important parameter - besides capacity - is their operating frequency and series resistance ESR. The basic capacitor model - presented in Fig. 2.8 - contains: the capacitance C, the equivalent series resistance (ESR), the equivalent series inductance (ESL) and the leakage resistance (R_σ).

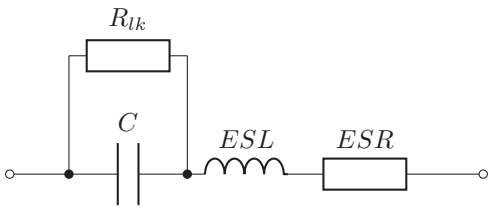

Fig. 2.8: Capacitor models

The capacitor impedance results from the production technology. The examples of impedance spectra for produced in various technology capacitors $C = 2\mu F$ are presented in Fig. 2.9. The selection of the appropriate technology depends on the application, but in practice e.g in input – output filters, it is preferred to use parallel connection of capacitor produced in various technology.

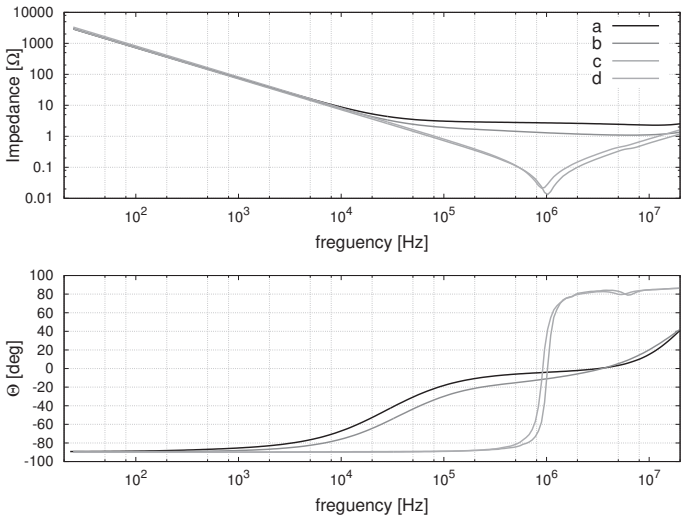

Fig. 2.9: Capacitor impedance a) electrolytic b) tantalum c) polyester d) polypropylene

The standalone capacitors can be a resonant circuit due to interaction between the capacitance and inductance ESL, especially for components produced in THT (Through-Hole Technology). In the converter, ESL parameter influences

on the interference propagation, particularly for low power devices – the use of SMD (Surface Mounted Devices), practically solves this problem.
The capacitor parameters change during operation, because of aging and deterioration processes, especially in high temperature. The most susceptible are electrolytic capacitors, where e.g after 6000 working hours, the value of capacitance can decrease about 10% but the ESR increases even 5 times, because the temperature condition and the current ripples lead to acceleration of the electrolyte evaporation of the electrolyte [9]. In Fig. 2.10 the impedance of electrolytic capacitor is presented: (blue) „new" and (green) after 9000 hour operation. The capacitor aging has great impact on the effectiveness of filtering and EMI generation in Power Electronics converters change during working time [10].

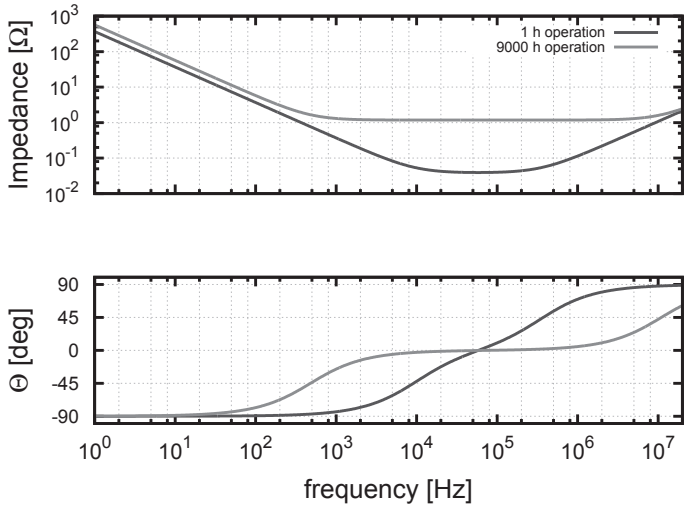

Fig. 2.10: Deterioration of electrolytic capacitor impedance

2.2.3 Transformer

The transformer is basic component of all isolated converters. It is a device to transform alternating current electrical energy between two or more circuits through the magnetic field according to the Faraday's law. The physical transformer consists of the windings located on core. In some applications (e.g in

the flyback converter (see Chapter 4)) this structure is additionally used for store energy.
The main parameters of the transformer model are:

- n-turns ratio $\vartheta = \frac{u_2}{u_1} = \frac{i_{n_1}}{i_{n_2}} = \frac{n_2}{n_1}$
- magnetizing inductance L_M
- primary and secondary winding resistance R_1 and R_1
- primary and secondary leakage inductances $L_{\sigma 1} = \vartheta^2 L_{\sigma 2}$
- core losses R_c

From the EMC point of view, the parasitic capacitance should be included, but in producer data-sheets, the parameters from list are principally specified, however the stray capacitances are usually neglected. The high frequency transformer lumped circuit model [11] is assumed as in Fig. 2.11 including primary C_1 and secondary C_2 winding capacitances and inter-winding capacitance is represented by capacitors C_{12}, C_{21}, C_{13} and C_{31}. The core losses R_c are neglected in this model, because it does not play a significant role in the EMC phenomena.
Much effort has been given in literature to the transformer parameters extraction. Geometrical dimension and electromagnetic models using finite element analysis have been applied to calculate parasitic capacitances [12, 13, 14, 15]. The experimental setup for the two-port network approach using the step response [16, 17] and the frequency response analysis [18, 19, 20] have been presented. Non-linear identification process, taking into account magnetic saturation and skin effects occurring in the windings, have been described in [21]. The model, presented in Fig. 2.11, includes all main lumped capacitances in the transformer, but in many situation a simple model can be used only with three capacitances C_1, C_2 and C_{12} as it is presented in Fig. 2.12.
In order to extract the value of lumped capacitors, the impedance analyzer or Wiener filtering [22] can be used to identify resonant frequencies, which can be observed in impedance spectra. The origin of these phenomena is interaction between inductances and capacitances of different transformer sides, layers, wires and other parts. The first lowest resonant frequency represents resonances between transformer inductance and the lumped equivalent capacitance. These

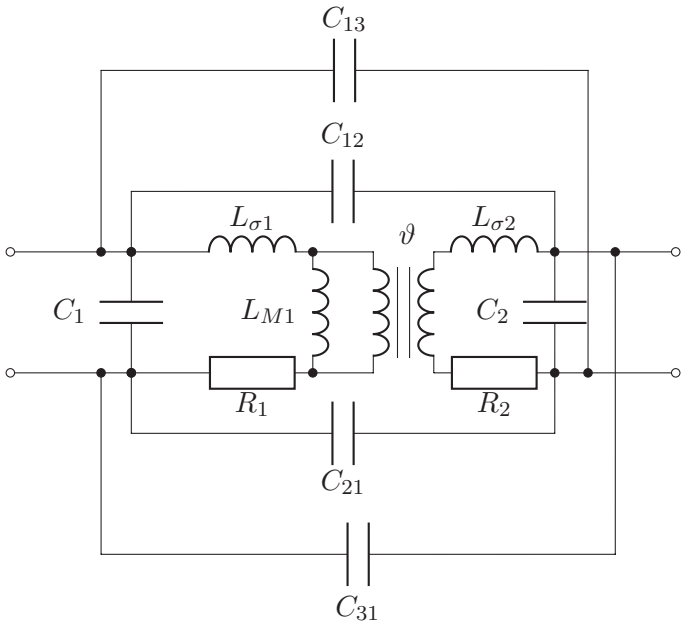

Fig. 2.11: Two winding transformer model with six stray capacitances

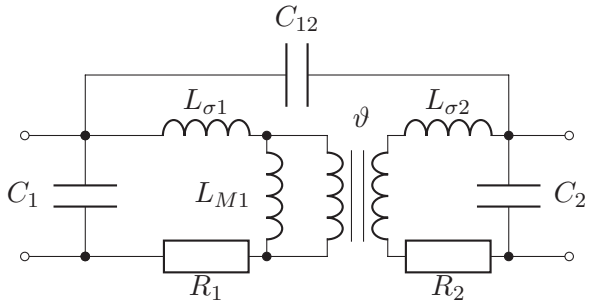

Fig. 2.12: Two winding transformer with three stray capacitances

lumped capacitances can be estimated by analyzing impedance spectra of three setup circuits [23]:

- with open secondary side (Fig. 2.13),
- short circuit between primary winding end and secondary winding beginning (Fig. 2.15)
- shorted secondary side terminals. (Fig. 2.14),

The equivalent capacitance seen from primary winding terminals C_{M1} can be estimated using the circuit presented in Fig. 2.13, where secondary winding terminals are open. Assuming the model from Fig. 2.12, it can be noticed that C_{M1} is a parallel connection of C_1 and C_2 referred to the primary side. The equivalent input capacitance C_{M1} is given by formula 2.4:

$$C_{M1} \approx C_1 + \frac{C_2}{\vartheta^2} \tag{2.4}$$

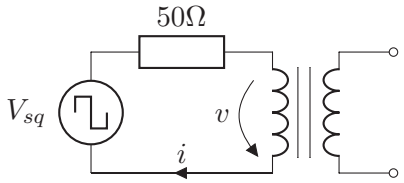

Fig. 2.13: C_{M1} measurement setup

In figure 2.15, the short connection between primary winding end and secondary winding beginning is presented. The first resonant frequency results from interaction between input inductance $L_0 = L_{M1+}L_{\sigma 1}$ and capacitance C_{M2}, which is a parallel connection of C_1, C_{12} and C_2 referred to the primary side. The equivalent input capacitance C_{M2} is given by formula 2.5:

$$C_{M2} \approx C_1 + C_{12} + \frac{C_2}{\vartheta^2} \tag{2.5}$$

In figure 2.14 the short circuit is between the terminals of secondary winding. It allows to oust the capacitances C_2 and C_{12} from impedance. The main resonant frequency results from interaction between C_1 and $L_{\sigma 1}$. The equivalent input capacitance C_{M3} is given by formula 2.6:

$$C_{M3} \approx C_1 \tag{2.6}$$

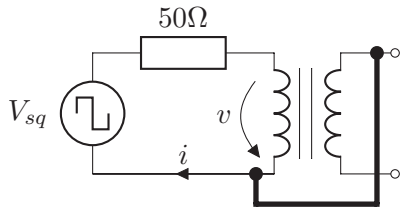

Fig. 2.14: C_{M2} measurement setup

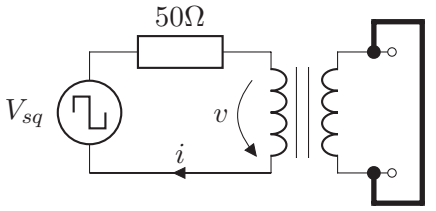

Fig. 2.15: C_{M3} measurement setup

The capacitances C_{M1}, C_{M2} and C_{M3} can be derived using identified resonant frequencies by the Wiener filtering method.

$$C_{M1} = \left[L_0 * (f_1 * 2 * \pi)^2\right]^{-1} \tag{2.7}$$

$$C_{M2} = \left[L_0 * (f_2 * 2 * \pi)^2\right]^{-1} \tag{2.8}$$

$$C_{M3} = \left[2 * L_{\sigma 1} * (f_3 * 2 * \pi)^2\right]^{-1} \tag{2.9}$$

where:

- f_1, f_2, f_3 are resonant frequencies obtained from impedance analyzer or filter transfer function,
- $L_0 = L_{M1+}L_{\sigma 1}$ input inductance,

- $2 * L_{\sigma 1} \approx L_{\sigma 1} + \vartheta^2 * L_{\sigma 2}$ sum of leakage primary and secondary inductances.

Based on equations (2.7), (2.8) and (2.9), capacitances of the transformer model (Fig. 2.12) are calculated.

$$C_1 = C_{M3} \tag{2.10}$$

$$C_2 = \vartheta^2 * (C_{M1} - C_{M3}) \tag{2.11}$$

$$C_{12} = C_{M2} - C_{M1} \tag{2.12}$$

2.3 Connections

In typical analysis of converter operation, the connection like wires, cables, bonding or PCB tracks, are usually neglected. From the EMC point of view, these are important parts in interference generation and propagation. In environment of every conductor with flowing current, there is the electromagnetic filed, according to two Maxwell equations, Faraday's Law, Lorentz force law and the Ampère-Maxwell Law. In the equivalent circuit, the connection behavior can be described as a matrix of passive elements. There are few formulas which allow finding dependencies between geometrical and physical properties of conductors and their RLC models [24, 25]. In many cases, the non ideal behavior of conducting tracks can be described by lumped models.
The power dissipation in conductors is negligently small. The value of DC resistance of rectangular PCB track depends on track material properties and dimensions:

$$R = \frac{\rho * l}{A} \tag{2.13}$$

where: R – begin-to-end track resistance [Ω], ρ –resistivity of the track material [Ω m], l - the track length $[m]$ and $A = w * h$ – the track cross sectional area $[m^2]$.
Density distribution of the track current tends to crowd to outside when frequency increases. The *skin effect* causes that for high frequency the total value of track resistance increases since the current flows mainly at the edges of track. In Fig. 2.16 the current density in function of distance from the middle of the track is presented for frequency in range for 0 to 30MHz for the PCB copper track thickness $20\mu m$. It can be noticed that for DC and low frequencies the

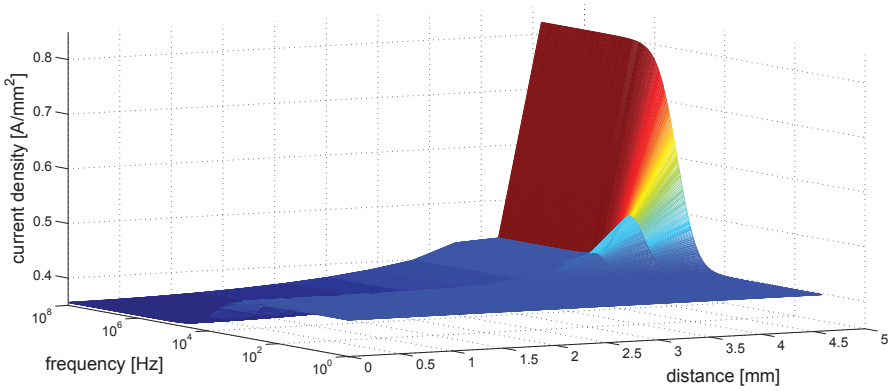

Fig. 2.16: Skin effect – current density in function of distance from conductor middle for frequency in range for 0 to 30MHz

current distribution is even, but for higher frequencies it is concentrated in the outer periphery. The resistance for high frequency can be estimated by [24]

$$R \approx \frac{l}{\rho(2\sigma w + 2\sigma t)} \tag{2.14}$$

where: w – track width, t – track thickness and $\sigma = \sqrt{\frac{2\rho}{2\pi f \mu}}$ – skin effect depth (μ -magnetic permeability of the conductor). The proximity effect has the same nature as the skin effect, where the current distribution in one conductor is determined by current in the neighboring conductor. The alternating magnetic field induces eddy currents in adjacent conductors increasing the current density at the edge of conductor.
The skin and proximity effects also affect inductance of conductor. The measurement of self or mutual inductance is very difficult because of their relatively small value, but it can be calculated using the partial element equivalent circuit (PEEC) [25, 26]. It is based on analytical electromagnetic formulas to compute inductance and coupling, provided the uniform current density. Electromagnetic behavior of the conductor is modeled by lumped electrical resistance self and mutual inductance as it is shown in Fig. 2.17. Using the PEEC method self and mutual inductance for all conductors in the converter can be calculated, but it usually requires dedicated software e.q InCa3D.

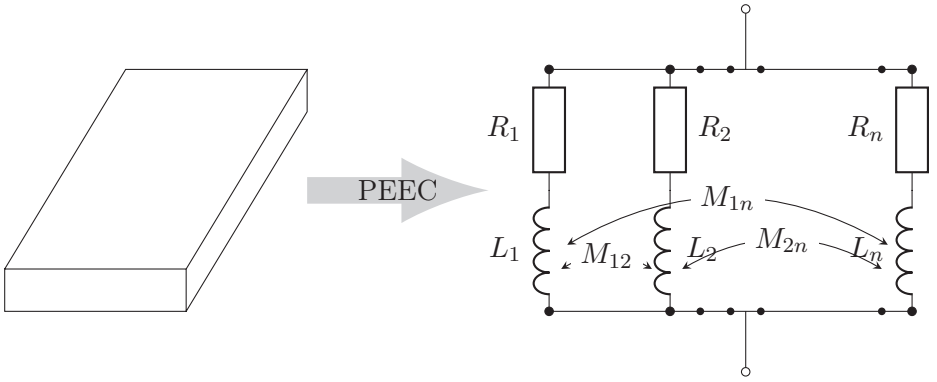

Fig. 2.17: One dimension PEEC PCB track model

The value of per-unit-length inductance can be calculated using characteristic impedance Z_C defined by C.R Paul in [24]:

$$Z_C = \begin{cases} \dfrac{60}{\sqrt{\epsilon_r'}} \ln\left[\dfrac{8h}{w} + \dfrac{w}{4h}\right] & \dfrac{w}{h} \leq 1 \\ \dfrac{120\pi}{\sqrt{\epsilon_r'}} \left[\dfrac{w}{h} + 1.393 + 0.667 \ln\left(\dfrac{w}{h} + 1.444\right)\right] & \dfrac{w}{h} > 1 \end{cases} \tag{2.15}$$

where h is board thickness and the ϵ_r' is effective relative permittivity follows that electric field is partly out of the conductor as it is presented in Fig. 2.18:

$$\epsilon_r' = \frac{\epsilon_r + 1}{2} + \frac{\epsilon_r - 1}{2} \frac{1}{\sqrt{1 + 10h/w}} \tag{2.16}$$

Using Eq. (2.15) the value of conducting track per-unit-length inductance is equal:

$$l = \frac{Z_C}{\upsilon}[H/m] \tag{2.17}$$

where υ is the wave velocity.
The parasitic capacitance is a critical element in many converters (eq in flyback converter (see Section 4.2.1)) and it can have a decisive role in EMI propagation. The values of parasitic capacitances are dependent on the geometry of

physical properties of insulate material. It can be measured using impedance bridge or an impedance analyzer or it can be calculated. The plate parallel formula (Eq. (2.18)) allows to estimate the value of parasitic capacitance of the track, but it does not take into account the uneven distribution of electrical field (Fig. 2.18).

$$C = \epsilon_0 \epsilon_r \frac{w}{h} [F/m] \tag{2.18}$$

More accurate results can be obtained with the Wheeler/Schneider formula [27] which takes into consideration the edge effect.

$$C = \frac{1.122\epsilon_{eff}}{ln\left[1 + \frac{1}{2}\left(\frac{8h}{w_{eff}}\right)\left(\frac{8h}{w_{eff}} + \sqrt{\left(\frac{8h}{w_{eff}}\right)^2 + \pi^2}\right)\right]} [pF/m] \tag{2.19}$$

where:

$$\epsilon_{eff} = \frac{\epsilon_r + 1}{2} + \frac{\epsilon_r - 1}{2}\left(1 + \frac{10h}{w}\right)^{-1/2} \tag{2.20}$$

and the effective conductor width is defined:

$$w_{eff} = w + \frac{t}{\pi} ln\left[\frac{4e}{\sqrt{(\frac{t}{h})^2 + \frac{1}{\pi(\frac{w}{t}+1.1)^2}}}\right] \tag{2.21}$$

The parasitic capacitance can be obtained from characteristic impedance from Eq. (2.15).

$$C = \frac{1}{Z_c \upsilon} [F/m] \tag{2.22}$$

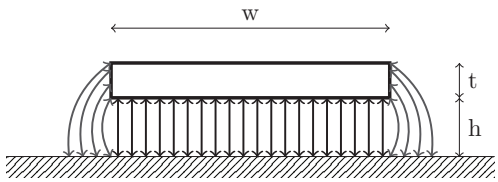

Fig. 2.18: Egde effect - uneven distribution of the electric field around the conductor

The cables connected to input and output of the converter can have an influence on interference propagation. If they are relatively short, their impact can be neglected, but if they are sufficiently long they can operate like an interference filter or amplifier (if long line reflection or resonant phenomena occurs). For the system including converters distant from the power source or load – like in photovoltaic installation – the cable impact should be taken into consideration. The physical properties and formulas for cable parameters using geometrical dimensions are presented in [24]. The per-unit-length model of cable based on telegrapher's equations is presented in Fig. 2.19.

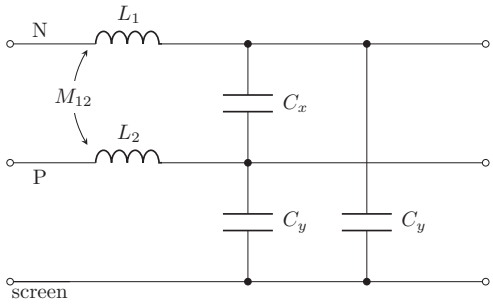

Fig. 2.19: Per-unit-length model of cable

2.4 Line Impedance Stabilization Network

The basic devices for conducted EMI measurement is Line Impedance Stabilization Network ($LISN$). It is a low-pass filter placed between power supply and tested devices or system. Its construction, parameters, characteristic and method of use are specified by standards (e.g EN 55032:2015). There are several $LISN$ topologies, they all should assure blocking a noise from the power supply network and provide the line impedance with a known high frequency characteristic (usually from 9kHz (150kHz) to 30MHz according to CISPR 16-1-2). The LISN types differ in their parameters such as impedance, frequency range, operating voltage and current, losses or connectors.
The example of the LISN topology is presented in Fig. 2.21. The impedance between EUT (Equipment Under Test) nodes with measured node terminated with 50Ω of the presented example is shown in Figure 2.22. It can be noticed

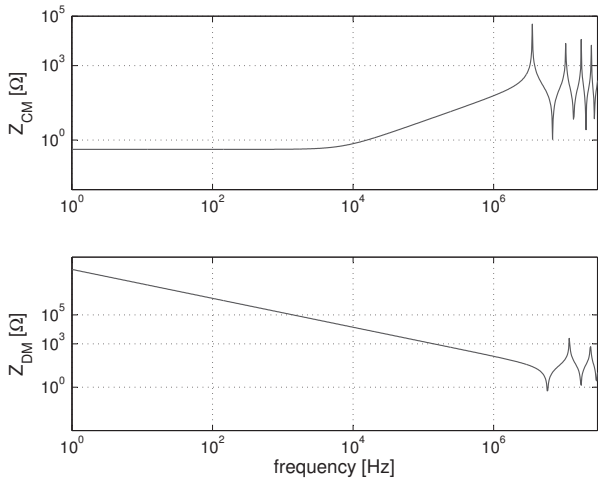

Fig. 2.20: 30 m cable common and differential impedance spectra

that for typical DC-DC converter operation frequency (here for 0 to 100 kHz) the impedance is relatively low and for higher frequency noise equals 50Ω. In the measurement, the power supply is connected to P and N nodes, the tested device to $EUT+$ and $EUT-$ and the measurement equipment registers the voltage U_{L1} or U_{L2}. Typically, a spectrum analysis or EMI receiver are used as the measurement meter, but also an oscilloscope can be applied. The measurement procedure is precisely described in the standards. The incorrect choice of topology can generated measurement errors [28]. The $LISN$ can also be used to preform decomposition of the interference to CM and DM noise [29]:

$$U_{CM} = \frac{U_{L1} + U_{L2}}{2} \qquad U_{DM} = U_{L1} - U_{L2} \tag{2.23}$$

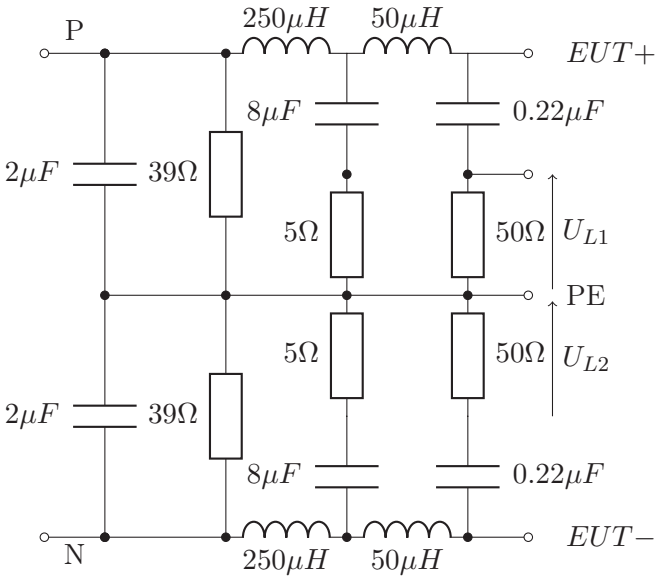

Fig. 2.21: Line Impedance Stabilization Network

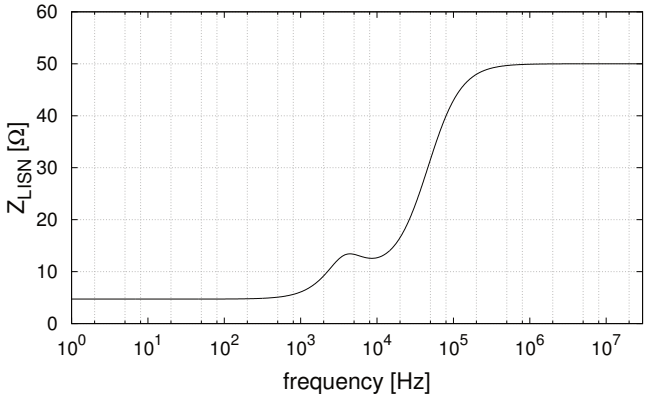

Fig. 2.22: LISN impedance between $EUT+$ and $EUT-$

Chapter 3

Non isolated converters

3.1 Introduction

DC-DC converters are devices for transforming direct voltage and current to the different level. Depending on topology the voltage can be steps down, steps up or both. It usually contains elements for storage energy like inductors or transformers. In transformerless converters, mainly parasitic capacitances and inductances have an influence on the EMI. The perturbation generation mechanism is depended on interaction between semiconductor switch Q, passive elements and parasitics. There are many different topologies, such as buck, boost, buckboost, SEPIC or Ćuk converters. The basic schemes of three most popular topologies are presented in Figs. 3.1 to 3.3. In order to understand the nature of generated interference – knowledge about the basic functionality and influence of the most important components is necessary. The basic operation, electromagnetic interference generation and propagation or sensitive study are explained on the example of boost converter.

3.2 Boost converter - basic operation

The boost converter – presented in Fig. 3.2 – is used to increase average output voltage U_o with the same polarity in relation to the input voltage E. The power electronic switch Q (most commonly used in this role are MOSFET or IGBT

(*)based on https://github.com/diegotrap/electronics

https://doi.org/10.2478/9783110623925-003

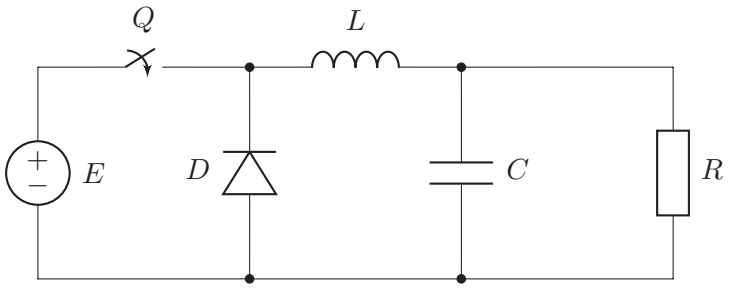

Fig. 3.1: Buck (Step-down Converter) (*)

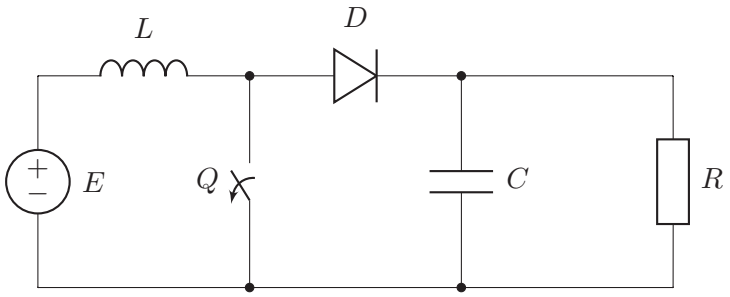

Fig. 3.2: Boost (Step-up Converter)

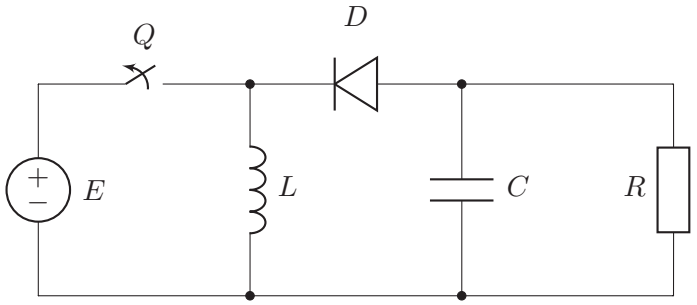

Fig. 3.3: Buck-Boost Converter

transistors) is switched cyclically (at the time $t = k \cdot T$ is turned on and at the time $t_1 = k \cdot T + t_{ON}$ is turned off). The relationship between the conduction time and the period T is described by duty cycle $\gamma = t_{ON}/T$.
In the time interval when the switch Q is in the ON state ($t_{ON} \in (0, t_1)$), current flows from the source of U_i through inductor L and switch Q (Fig. 3.4). At this time, the energy is transferred from the capacitor C to the load R , which requires their earlier charge in the previous cycle.

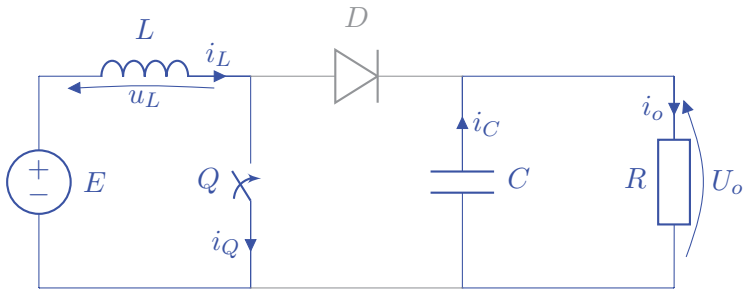

Fig. 3.4: Boost convert - equivalent circuit for time from 0 to t_1

In the time interval , when switch Q enters in the blocking state ($t_{OFF} \in (t_1, T)$), the current flows from the source E through the inductor L, diode D to the load R (Fig. 3.5). Energy delivered to the load R and to the capacitor C comes from the input source and inductor L (stored in its magnetic field at time t_{ON})). The diode current i_D is discontinuous and the capacitor C is periodically charged (at time T_{OFF}) and discharged (at the time t_{ON}). The input current can be continuous or discontinuous, which determines the mode of operation of the converter.

3.2.1 Continuous mode

During one operation cycle T, the switch Q is turned on at time t_{ON}. The inductor voltage u_L – assuming that all converter elements are ideal – is equal to input voltage E:

$$E = u_L(t) \Rightarrow U_{L(\mathrm{AV})} = E \tag{3.1}$$

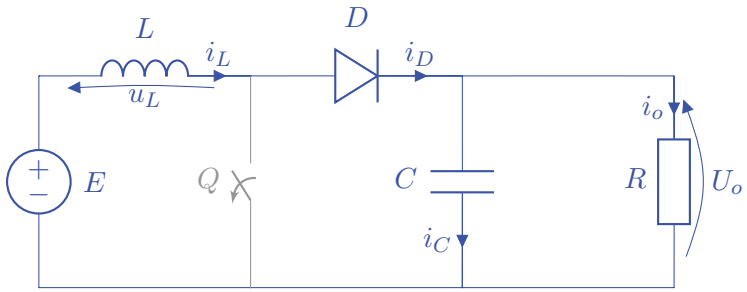

Fig. 3.5: Boost convert - equivalent circuit for time from t_1 to T

The Kirchhoff's voltage law – when switch Q is turned off ($t_{off} \in (t_1, T)$) – is defined by the relation:

$$u_i(t) = u_L(t) + u_O(t) \Rightarrow U_{L(\mathrm{AV})} = E - U_{o(\mathrm{AV})} \tag{3.2}$$

The average inductor voltage $U_{L(\ AV)}$ for the full one or multiple periods its should equal to 0:

$$\frac{1}{T}\int_0^T u_L(t)\mathrm{d}t = 0 \Leftrightarrow \frac{1}{T}\int_0^{t_1} E\mathrm{d}t + \frac{1}{T}\int_{t_1}^{T}(E - U_{o(\mathrm{AV})})\mathrm{d}t = 0 \tag{3.3}$$

Solving the equation Eq. (3.3) is obtained:

$$\begin{aligned}
&\frac{1}{T}\cdot E\cdot t\Big|_0^{t_1} + \frac{1}{T}\cdot(E - U_{o(\mathrm{AV})})\cdot t\Big|_{t_1}^{T} = 0 \Leftrightarrow \\
&\frac{1}{T}\cdot E\cdot t_1 + \frac{1}{T}\cdot(E - U_{o(\mathrm{AV})})\cdot(T - t_1) = 0 \\
&\qquad\qquad \Leftrightarrow E - U_{o(\mathrm{AV})} + U_{o(\mathrm{AV})}\cdot\gamma = 0.
\end{aligned} \tag{3.4}$$

The relationship between the input voltage E and the load voltage $U_{o(\mathrm{AV})}$ is given by:

$$\frac{U_{O(\mathrm{AV})}}{E} = \frac{1}{1-\gamma}. \tag{3.5}$$

The average source current is equal to the average inductor current $I_{L(\mathrm{AV})}$. The average active input power – assuming ideal operation and components –

should of equal the output power:

$$P_I = P_O \Leftrightarrow E \cdot I_{E(\mathrm{AV})} = U_{O(\mathrm{AV})} \cdot I_{O(\mathrm{AV})} \tag{3.6}$$

Transforming Eq. (3.6), the average inductor current $I_{L(\mathrm{AV})}$ can be obtained:

$$I_{L(\mathrm{AV})} = \frac{U_{O(\mathrm{AV})} \cdot I_{O(\mathrm{AV})}}{E} = \frac{\frac{E}{1-\gamma} \cdot I_{O(\mathrm{AV})}}{E} = \frac{I_{O(\mathrm{AV})}}{1-\gamma} = \frac{U_{O(\mathrm{AV})}}{R_O \cdot (1-\gamma)}. \tag{3.7}$$

Regarding waveforms in Fig. 3.6, the minimal value of inductor current i_L is obtained:

$$I_{L(\min)} = I_{L(\mathrm{AV})} - \frac{1}{2} \cdot \Delta i_L \tag{3.8}$$

where: Δi_L is determined by voltage Kirchhoff's law for time $t \in (0, t_1)$:

$$\begin{aligned} L \cdot \frac{\mathrm{d}i_L(t)}{\mathrm{d}t} = E \Leftrightarrow \frac{\mathrm{d}i_L(t)}{\mathrm{d}t} = \frac{E}{L} \Leftrightarrow \frac{\Delta i_L(t)}{\Delta t} = \frac{E}{L} \Leftrightarrow \\ \Delta i_L(t) = \frac{E}{L} \cdot t_1 = \frac{U_{O(\mathrm{AV})} \cdot (1-\gamma)}{L} \cdot \gamma \cdot T. \end{aligned} \tag{3.9}$$

Thus $I_{L(\min)}$:

$$\begin{aligned} I_{L(\min)} = \frac{U_{O(\mathrm{AV})}}{R_0 \cdot (1-\gamma)} - \frac{1}{2} \cdot \frac{U_{O(\mathrm{AV})} \cdot (1-\gamma)}{L} \cdot \gamma \cdot T = \\ U_{O(\mathrm{AV})} \cdot \left[\frac{1}{R_0 \cdot (1-\gamma)} - \frac{(1-\gamma) \cdot \gamma \cdot T}{2L} \right]. \end{aligned} \tag{3.10}$$

Analogously $I_{L(\max)}$ is determined by:

$$I_{L(\max)} = U_{O(\mathrm{AV})} \cdot \left[\frac{1}{R_0 \cdot (1-\gamma)} + \frac{(1-\gamma) \cdot \gamma \cdot T}{2L} \right]. \tag{3.11}$$

The relation between minimal, maximal and average values of inductor currents is given by:

$$I_{L(\mathrm{AV})} = \frac{I_{L(\max)} + I_{L(\min)}}{2} \tag{3.12}$$

The average and RMS value of the switch (transistor) Q and diode D currents – useful in converter design process – are described by the following equations:
– for switch:

$$i_Q(t) = \frac{I_{L(\max)} - I_{L(\min)}}{t_{ON}} \cdot t + I_{L(\min)} \tag{3.13}$$

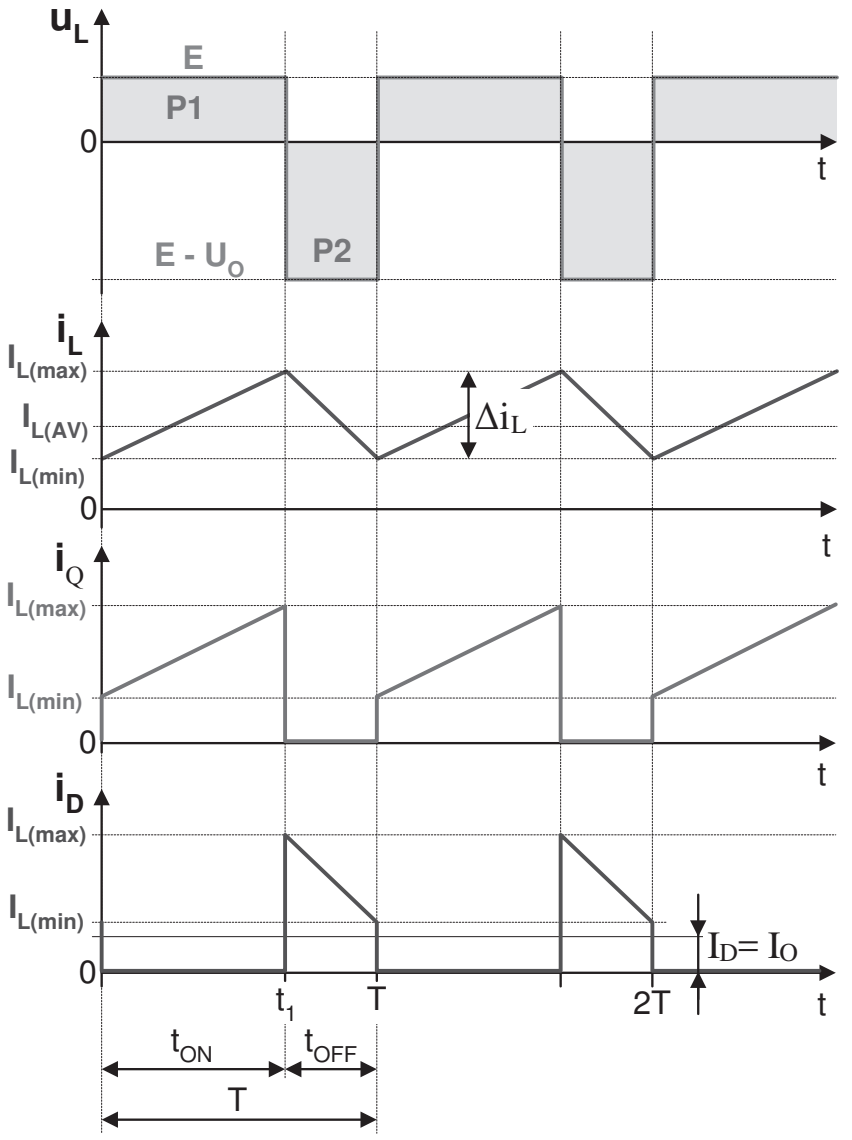

Fig. 3.6: Boost converter waveforms operating in continuous mode: inductor voltage u_L and current i_L, switch current i_Q, diode current i_D

$$I_{Q(\mathrm{AV})} = \frac{1}{T}\int_0^{t_{ON}} \left(\frac{I_{L(\max)} - I_{L(\min)}}{t_{ON}} \cdot t + I_{L(\min)}\right) \mathrm{d}t = \frac{I_{L(\max)} + I_{L(\min)}}{2} \cdot \gamma = I_{L(\mathrm{AV})} \cdot \gamma = I_{E(\mathrm{AV})} \cdot \gamma = I_{O(\mathrm{AV})} \cdot \frac{\gamma}{1-\gamma}. \tag{3.14}$$

$$I_{Q(\mathrm{RMS})} = \sqrt{\frac{1}{T}\int_0^{t_{ON}} \left(\frac{I_{L(\max)} - I_{L(\min)}}{t_{ON}} \cdot t + I_{L(\min)}\right)^2 \mathrm{d}t} = \sqrt{\frac{\left(I_{L(\max)}^2 + I_{L(\max)} \cdot I_{L(\min)} + I_{L(\min)}^2\right) \cdot \gamma}{3}}. \tag{3.15}$$

– for diode:

$$i_D(t) = \frac{I_{L(\max)} - I_{L(\min)}}{t_{ON} - T} \cdot t + \frac{I_{L(\min)} \cdot t_{ON} - I_{L(\max)} \cdot T}{t_{ON} - T} \tag{3.16}$$

$$I_{D(\mathrm{AV})} = \frac{1}{T}\int_{t_{ON}}^{T} \left(\frac{I_{L(\max)} - I_{L(\min)}}{t_{ON} - T} \cdot t + \frac{I_{L(\min)} \cdot t_{ON} - I_{L(\max)} \cdot T}{t_{ON} - T}\right) \mathrm{d}t = \frac{I_{L(\max)} + I_{L(\min)}}{2} \cdot (1-\gamma) = I_{L(\mathrm{AV})} \cdot (1-\gamma) = I_{E(\mathrm{AV})} \cdot (1-\gamma) = I_{O(\mathrm{AV})} \tag{3.17}$$

$$I_{D(\mathrm{RMS})} = \sqrt{\frac{1}{T}\int_{t_{ON}}^{T} \left(\frac{I_{L(\max)} - I_{L(\min)}}{t_{ON} - T} \cdot t + \frac{I_{L(\min)} \cdot t_{ON} - I_{L(\max)} \cdot T}{t_{ON} - T}\right)^2 \mathrm{d}t} = \sqrt{\frac{\left(I_{L(\max)}^2 + I_{L(\max)} \cdot I_{L(\min)} + I_{L(\min)}^2\right) \cdot (1-\gamma)}{3}} \tag{3.18}$$

3.2.2 Boundary conduction mode

The inductor current i_L can be pulse or continuous, depending on the operation condition and the load. The converter is in boundary conduction mode when

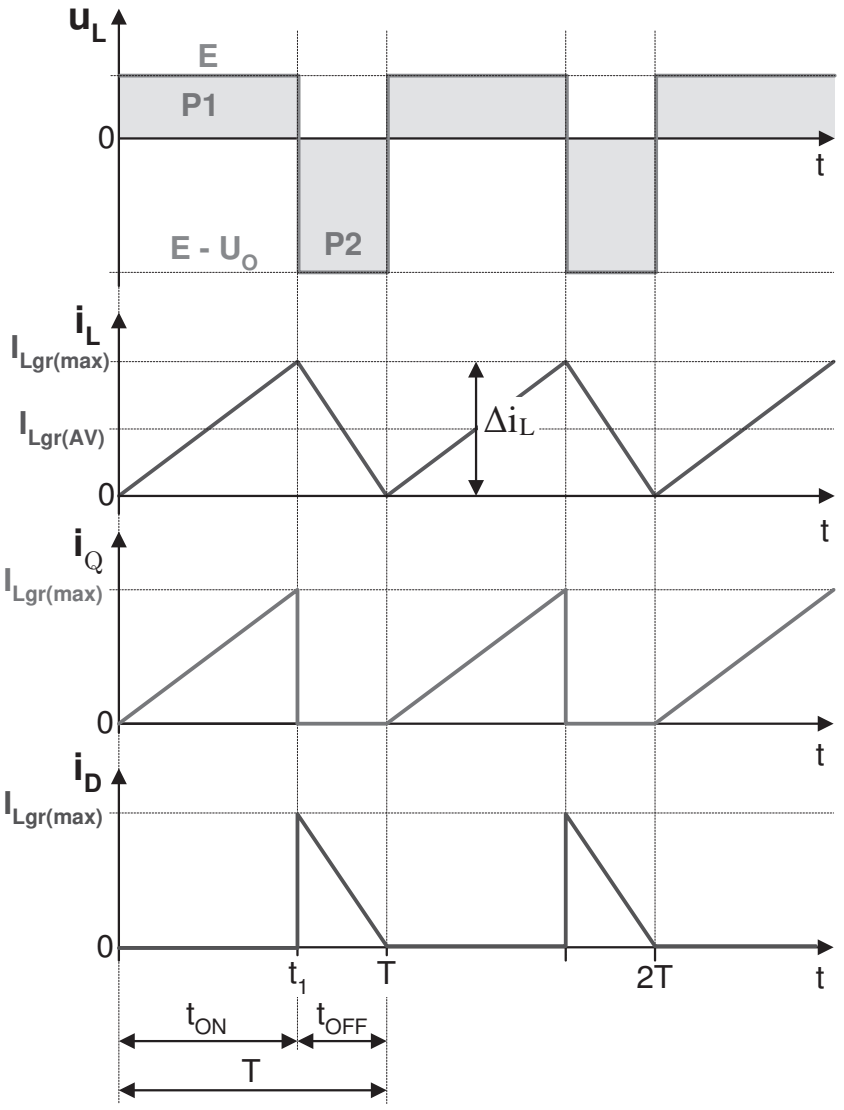

Fig. 3.7: Boost converter waveforms operating in boundary conduction mode: inductor voltage u_L and current i_L, switch current i_Q, diode current i_D

.

i_L falls to zero only at time $t = k \cdot T$ (for k= 1,2,3 ...) as it is presented in Figure 3.7. The average value of the inductor current i_L equals:

$$I_{Lgr(\mathrm{AV})} = \frac{1}{T}\int_0^T i_L \mathrm{dt} =$$

$$\frac{1}{T}\left[\int_0^{t_1} \frac{I_{Lgr(\max)}}{t_1}\cdot t \mathrm{dt} + \int_{t_1}^{T}\left(\frac{L_{Lgr(\max)}}{t_1 - T}\cdot t - \frac{I_{Lgr(\max)}\cdot T}{t_1 - T}\right)\mathrm{dt}\right] =$$

$$\frac{1}{T}\left(\frac{I_{Lgr(\max)}}{2t_1}\cdot t^2\Big|_0^{t_1} + \frac{I_{Lgr(\max)}}{2(t_1 - T)}\cdot t^2\Big|_{t_1}^{T} - \frac{I_{Lgr(\max)}\cdot T}{t_1 - T}\cdot t\Big|_{t_1}^{T}\right) = \frac{1}{2}I_{Lgr(\max)} \tag{3.19}$$

where maximal value of inductor current $I_{Lgr(\max)}$ is defined:

$$I_{Lgr(\max)} = \frac{u_L(t_1)}{L}\cdot t_{ON} = \frac{E}{L}\cdot t_{ON}. \tag{3.20}$$

Using Equations 3.19 and 3.20 the formula for average inductor current $I_{Lgr(\mathrm{AV})}$ depending on duty cycle γ can be obtained:

$$I_{Lgr(\mathrm{AV})} = \frac{1}{2}I_{Lgr(\max)} = \frac{E}{2L}\cdot t_{ON} = \frac{T\cdot U_{O(\mathrm{AV})}}{2L}\cdot\gamma(1-\gamma). \tag{3.21}$$

It can be noticed that the inductor current is also the input current, thus – for the idealized circuit when the input power is losslessly transferred to load $P_d = P_O$, so $U_I \cdot I_{L(\mathrm{AV})} = U_{O(\mathrm{AV})} \cdot I_{O(\mathrm{AV})}$ – the voltages and currents ratio for boundary conduction mode is equal to:

$$\frac{I_{O(\mathrm{AV})}}{I_{L(\mathrm{AV})}} = \frac{E}{U_{O(\mathrm{AV})}} = 1 - \gamma. \tag{3.22}$$

Transforming Eq. (3.22), it is possible to define the average output current $I_{Ogr(\mathrm{AV})}$:

$$I_{Ogr(\mathrm{AV})} = \frac{T\cdot U_{O(\mathrm{AV})}}{2L}\cdot\gamma(1-\gamma)^2. \tag{3.23}$$

In Fig. 3.8 the dependence between the average inductor current $I_{Lgr(\mathrm{AV})}$, the average output current $I_{Ogr(\mathrm{AV})}$ and duty cycle γ is presented. It can be notice

that $I_{Lgr(\mathrm{AV})}$ reaches the maximal value for $\gamma = 1/2$ while $I_{Ogr(\mathrm{AV})}$ for $\gamma = 1/3$. The maximum value of this currents equals:

$$I_{Ogr(\mathrm{AV})}\left(\gamma = \frac{1}{3}\right) = I_{Ogr(\mathrm{AV})(\max)} = \frac{2 \cdot T \cdot U_{O(\mathrm{AV})}}{27L} \tag{3.24}$$

$$I_{Lgr(\mathrm{AV})}\left(\gamma = \frac{1}{2}\right) = I_{Lgr(\mathrm{AV})(\max)} = \frac{T \cdot U_{O(\mathrm{AV})}}{8L}. \tag{3.25}$$

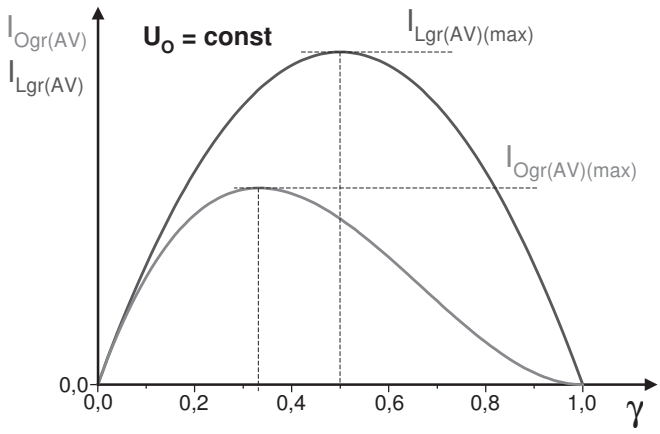

Fig. 3.8: Characteristics of $I_{Lgr(\mathrm{AV})}$ and $I_{Ogr(\mathrm{AV})}$ depending on duty cycle γ

The operation mode of the boost converter depends on the parameters and the load. In many cases, the value of the power consumed by the load is not constant, therefore it is preferable to determine the value of the boundary resistance R_{Ogr}, which – for the other converter parameters constants – operates in the bound between continuous and discontinuous modes. If the resistance $R_O > R_{Ogr}$, the converter operates in discontinuous mode.

$$R_{Ogr} = \frac{U_{O(\mathrm{AV})}}{I_{O(\mathrm{AV})}} = \frac{U^2_{O(\mathrm{AV})}}{E \cdot I_{Lgr(\mathrm{AV})}} \tag{3.26}$$

Using Eq. (3.21) and (3.26), the value of boundary resistance can be defined:

$$R_{Ogr} = \frac{U^2_{O(\mathrm{AV})} \cdot 2L}{E^2 \cdot t_{ON}} = \frac{2L}{T \cdot \gamma(1-\gamma)^2} = \frac{X_L}{\pi \cdot \gamma(1-\gamma)^2} \tag{3.27}$$

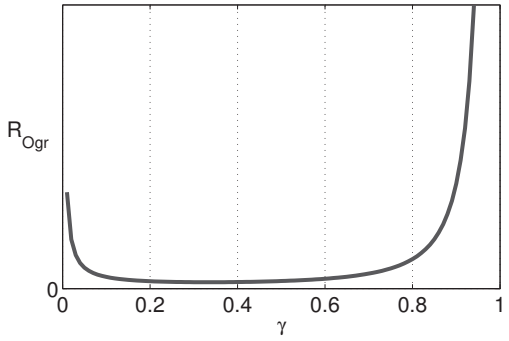

Fig. 3.9: $R_{Ogr} = \mathrm{f}(\gamma)$

where: $X_L = 2 \cdot \pi f L$, $f = 1/T$.
Similarly, the bound inductance L_{gr} for boundary condition mode can be defined:

$$L_{gr} = \frac{(1-\gamma)^2 \gamma R}{2f} \tag{3.28}$$

3.2.3 Discontinuous mode

In the discontinuous mode, the inductor current i_L reaches the zero amperes for some time. The operation mode of the converter depends on operation conditions e.g. for low values of input i_L and output i_O and high value of the current ripple Δi_L, what can happen when the load resistance is high enough and the inductor current i_L decreases to zero at the instant $t = t_1 + \Delta_1 T$ as it is presented in Fig. 3.10.
Knowing that the average voltage on inductor $U_{L(\mathrm{AV})}$ – for whole period – should be equal zero, the expression between the input voltage E and the average output voltage U_O for the discontinuous operation mode can be calculated:

$$\frac{U_{O(\mathrm{AV})}}{E} = \frac{\Delta_1 + \gamma}{\Delta_1} \tag{3.29}$$

and similarly for current (using ideal converter properties ($P_I = P_O$):

$$\frac{I_{O(\mathrm{AV})}}{I_{Lp(\mathrm{AV})}} = \frac{\Delta_1}{\Delta_1 + \gamma}. \tag{3.30}$$

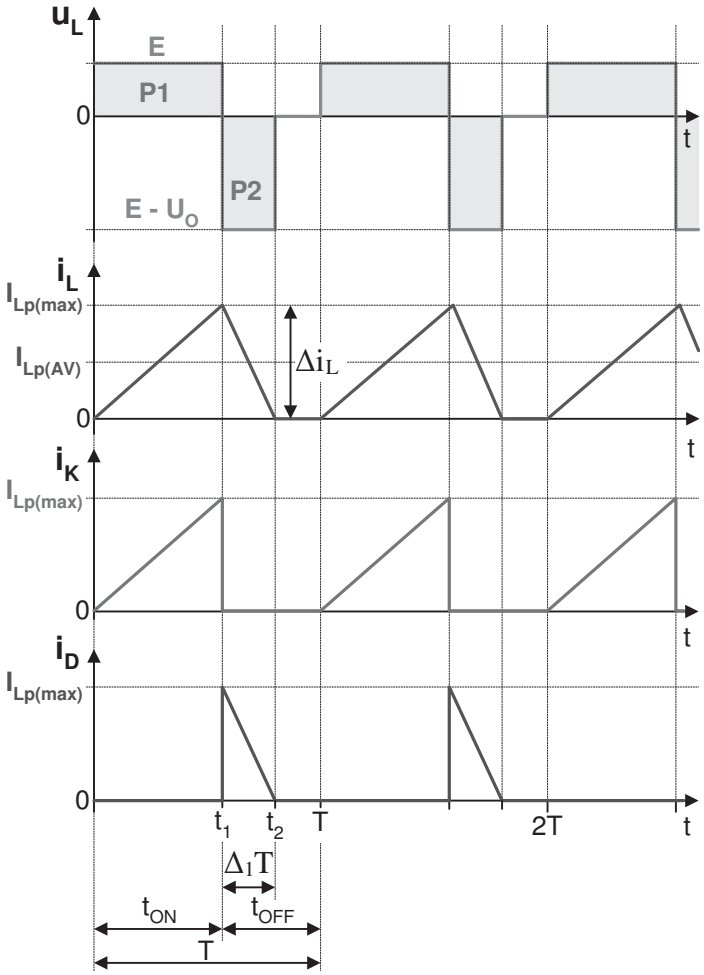

Fig. 3.10: Boost converter waveforms operating in discontinuous mode: inductor voltage u_L and current i_L, switch current i_Q, diode current i_D

The average inductor current is equal to:

$$I_{Lp(\mathrm{AV})} = \frac{1}{T}\int_0^T i_L \mathrm{dt} =$$

$$\frac{1}{T}\left[\int_0^{t_1}\frac{I_{Lp(\max)}}{t_1}\cdot t\,\mathrm{dt}+\int_{t_1}^{t_2}\left(\frac{L_{Lp(\max)}}{t_1-t_2}\cdot t-\frac{I_{Lp(\max)}\cdot t_2}{t_1-t_2}\right)\mathrm{dt}\right]=$$

$$\frac{I_{Lp(\max)}}{2T}\cdot(\gamma T+\Delta_1 T)=\frac{I_{Lp(\max)}}{2}\cdot(\gamma+\Delta_1). \tag{3.31}$$

Transforming Eq. (3.31) gives shall be finally:

$$I_{Lp(\mathrm{AV})}=\frac{E}{2L}\cdot t_{ON}\cdot(\gamma+\Delta_1)=\frac{E\cdot T}{2L}\cdot\gamma(\gamma+\Delta_1), \tag{3.32}$$

Using Eq. (3.30), the average value of the output current can be calculated:

$$I_{Op(\mathrm{AV})}=I_{Lp(\mathrm{AV})}\cdot\frac{\Delta_1}{\Delta_1+\gamma}=\frac{E\cdot T\cdot\gamma\cdot\Delta_1}{2L}=\frac{E\cdot(1-\gamma)\gamma\cdot T}{2L}. \tag{3.33}$$

Substituting Eq. (3.20) and Eq. (3.30) for Eq. (3.30) gives:

$$\frac{U_{O(\mathrm{AV})}}{E}=1+\frac{E\cdot\gamma^2\cdot T}{2L\cdot I_{Op(\mathrm{AV})}}. \tag{3.34}$$

Theoretically, the output voltage $U_{O(\mathrm{AV})}$ tends to infinity when the current $I_{Op(\mathrm{AV})}$ tends to zero. In practice, these values are limited by strength converter components, in particular semiconductor devices and the output capacitor, and therefore it is preferable to use supplementary security preventing the voltage increase above the values permissible. In order to maintain the output voltage constant $I_{Op(\mathrm{AV})}=const$, it is preferred to determine the value of the duty cycle γ transforming Eq. (3.34):

$$\gamma=\sqrt{\frac{2L\cdot I_{Op(\mathrm{AV})}\cdot(U_{O(\mathrm{AV})}-E)}{E^2\cdot T}}=\sqrt{\frac{2L\cdot I_{Op(\mathrm{AV})}}{\frac{E^2\cdot T}{U_{O(\mathrm{AV})}-E}}}=$$

$$\sqrt{\frac{2L}{U_{O(\mathrm{AV})}\cdot T}\cdot\frac{I_{Op(\mathrm{AV})}\cdot(U_{O(\mathrm{AV})}-E)\cdot U_{O(\mathrm{AV})}}{E^2}}= \tag{3.35}$$

3.2.4 Output voltage ripple

In previous sections, it is assumed that the output voltage is constant by employing a capacitor with a very high capacitance. However, in practice, there

are some voltage ripples caused by the cyclic charging and discharging of the capacitor. The value of these ripples can be estimated by studying the variations of the capacitor charging and discharging:

$$\Delta u_O = \frac{\Delta Q}{C} = \frac{I_{O(\mathrm{AV})} \cdot \gamma \cdot T}{C} = \frac{U_{O(\mathrm{AV})} \cdot \gamma \cdot T}{R \cdot C}. \tag{3.36}$$

To determine the absolute value, the formula can be used:

$$\frac{\Delta u_O}{U_{O(\mathrm{AV})}} = \frac{\gamma \cdot T}{RC} = \gamma \cdot \frac{T}{\tau} \tag{3.37}$$

where: $\tau = RC$ – load time constants. It is apparent from the Eq. (3.37) that reducing the output voltage ripple can be achieved by increasing the time constant τ or switching frequency $f = 1/T$.

3.3 EMI propagation paths

The generation and propagation phenomena in all non isolated (transformerless) converters has the same nature, so for the EMI analysis of the boost converter is presented as an example. The device does not contain any of damping like snubber or clamps and some parts were specially over-sized in order to make more visible the influence of selected elements.
The main EMI origin in all – isolated and non-isolated – converters are fast changing of the voltage and current in semiconductor devices. The interference is propagated through all basic components and also wires and conducting tracks. Moreover, there are electric and magnetic couplings between them. The main EMI propagation paths are shown in Fig. 3.11, where common mode noise is represented by brown lines and differential mode by other colors.
The boost converter prototype and simulation model have been used for EMI analyzes. In Fig. 3.12 converter scheme is presented, where – besides the main components – Line Impedance Stabilization Network ($LISN$) and PCB parasitics (highlighted in blue) are included. In simulation, models presented in Chapter 2 are applied.
The spectra of transistor voltage U_{DS}, diode voltage U_D and voltage across 50Ω LISN resistor are presented in Fig. 3.13. The interference obtained from LISN is mainly in common mode. The switching frequency is 100 kHz with

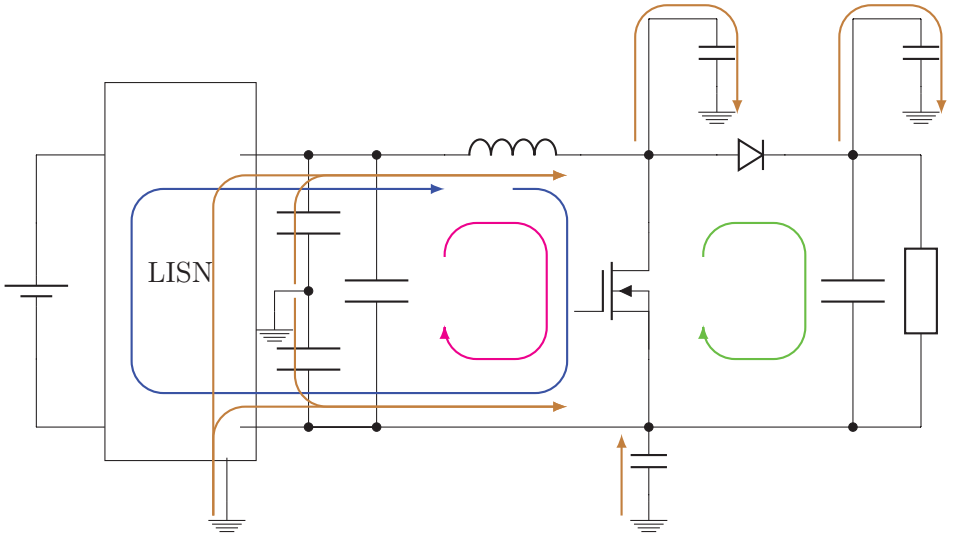

Fig. 3.11: Propagation paths in boost converter

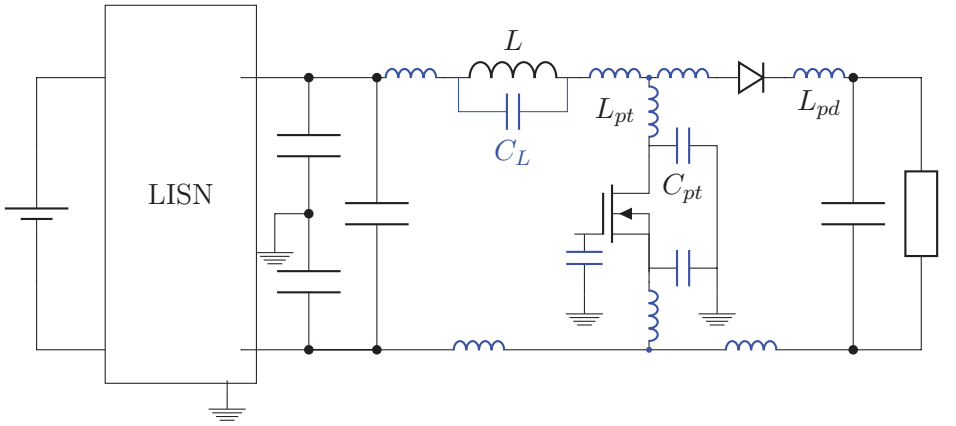

Fig. 3.12: Boost converter - equivalent circuit with parasitic

duty cycle D=0.7 what is visible in spectra in the range up to 1 MHz, where its harmonics dominate. Above 1 MHz interference peaks are linked with the

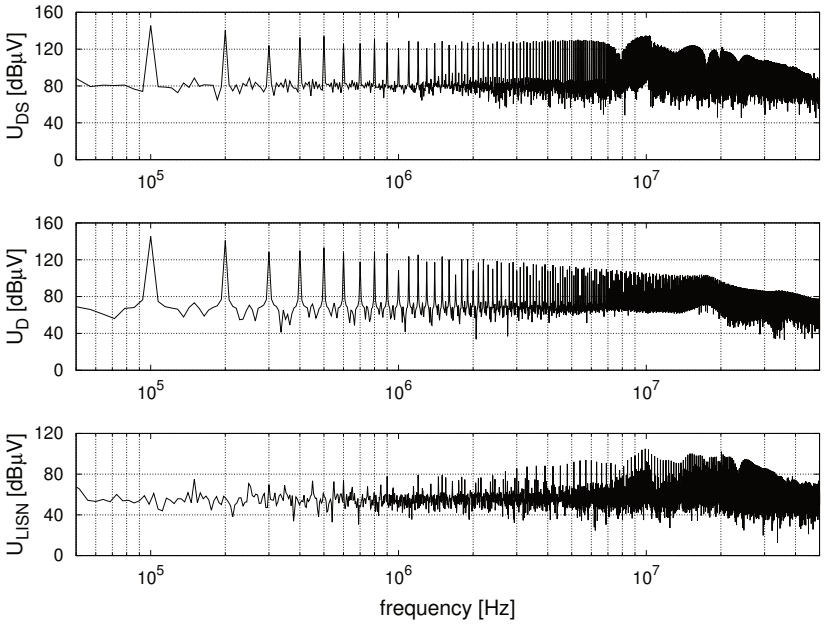

Fig. 3.13: Boost converter voltages spectra

resonant between parasitics. Of course this scope is individual for the converter and it depends on its parameters, components and geometrical dimensions. In the spectra (Fig. 3.13) the distinctive peaks appear:

- the operation frequency (here for 100 kHZ)
- the harmonics (in the range 0.2 - 1 MHz)
- peak links with transistor slew rate (for 10 MHz)
- ringing oscillation during transistor turn on (for 16 MHz)
- oscillation in discontinuous mode during transistor turn off (for 20 MHz)
- ringing oscillation during diode turn on (for 17 MHz)

Next, the impact of chosen components is discussed, where only one parameter is changed and its influence on the spectra is considered.

3.3.1 Transistor capacitance

The main interference origin is the fast switching of transistor. The transistor is periodically turned on and off. After switch commutation, a voltage U_{DS} oscillation appears and it is propagated as interference. One of the main parameters which are responsible for perturbation level is the internal capacitance, as it is described in Section 2.1.2. The internal capacitance is non linear, thus it has different values during switch on and off. In Fig. 3.14 voltage spectra are presented when the capacitance of transistor increases 10 times. Compared to Fig. 3.13, it can be notice that this capacitance impacts mainly on spectra envelopes' shape in range above 1 MHz but it has a negligible impact on their level. It is involved mainly in the interference generation and has less impact on the propagation process. Increasing MOSFET capacitance causes its ringing frequency f_{tr} shifts to the left. The MOSFET ringing frequency is difficult to calculate. It depends on almost all physical and geometrical properties of the circuit and input filter.

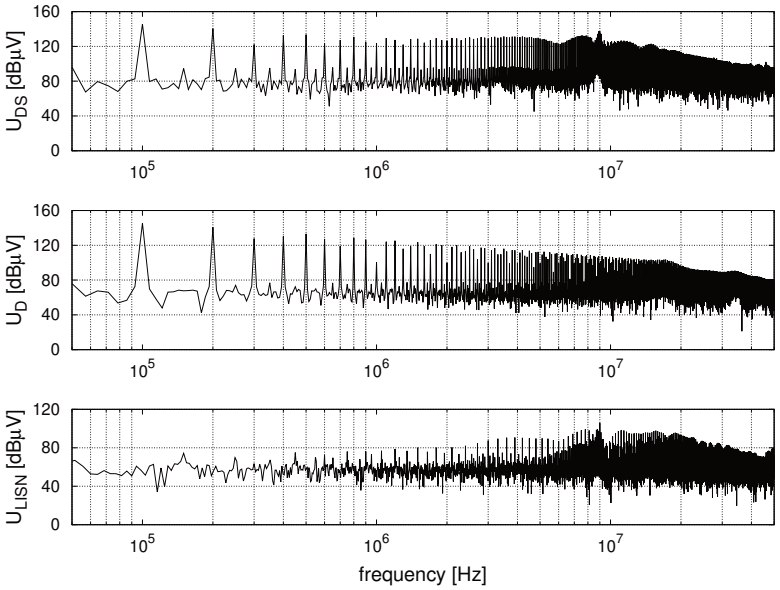

Fig. 3.14: Influence of MOSFET internal capacitance

The MOSFET ringing frequency can be estimated using Eq. (3.38).

$$f_{tr} \approx \frac{1}{2 * \Pi * \sqrt{k(C_{troff} + C_L) * (\sum L_p + L)}} \tag{3.38}$$

where:

C_{troff}	–	transistor capacitance at its turns off
C_L	–	inductor internal capacitance
$\sum L_p$	–	sum of parasitic inductance in branches where current flows before transistor switch off
L	–	inductor inductance
k	–	influence of input filter factor L/C_{in}

It should be noticed that parasitic ground capacitance impacts on the ringing frequency, but in typical application, it is incomparably smaller than the transistor and inductor and it is insignificant in EMI generation but it is essential in EMI propagation.
The example application was validated for DC-DC boost converter prototype for the photovoltaic system. The simulation and laboratory measurements have been done and compared with results obtained with formula 3.38 with following parameters: C_{DSoff}=200e-12F, L=4.752e-4H, C_L=6e-11F, $\sum L_p$=2.26e-07 H, C_{input}=5.37e-04F.
The ringing frequency – calculated using Equation 3.38 – is f_r = 22 MHz, which is in agreement with the measurement results presented in Fig 3.15

3.3.2 Diode capacitance

The diode is a basic element in DC-DC converters. After diode commutation, a voltage U_D (anode - cathode voltage) oscillation appears. The level and frequency of this oscillation depends mainly on the output circuit parasitic parameters like diode, output filter and ground capacitance, PCB inductance and load. From EMC point of view, the most important parameter is its internal capacitance C_{ds}. As in all semiconductors, it is nonlinear and depends on diode state and U_D .
In Fig. 3.16 the diode capacitance has been increased ten times in comparison to Fig. 3.13. It is highly visible that diode ringing oscillation is shifted to the left and the level increased significantly. It follows that internal diode capacitance

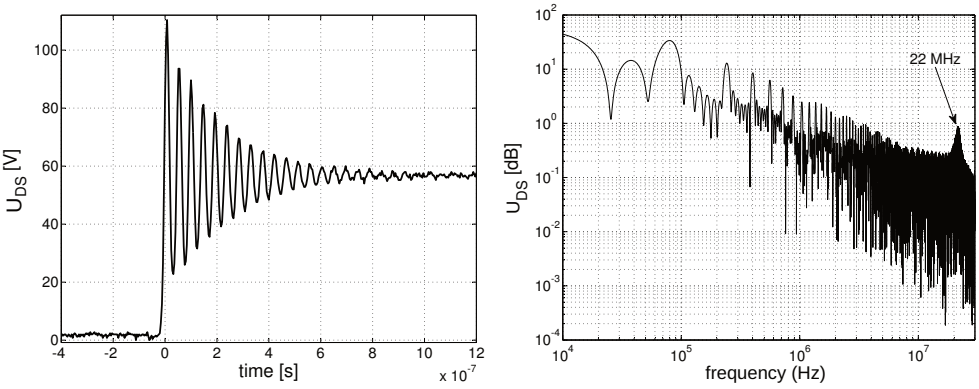

(a) waveform (b) spectra

Fig. 3.15: Experimental U_{DS} measurement - ringing frequency

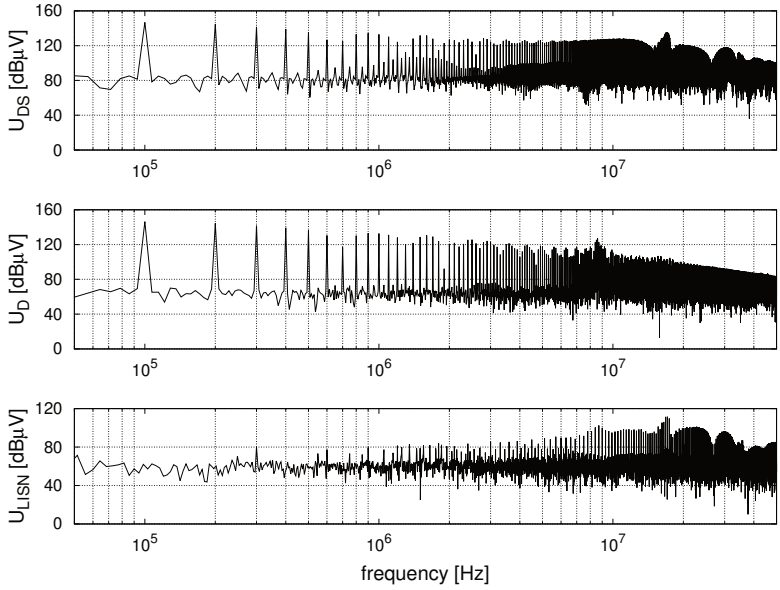

Fig. 3.16: Influence of Diode internal capacitance

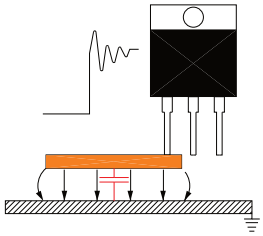

Fig. 3.17: Parasitic capacitance phenomena

impacts on the frequency and also on the level of interference registered on LISN.

3.3.3 Parasitic capacitance connected to MOSFET terminals

In typical converter, a transistor is located on the board and connected with other elements through the conducting tracks. The track is a flat copper part and it can be characterized by resistance, self and mutual (with other components) inductance and ground capacitance. Due to fast changes of potential connected to drain or source terminal ($\mathrm{d}u/\mathrm{d}t$), the current flows to the ground and beyond the converter. In Fig. 3.14 the parasitic capacitance connected to drain C_{pt} was reduced (a) 10 times and increase 10 times (b) according to spectra presented in Fig. 3.13 which may be caused by the change of the distance to the ground. It can be noticed that the peak level in the range above 10 MHz is most noticeable.
The parasitic capacitance of the track connected to MOSFET drain node has great impact on the level of U_{DS} oscillation and generated perturbation U_{LISN} and minimal on interference frequency – of course it depends on individual geometrical properties of the PCB and parasitic current paths. In the present case, there is no visible impact on diode voltage U_D, but this is an individual property of the investigated circuit and depending on the couplings of the electric field near the PCB, the parasitic capacitance connected to the transistor terminals have the influence on its level or less on the resonant frequency.

3.3.4 Parasitic inductance in transistor branch

The parasitic inductance connected in series with the transistor, both drain and source terminals, takes a part in interference generation. When transistor

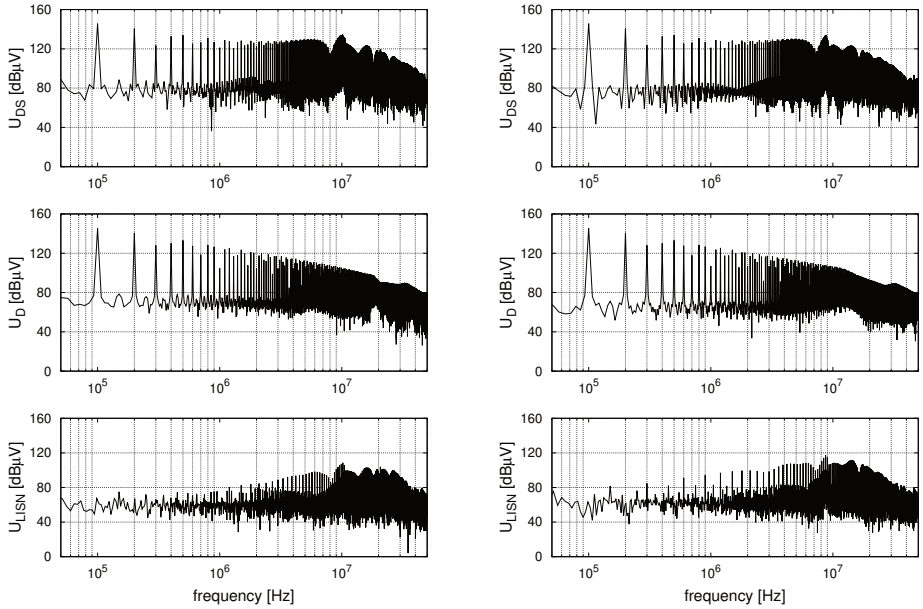

(a) $C_{pd}/10$ (b) C_{pd}*10

Fig. 3.18: Influence of parasitic capacitance connected to drain

or diode is turned on, it is the part of the resonant circuit in which oscillation is generated. During transistor turning off, its impact is less significant because it is serially connected to inductor L, which the inductance value is typically much larger than parasitic inductance. During the diode turning off, the influence of the inductor inductance is significant, so resonate circuit includes parasitic inducance and semiconductors capacitance. In Fig. 3.19 the parasitic inductance in transistor branch L_{pt} was reduced (a) 10 time and increase 10 time (b) according to spectra presented in Fig. 3.13. Increasing the L_{pt} shifts the ringing frequency peaks to the left. The level of disturbance also increases. In practical application, the PCB tracks between transistor, diode and inductor should be as short as possible in order to avoid increasing the EMI level or increasing the resonant frequency oscillation after the diode is turned off, which allows efficiently their attenuating or filtering.

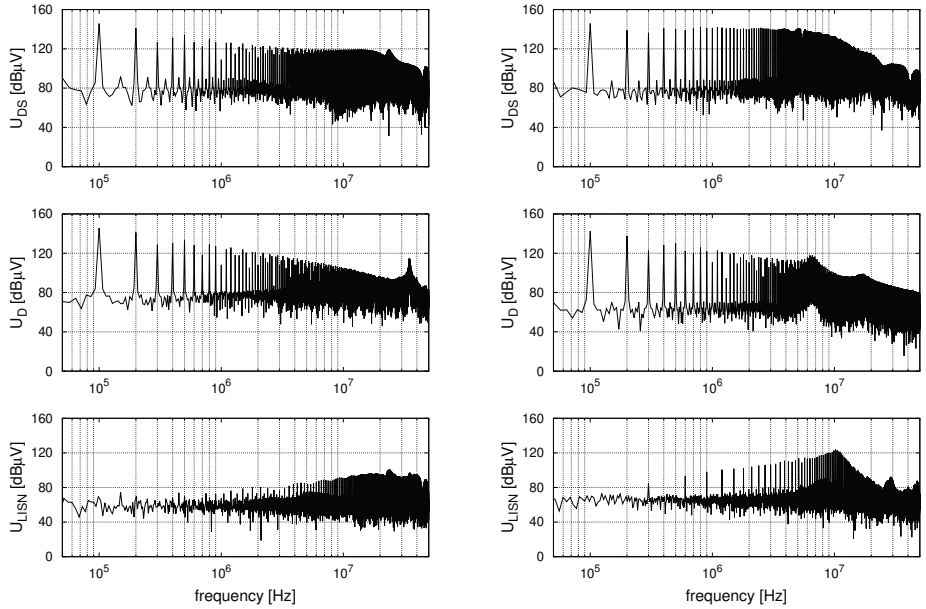

(a) $L_{pt}/10$ (b) L_{pt}*10

Fig. 3.19: Influence of parasitic inductance in MOSFET branch

3.3.5 Driver

EMI interference generation is strongly connected with transistor current and voltage slew rate during commutation. Generally, when transistor is switched faster, the over voltage and the interference level are greater. On the other side, the longer commutation time may cause higher losses. In some range, it can be controlled by the driver gate resistor. Moreover, parasitics in the gate circuit have also the influence on U_{gs} and U_{ds} slew rate. In order to limit the interference from control circuit, the transistor driver should be located as close as possible to transistor. In some cases, disruption is generated in driver or its supply, but it can be disabled by applying the common mode filter as it is shown in Fig. 3.20.

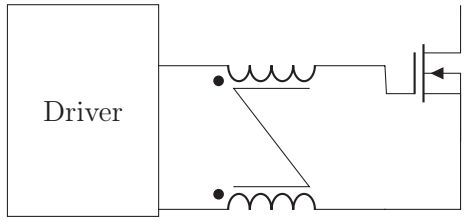

Fig. 3.20: The common mode filter between driver and transistor

3.3.6 Parasitic inductance in diode branch

The parasitic inductance serial linked with diode L_{pd} depends on the load and its connections, thus its value depends on the PCB layout of the converter and also on the external load properties. The output differential mode current noise flows through the load, so it properties depend on L_{pd}. The influence of load is typically reduced by the output filter, but it can not be totally cut down. The value of L_{pd} is normally much smaller than the inductor inductance, so it impacts only during diode turning off. In Fig. 3.21 the parasitic inductance in diode branch L_{pd} was reduced (a) 10 times and increased 10 times (b) according to spectra presented in Fig. 3.13. It can be noticed that it affects mainly on the diode voltage U_d (distinctive peak near 13MHz in Fig. 3.21b), but the influence on interference registered on LISN is slight because of the filters operation.
The oscillation – which appears after diode turn off – derives from interaction between L_{pd} and the parasitic diode capacitance, but if the output filter is not designed correctly (the right way can be found in [30]), the EMI level and frequency impact deteriorates. The components should be geometrically located as close as possible but if it is impossible, the distance between diode, output filter and output terminals can be increased.

3.3.7 Inductor

The inductor is a passive element used for storage and transfer of energy. The non ideal inductor can be described as inductance L, wire resistance R_L and parasitic (between wires) capacitance C_L as it is presented in Section 2.2.1. Interaction between these parameters and other parasitics during transistor commutation can be the origin of interference. For practical reasons the ge-

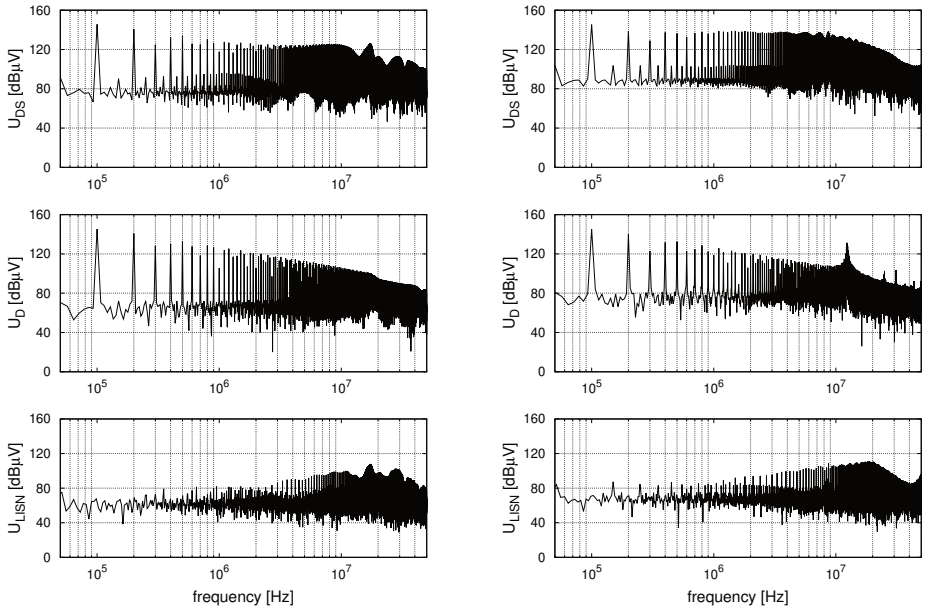

(a) $L_{pd}/10$ (b) L_{pd}*10

Fig. 3.21: Influence of parasitic inductance in diode branch

ometrical dimensions and L, R_L and C_L values should be small as possible, but for EMC point of view the inductor can operate as the low pass filter. In Fig. 3.22, the impact of the inductance L is presented. It influences on the frequency and level of interference in the range above 1MHz.

The parasitic capacitance of inductor C_L represents the electrical field behaviour of wires or other conductors. The total capacitance – viewed from inductor terminals – consists a partial capacitances between coils or coils and magnetic core or inductor housing. This capacitance has the strong impact on the ringing frequency – especially during diode turn off. In Fig. 3.23b, in the U_D spectra a characteristic peak appears close to 13 MHz.
In some cases – depending on individual properties of the PCB – the C_L could operate as the high pass filter, which limits the perturbation register in LISN – in the frequency range below ringing frequency.

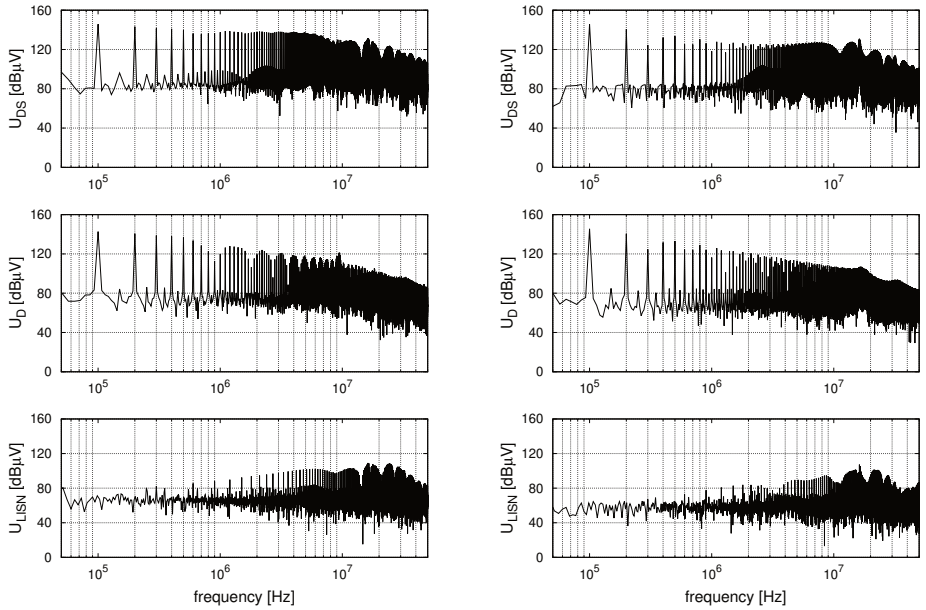

(a) $L_L/10$ (b) L_L*10

Fig. 3.22: Influence of inductor L inductance

3.4 Conclusion

The boost converter is a quite good example to analyze and understand the EMI generation and propagation phenomena in all non isolated DC-DC converters. From the electromagnetic point of view, converters like boost, buck or sepic are similar, where there is only one interference source – the fast switching pair transistor - diode. The level of the perturbation depends mainly on the voltage and current rising and falling rate and the physical and geometrical properties of converter. The parasitic capacitances in the immediate vicinity of transistors have the impact on total EMI level. The inductor and parasitic capacitance of semiconductors affects on the ringing frequency. For fast forecast of the EMI level, the simple model can be built including only one capacitance, inductor, input capacitor, trapezoidal voltage source (as a CM source) and the

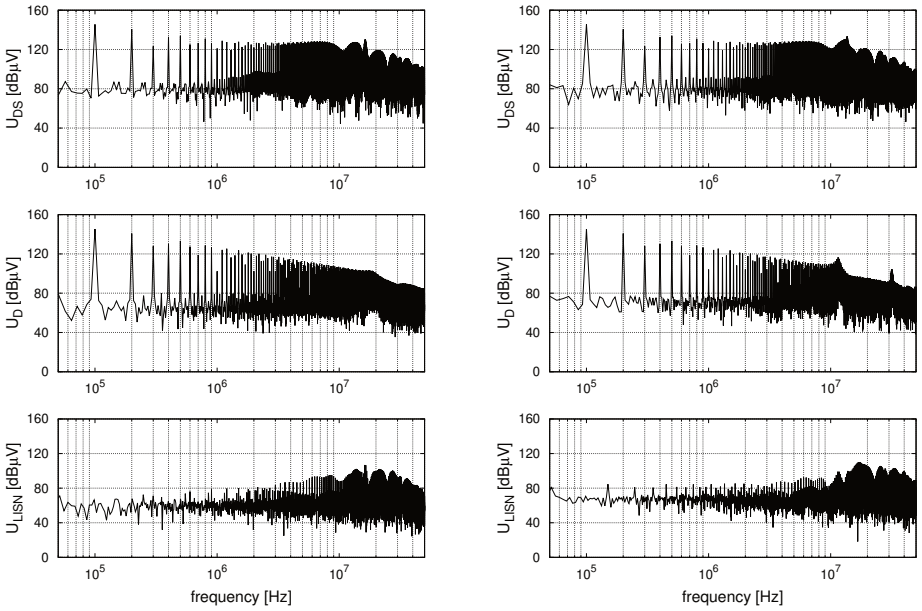

(a) $C_L/10$ (b) C_L*10

Fig. 3.23: Influence of inductor L capacitance

trapezoidal current source (as a DM source) [31, 32]. The result of simulation is presented in Fig. 3.25.

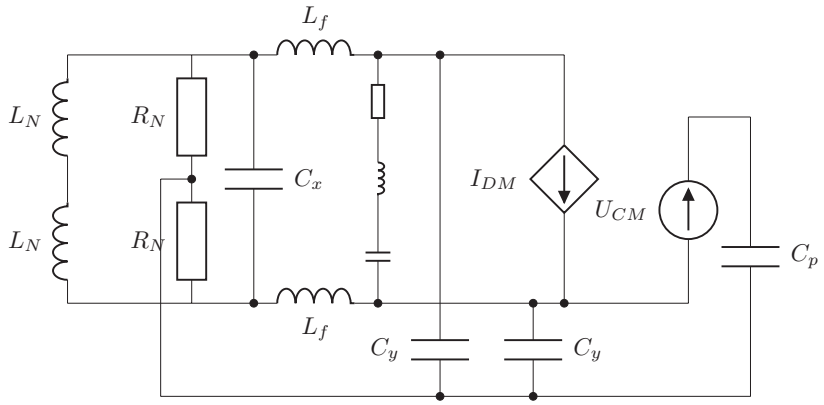

Fig. 3.24: Simple model for EMI estimation of boost converter

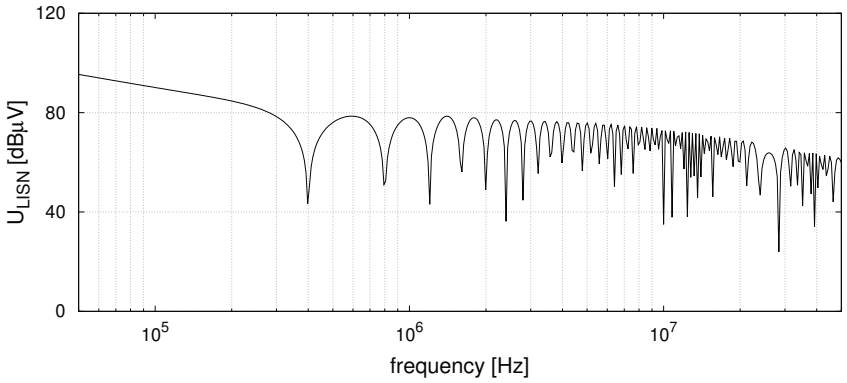

Fig. 3.25: U_{LISN} spectra obtained using the simple model of boost converter

Chapter 4

Flyback converter

4.1 Introduction - basic operation

The extended properties of isolated DC-DC converters are achieved in the flyback converter, where the inductor is replaced by the transformer consists of two inversely wound magnetically coupled coils. In literature this kind of transformer is often called the coupled inductor. In Fig. 4.1 the basic schema of flyback converter is presented. The DC power supply feeds the circuit consisted of transformer primary winding and the switch Q. In a typical application, as the switch Q, transistors MOSFET are widely used. The secondary circuit includes the diode, the capacitor and the load. The role of the capacitor is filtering and energy storage.
Idealized transformer turns ratio is equal to the voltage and current ratios.

$$\vartheta = \frac{u_2}{u_1} = \frac{i_{n_1}}{i_{n_2}} = \frac{n_2}{n_1} \tag{4.1}$$

During typical operation of the converter, energy is stored in the magnetic field of the transformer, and then provided to the load. Properties of the magnetic circuit are associated with the amount and speed of energy accumulation, which affects the total power of the inverter. The operation periods depend on the state of the power electronic switch Q, which may be in the two states. When the switch Q is turned on (Fig. 4.2), the primary winding is fed from the source E. The i_{n1} current linear increase and flowing through primary winding causes increasing the magnetic field in the core of the transformer, where the

https://doi.org/10.2478/9783110623925-004

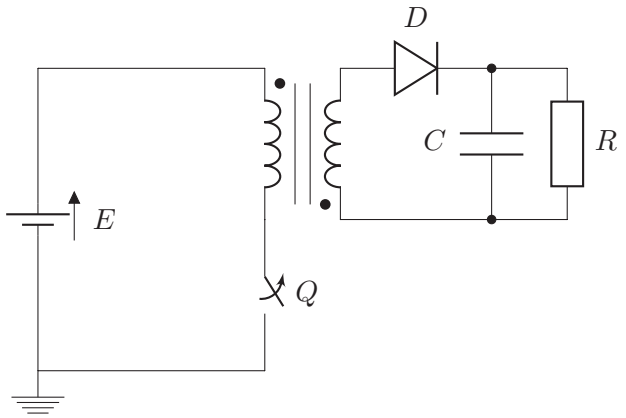

Fig. 4.1: Flyback converter – basic schema

energy is stored. In this converter topology, where the beginning of windings are connected as is shown in Fig. 4.1, the diode is reverse biased and the secondary winding current i_{n1} is equal to zero. The load is fed from the capacitor, because the energy has been stored there in the previous period.

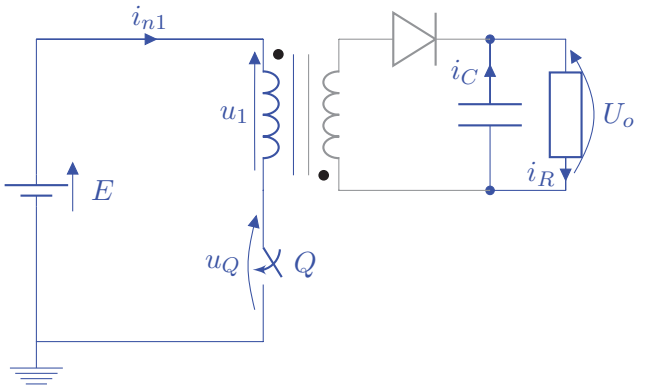

Fig. 4.2: Flyback converter – switch Q turned on

In the next cycle, the power switch Q is turned off (Fig. 4.3), the primary side current stops to flow. The magnetic flux in the transformer core decreases and the secondary voltage u_{n2} changes polarization causing the diode is forward biased. As the current i_{n2} flows, the energy stored in the transformer core in the first cycle is transferred to the load.

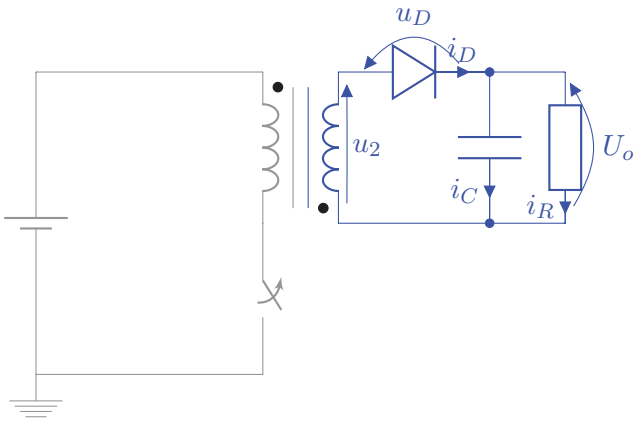

Fig. 4.3: Flyback converter – switch Q turned off

Mode of operation of the converter depends on the transformer flux – while it is always greater than zero – the converter operates in the continuous mode, otherwise the converter operates in the discontinuous mode. In discontinuous mode, the third cycle occurs when the energy in the transformer core reaches zero before the beginning of the next period. The load is fed from output capacitor as it is shown in Fig. 4.4

4.1.1 Continuous current mode

The typical current and voltage waveforms for flyback converter operation in continuous mode are presented in Fig. 4.5. Assuming that the output capacitor C has a sufficiently high capacity, the output voltage u_O is constant during the whole period:

$$u_O(t) = U_{O(\mathrm{AV})}. \tag{4.2}$$

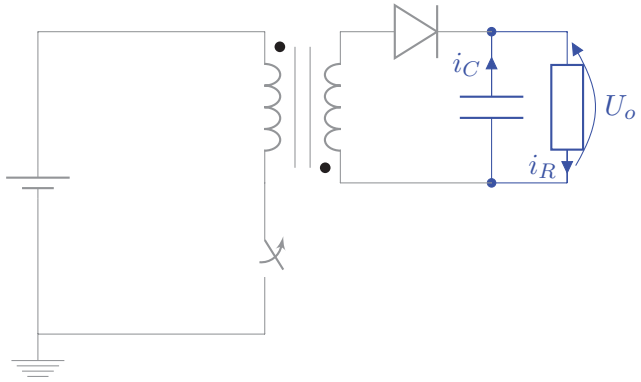

Fig. 4.4: Flyback converter – load is fed from capacitor

In time interval $t \in (0, t_1)$, when the switch Q is turned on, the voltage drop across the transformer primary winding $u_{n1} = E$ is constant. The flux φ in transformer core increases according to the relation:

$$u_1(t) = n_1 \frac{\mathrm{d}\varphi}{\mathrm{d}t} \Leftrightarrow \mathrm{d}\varphi = \frac{u_1}{n_1}\mathrm{d}t \tag{4.3}$$

by integrating both sides:

$$\varphi(t) = \int \frac{u_1}{n_1}\mathrm{d}t\,. \tag{4.4}$$

Because $u_1 = E = const$, hence the flux derivative $\mathrm{d}\varphi/\mathrm{d}t$ is also constant, what means that the flux increase is linear.

$$\varphi(t) = \frac{E}{n_1}\ t + \varphi_{(\min)}, \tag{4.5}$$

where: $\varphi_{(\min)}$ is the minimal flux value at time $t = 0$. For the continuous mode, the flux $\varphi_{(\min)}$ is always greater than zero in the whole period. The secondary side voltage u_{n2} is described by formula:

$$u_2(t) = -n_2 \frac{\mathrm{d}\varphi}{\mathrm{d}t} = -\frac{n_2}{n_1}\,E. \tag{4.6}$$

The magnetic flux φ – in the associated interval – is related to the flow of primary winding current, described by the relation:

$$i_{n1}(t) = \int \frac{u_1}{L_1}\mathrm{d}t = \frac{E}{L_1}t + I_{n1(\min)}\,. \tag{4.7}$$

In the time instant t_1 the i_{n1} current reaches the maximum value, determining the end of the cycle t_{ON}:

$$i_{n1}(t_1) = I_{n1(\max)} = \frac{E \cdot t_1}{L_1} + I_{n1(\min)} = \frac{E \cdot \gamma \cdot T}{L_1} + I_{n1(\min)} \,. \tag{4.8}$$

where: $\gamma = t_{ON}/T$ - duty cycle, L_1 - primary transformer magnetic inductance. In time t_1, the switch Q opens, the current i_{n1} stops to flow, but due to conservation of magnetic flux in the transformer core.

$$\varphi(t_1) = \varphi_{(\max)} \Longleftrightarrow n_1 \cdot I_{n1(\max)} = n_2 \cdot I_{n2(\max)} \,. \tag{4.9}$$

the current i_{n2} equals the maximum value:

$$I_{n2(\max)} = \frac{n_1}{n_2} \cdot I_{n1(\max)} \,. \tag{4.10}$$

During the sub cycle $t_{OFF} \in (t_1, T)$, the switch remains turned off and the relation between flux and voltage u_2 is described by:

$$u_2(t) \; = \; -n_2 \frac{\mathrm{d}\varphi}{dt} \Leftrightarrow \varphi(t) = -\int \frac{u_2}{n_2} dt \,. \tag{4.11}$$

Because the flux derivative $\mathrm{d}\varphi/\mathrm{d}t$ is constant, it decreases linearly:

$$\varphi(t) = -\frac{U_{O(\mathrm{AV})}}{n_2} \; (t - t_1) + \varphi_{(\max)}. \tag{4.12}$$

Using Eq. (4.11), the primary transformer side voltage u_2 can be obtained:

$$u_1(t) \; = \; n_1 \frac{\mathrm{d}\varphi}{\mathrm{d}t} = -\frac{n_1}{n_2} U_{O(\mathrm{AV})}. \tag{4.13}$$

The voltage across switch terminals u_Q is equal to the difference between input voltage E and u_1.

$$u_K \; = E \; - \; u_1 = E \; + \frac{n_1}{n_2} U_{O(\mathrm{AV})}. \tag{4.14}$$

The diode current i_{n2} is linked with magnetic flux and it is equal:

$$i_{n2}(t) = \int \frac{u_2}{L_2} \mathrm{d}t = \; - \; \frac{U_{O(\mathrm{AV})}}{L_2} (t - t_1) + I_{n2(\max)} \,. \tag{4.15}$$

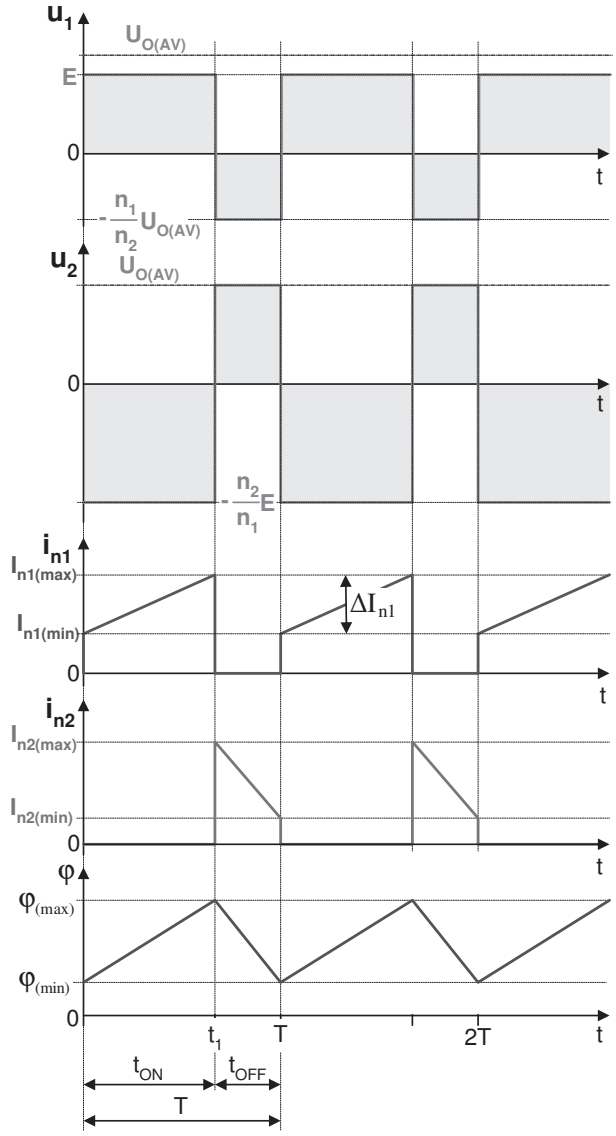

Fig. 4.5: Current and voltage waveforms of flyback converter operation in continuous mode

The i_{n2} reaches the minimal value at the end of t_{OFF}, at time T.

$$I_{n2(\min)} = I_{n2(\max)} - \frac{U_{O(\mathrm{AV})} \cdot (T - t_1)}{L_2} =$$

$$I_{n2(\max)} - \frac{U_{O(\mathrm{AV})} \cdot t_{OFF}}{L_2} = I_{n2(\max)} - \frac{U_{O(\mathrm{AV})} \cdot (1-\gamma)\, T}{L_2}, \tag{4.16}$$

where : L_2 is magnetic inductance of secondary side winding. In the steady state, the minimal flux value $\varphi_{(\min)}$ at time T at the end of operation period is equal to the flux value at the beginning of operation period at time $t = 0$.

$$\varphi(T) = \varphi_{(\min)} = -\frac{U_{O(\mathrm{AV})}(T - t_1)}{n_2} + \varphi_{(\max)} = -\frac{U_{O(\mathrm{AV})} \cdot t_{OFF}}{n_2} + \varphi_{(\max)}, \tag{4.17}$$

hence the flux value at the time instant t_1:

$$\varphi(t_1) = \varphi_{(\max)} = \varphi_{(\min)} + \frac{U_{O(\mathrm{AV})} \cdot t_{OFF}}{n_2}. \tag{4.18}$$

The flux value at time t_1 can also be calculated using Eq. (4.5):

$$\varphi(t_1) = \varphi_{(\max)} = \frac{E}{n_1}\ t_1 + \varphi_{(\min)} = \frac{E}{n_1}\ t_{ON} + \varphi_{(\min)}\,. \tag{4.19}$$

The input-output voltage gain can be obtained using Eqs. (4.18) and (4.19) comparing the flux at time t_1:

$$\varphi(t_1) = \frac{E}{n_1}\ t_{ON} + \varphi_{(\min)} = \varphi_{(\min)} + \frac{U_{O(\mathrm{AV})} \cdot t_{OFF}}{n_2} \tag{4.20}$$

$$\frac{U_{O(\mathrm{AV})}}{E} = \frac{n_2}{n_1}\frac{t_{ON}}{t_{OFF}} = \frac{n_2}{n_1}\frac{t_{ON}}{T - t_{ON}} = \frac{n_2}{n_1}\frac{\gamma}{1-\gamma}. \tag{4.21}$$

It can be noticed that the flyback converter can be used both as the step-down and step-up converter. The voltage gain depends only on the duty cycle and transformer turns ratio. The average value of the output current equals:

$$I_{O(\mathrm{AV})} = \frac{U_{O(\mathrm{AV})}}{R_O} \tag{4.22}$$

Assuming that converter is lossless, the power supplied P_I is equal to the output power P_O:

$$P_I = P_O \quad \Longleftrightarrow E \cdot I_{n1(\mathrm{AV})} = U_{O(\mathrm{AV})} \cdot I_{O(\mathrm{AV})} \tag{4.23}$$

Hence, the current ratio is equal:

$$\frac{I_{O(\mathrm{AV})}}{I_{n1(\mathrm{AV})}} = \frac{E}{U_{O(\mathrm{AV})}} = \frac{n_1}{n_2}\frac{1-\gamma}{\gamma}. \tag{4.24}$$

The average value of the primary transformer side $I_{n1(\mathrm{AV})}$ can be determined by:

$$\begin{aligned} I_{n1(\mathrm{AV})} = \frac{1}{T}\int_0^T i_{n1}(t)\mathrm{d}t = \frac{1}{T}\int_0^{t_{ON}} (\frac{E}{L_1}t + I_{n1(\mathrm{min})})\mathrm{d}t = \\ = \frac{1}{T}\left(\frac{E}{2L_1}\cdot t_{ON}^2 + I_{n1(\mathrm{min})}\cdot t_{ON}\right) = \\ = \gamma\left(\frac{E\cdot t_{ON}}{2L_1} + I_{n1(\mathrm{min})}\right) = \gamma\left(\frac{E\cdot\gamma\cdot T}{2L_1} + I_{n1(\mathrm{min})}\right) \end{aligned} \tag{4.25}$$

Rearranging Eqs. (4.24) and (4.25) allows to obtain the minimum value of the primary current $I_{n1(\mathrm{min})}$:

$$I_{n1(\mathrm{min})} = \frac{I_{n1(\mathrm{AV})}}{\gamma} - \frac{E\cdot\gamma\cdot T}{2L_1} = \frac{n_2}{n_1}\frac{I_{O(\mathrm{AV})}}{1-\gamma} - \frac{E\cdot\gamma\cdot T}{2L_1} \tag{4.26}$$

The increase of the primary side current ΔI_{n1} at time t_{ON} is equal to:

$$\Delta I_{n1} = \frac{E\cdot t_1}{L_1} = \frac{E\cdot t_{ON}}{L_1} = \frac{E\cdot\gamma\cdot T}{L_1}, \tag{4.27}$$

hence the maximum value of $I_{n1(\mathrm{max})}$:

$$I_{n1(\mathrm{max})} = I_{n1(\mathrm{min})} + \Delta I_{n1} = \frac{n_2}{n_1}\frac{I_{O(\mathrm{AV})}}{1-\gamma} + \frac{E\cdot\gamma\cdot T}{2L_1}. \tag{4.28}$$

Solving Eq. (4.10), the maximum value of secondary side current $I_{n2(\mathrm{max})}$ equals:

$$I_{n2(\mathrm{max})} = \frac{n_1}{n_2}\cdot I_{n1(\mathrm{max})} = \frac{I_{O(\mathrm{AV})}}{1-\gamma} + \frac{n_1}{n_2}\frac{E\cdot\gamma\cdot T}{2L_1}. \tag{4.29}$$

The minimal value of secondary side current $I_{n2(\min)}$ is equal:

$$I_{n2(\min)} = \frac{n_1}{n_2} \cdot I_{n1(\min)} = \frac{I_{O(\mathrm{AV})}}{1-\gamma} - \frac{n_1}{n_2} \cdot \frac{E \cdot \gamma \cdot T}{2L_1}. \tag{4.30}$$

4.1.2 Boundary current conduction mode

The increase of the load resistance R_O – with unchanged the other parameters of converter – leads to a reduction in the minimum current values i_{n1} and i_{n2} and therefore the minimum value of transformer flux $\varphi_{(\min)}$. For a certain value of the load resistance $R_O = R_{Ogr}$, the minimum transformer current and flux values reach zero only at the beginning (end) of period (Fig. 4.6). In that situation, the converter operates in the border of continuous and discontinuous flux. In the sub cycle $t \in (0, t_1)$, the current i_{n1} is determined by Eq. (4.31) with zero initial condition ($I_{n1(\min)} = 0$):

$$i_{n1}(t) = \int \frac{u_1}{L_1} dt = \frac{E}{L_1} t \tag{4.31}$$

The $I_{N1(\mathrm{AV})}$ average value can be obtained transforming the Eq. (4.26):

$$I_{n1(\mathrm{AV})} = \frac{E \cdot \gamma^2 \cdot T}{2L_1} \tag{4.32}$$

The maximum value $I_{n1(\max)}$ is determined from Eq. (4.31):

$$I_{n1(\max)} = \Delta I_{n1} = \frac{E \cdot t_1}{L_1} = \frac{E \cdot t_{ON}}{L_1} = \frac{E \cdot \gamma \cdot T}{L_1} \tag{4.33}$$

The magnetic flux increases linearly from zero to $\varphi_{(\max)}$ as follows:

$$\varphi(t) = \int \frac{u_1}{n_1} dt = \frac{E}{n_1} \; t \tag{4.34}$$

In the result of the flux continuity, the secondary side current – at time t_1, when switch Q turns off – reaches the maximum value $I_{n2(\max)}$ as it is described in Eq. (4.10). After t_1, the flux decreases linearly (Eq. (4.12)). In time $t = 0$ and $t = T$, the flux is equal to zero:

$$\varphi(0) = \varphi(T) = -\frac{U_{O(\mathrm{AV})}(T - t_1)}{n_2} + \varphi_{(\max)} = -\frac{U_{O(\mathrm{AV})} \cdot t_{OFF}}{n_2} + \varphi_{(\max)} = 0, \tag{4.35}$$

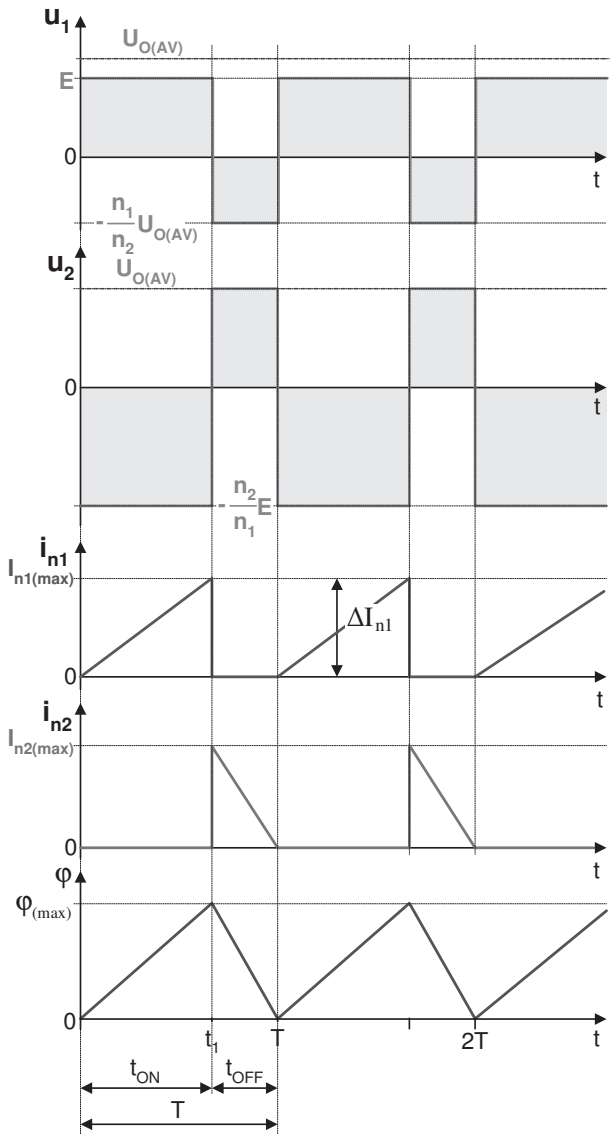

Fig. 4.6: Flyback converter waveforms – operation in boundary conduction mode

hence, the maximum flux value equals:

$$\varphi_{(\max)} = \frac{U_{O(\mathrm{AV})} \cdot t_{OFF}}{n_2} \ . \tag{4.36}$$

since from Eq. (4.34):

$$\varphi_{(\max)} = \frac{E}{n_1} \ t_{ON}. \tag{4.37}$$

The input-output voltage gain can be calculated comparing Eqs. (4.36) and (4.37):

$$\frac{U_{O(\mathrm{AV})}}{E} = \frac{n_2}{n_1} \frac{t_{ON}}{t_{OFF}} = \frac{n_2}{n_1} \frac{t_{ON}}{T - t_{ON}} = \frac{n_2}{n_1} \frac{\gamma}{1-\gamma}. \tag{4.38}$$

It can be notice that the input-output voltage ratio for continuous and boundary conduction modes is the same as it depends only on the transformer ratio n_2/n_1 and duty cycle γ. However, it is independent of the load. Similarly, the formula for current ratio remains unchanged (4.25). The average value of the primary side current for converter operating in boundary conduction mode is equal to:

$$\begin{aligned} I_{n1gr(\mathrm{AV})} &= \frac{1}{T} \int_0^T i_{n1}(t)\mathrm{d}t = \frac{1}{T} \int_0^{t_{ON}} \frac{E}{L_1} t \, \mathrm{d}t = \frac{1}{T} \left(\frac{E}{2L_1} \cdot t_{ON}^2 \right) \\ &= \gamma \left(\frac{E \cdot t_{ON}}{2L_1} \right) = \frac{E \cdot \gamma^2 \cdot T}{2L_1}. \end{aligned} \tag{4.39}$$

and the average value of the load current is described by:

$$I_{Ogr(\mathrm{AV})} = \frac{n_1}{n_2} (1-\gamma) \frac{E \cdot \gamma \cdot T}{2L_1} \tag{4.40}$$

Transforming the relationship Eqs. (4.38) and (4.40) obtains:

$$I_{Ogr(\mathrm{AV})} = \left[\frac{n_1}{n_2} (1-\gamma) \right]^2 \frac{U_{O(\mathrm{AV})} \cdot T}{2L_1 \cdot \gamma} \tag{4.41}$$

The average value of the load current $I_{Ogr(\mathrm{AV})}$ reaches maximum for duty cycle $\gamma = 1/3$ (Fig. 4.7):

$$I_{Ogr(\mathrm{AV})(\max)} = I_{Ogr(\mathrm{AV})}(\gamma = \frac{1}{3}) = \frac{4}{3} \left(\frac{n_1}{n_2} \right)^2 \frac{U_{O(\mathrm{AV})} \cdot T}{L_1} \tag{4.42}$$

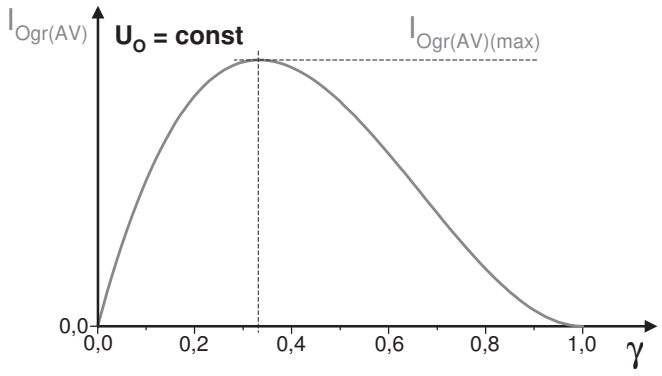

Fig. 4.7: Characteristics $I_{Ogr(\mathrm{AV})} = f(\gamma)$

From Eq. (4.40), the value of boundary resistance can be calculated:

$$R_{Ogr} = \frac{U_{O(\mathrm{AV})}}{I_{O(\mathrm{AV})gr}} = \frac{2L_1}{T} \frac{1}{\left[\frac{n_1}{n_2}(1-\gamma)\right]^2}\,. \tag{4.43}$$

The operation of the flyback converter in boundary conduction mode – in the author's opinion – is the most efficient, easy to control with minimal electromagnetic interference compared with the other two modes. There are many integrated circuits dedicated for this operation mode. It can be noticed – based on Eq. (4.43) – that the boundary resistance value, at which the converter operates in boundary conduction mode, depends on the operation period T (or frequency f), the duty cycle γ, inductance L and the transformer turns ratio ϑ. In Fig. 4.8 the characteristics $R_{Ogr} = f(\gamma)$ is presented for constant values of T, L and ϑ.

4.1.3 Discontinuous current mode

Depending on the operation condition, if the magnetic flux in the transformer is periodically equal to zero in the interval $t \in (t_2, T)$, the converter works in discontinuous mode. It means that in some phase of the cycle no current flows through the windings and the load is fed from the capacitor, where energy was stored in the electrical field during the previous cycle. The discontinuous mode can be obtained eg. by increasing the values of load resistance above the

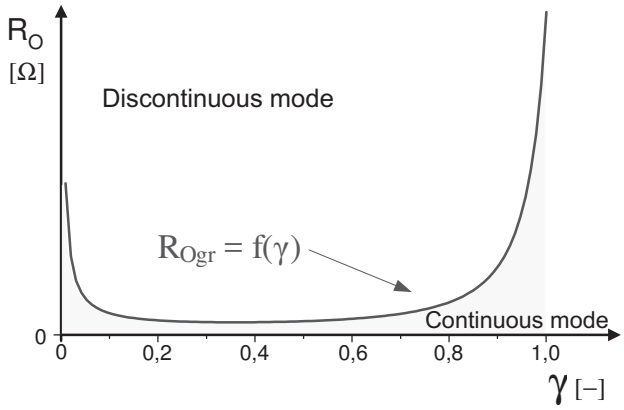

Fig. 4.8: The dependence of the load boundary resistance of the duty cycle γ

boundary resistance (Eq. (4.43)). In the first subcycle $t \in (0, t_1)$ – similarly as it is in continuous and boundary modes – the primary winding current increase linearly from the zero initial condition:

$$i_{n1}(t) = \int \frac{u_1}{L_1} \mathrm{d}t = \frac{E}{L_1} t. \tag{4.44}$$

The primary winding current reaches the maximum value at time t_1, when the switch Q is turned off.

$$i_{n1}(t_1) = I_{n1(\max)} = \frac{E}{L_1} t_1 = \frac{E}{L_1} t_{ON} = \frac{E \cdot \gamma \cdot T}{L_1}. \tag{4.45}$$

The maximum value of the current in the secondary winding $I_{n2(\max)}$ is equal to the current $I_{n1(\max)}$ multiplied by the value of transformer turns ratio:

$$I_{n2(\max)} = \frac{n_1}{n_2} \cdot I_{n1(\max)} = \frac{n_1}{n_2} \frac{E \cdot \gamma \cdot T}{L_1}. \tag{4.46}$$

In the time instant t_1, energy stored in the transformer magnetic field reaches the maximum value:

$$W_{(\max)} = \frac{L_1 \, I_{n1(\max)}^2}{2} = \frac{L_2 \, I_{n2(\max)}^2}{2}. \tag{4.47}$$

Assuming the switch Q is ideal (voltage drop is equal to zero), the primary

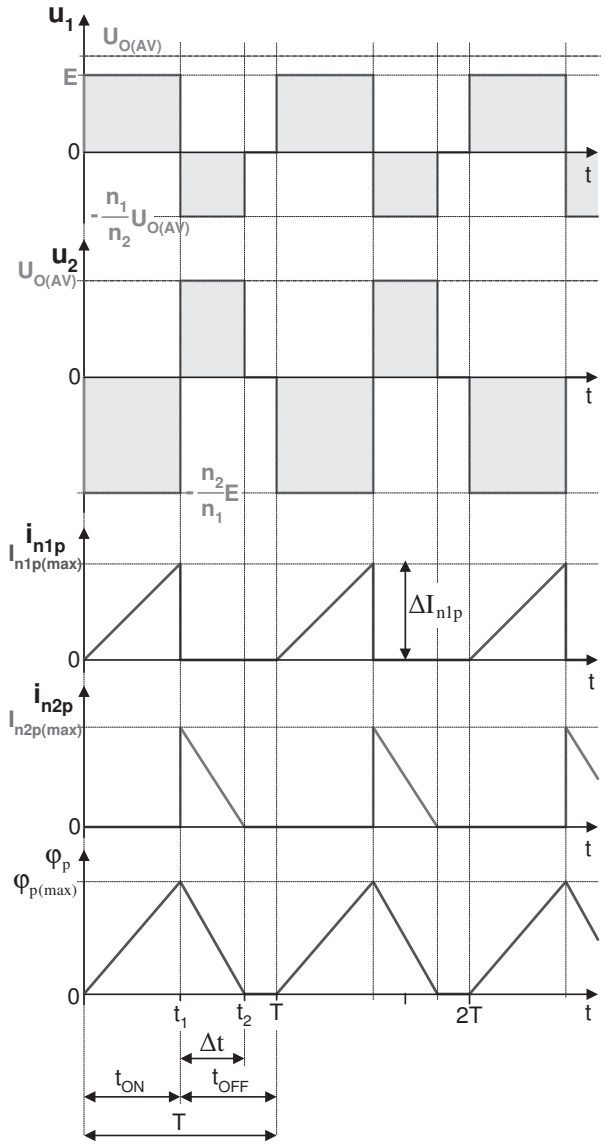

Fig. 4.9: Current and voltage waveforms of flyback converter operation in discontinuous mode

side voltage equals the input voltage $u_1 = E$, taking into account winding inverting, the value of the secondary side voltage $u_2(t_{OFF})$ is equal to:

$$u_2 = -\frac{n_2}{n_1} \cdot u_1 = -\frac{n_2}{n_1} \cdot E. \tag{4.48}$$

In the sub-period $t_{OFF} \in (t_1, T)$ the switch remains open, because the primary current stops to flow when switch turns off. The magnetic flux induced in the core at sub-period $t \in (t_1, t_2)$ causes the secondary side current flow i_{n2}, which decreases linearly and reaches zero at time t_2. Neglecting the voltage drop on the conductive diode, voltage $u_2 = U_{O(\mathrm{AV})} = const$, consequently:

$$u_2 = U_{O(\mathrm{AV})} = -L_2 \frac{\mathrm{d}i_{n2}}{\mathrm{d}t}. \tag{4.49}$$

The secondary current i_{n2} reaches the maximum value $I_{n2(\max)}$ at time t_2, so it can be described by:

$$\begin{aligned} i_{n2}(t) = -\int \frac{U_{O(\mathrm{AV})}}{L_2}\,\mathrm{d}t = -\frac{U_{O(\mathrm{AV})}}{L_2}(t - t_1) + I_{n2(\max)p} = \\ = -\frac{U_{O(\mathrm{AV})}}{L_2}(t - t_{ON}) + I_{n2(\max)p} = -\frac{U_{O(\mathrm{AV})}}{L_2}(t - \gamma T) + I_{n2(\max)p}\,. \end{aligned} \tag{4.50}$$

In time t_2 the secondary current drops to zero:

$$i_{n2}(t_2) = 0 = -\frac{U_{O(\mathrm{AV})}}{L_2}(t_2 - t_1) + I_{n2(\max)p} = -\frac{U_{O(\mathrm{AV})}}{L_2}\Delta t + I_{n2(\max)p}, \tag{4.51}$$

where Δt is time interval from t_1 to t_2.
Transforming Eq. (4.51), the interval Δt is calculated:

$$\Delta t = \frac{L_2 \cdot I_{n2(\max)p}}{U_{O(\mathrm{AV})}}. \tag{4.52}$$

Then substituting (Eq. (4.46)) into (Eq. (4.52)), we obtain:

$$\Delta t = \frac{L_2 \cdot I_{n2(\max)p}}{U_{O(\mathrm{AV})}} = \frac{n_1}{n_2}\,\frac{L_2}{L_1}\,\frac{E \cdot \gamma \cdot T}{U_{O(\mathrm{AV})}}. \tag{4.53}$$

It is known from the ideal transformer theory that the magnetizing inductance ratio L_2/L_1 determines the value of stored energy at a time t_1 (Eq. (4.47)) or (Eq. (4.9))

$$\frac{L_2}{L_1} = \left(\frac{I_{n1(\max)p}}{I_{n2(\max)p}}\right)^2 = \left(\frac{n_2}{n_1}\right)^2. \tag{4.54}$$

Substituting (Eq. (4.54)) into (Eq. (4.53)), the length interval Δt ultimately is:

$$\Delta t = \frac{L_2 \cdot I_{n2(\max)p}}{U_{O(\mathrm{AV})}} = \frac{n_2}{n_1} \frac{E \cdot \gamma \cdot T}{U_{O(\mathrm{AV})}}. \tag{4.55}$$

Hence the total converter voltage ratio is equal to:

$$\frac{U_{O(\mathrm{AV})}}{E} = \frac{n_2}{n_1} \frac{\gamma \cdot T}{\Delta t}. \tag{4.56}$$

Assuming the ideal converter is lossless (the input power P_i is equal to output power P_o), the current ratio for the flyback converter operating in discontinuous mode is equal to :

$$\begin{aligned} E \ \cdot I_{n1(\mathrm{AV})} &= U_{O(\mathrm{AV})} \cdot I_{Op(\mathrm{AV})} \\ \frac{I_{Op(\mathrm{AV})}}{I_{n1(\mathrm{AV})}} &= \frac{E}{U_{O(\mathrm{AV})}} = \frac{n_1}{n_2} \frac{\Delta t}{\gamma \cdot T}. \end{aligned} \tag{4.57}$$

The input current average value $I_{n1(\mathrm{AV})}$ is described by:

$$\begin{aligned} I_{n1(\mathrm{AV})} = \frac{1}{T} \int_0^T i_{n1}(t)\mathrm{d}t = \frac{1}{T} \int_0^{t_{ON}} \frac{E}{L_1} t \,\mathrm{d}t = \frac{1}{T} \left(\frac{E}{2L_1} \cdot t_{ON}^2 \right) = \\ = \gamma \left(\frac{E \cdot t_{ON}}{2L_1} \right) = \gamma \left(\frac{E \cdot \gamma \cdot T}{2L_1} \right). \end{aligned} \tag{4.58}$$

Substituting (4.58) into (4.57), the output current average value in discontinuous mode can be obtained:

$$I_{Op(\mathrm{AV})} = \frac{n_1}{n_2} \frac{\Delta t}{\gamma \cdot T} I_{n1(\mathrm{AV})} = \frac{n_1}{n_2} \frac{\Delta t}{\gamma \cdot T} \left(\frac{E \cdot \gamma^2 \cdot T}{2L_1} \right) \tag{4.59}$$

4.2 EMI propagation paths

The EMI generation in the flyback converter is directly connected with the periodical commutation of the switch Q (transistor). The fast increase and fall of voltage and current causes the oscillations in sub-circuits composed

of basic and parasitic elements [33, 34, 35, 36]. In the flyback converter the most important components – from the EMC point of view – are transistor, diode and transformer. Also parasitics – including wires, conduction tracks– are significant in perturbation propagation. The crucial parameters – presented in blue in Fig. 4.10 – are related to the transformer and semiconductors:

- transistor internal capacitance (see Section 2.1.2)
- magnetizing inductance L_{1m}, primary and secondary leakage inductance L_σ, primary C_{w1} and secondary C_{w2} windings capacitance, winding-to-winding capacitance C_{12}, C_{21} [11]
- parasitic capacitance C_{hs} between the transistor and heat sink, connected to the primary ground potential
- parasitic capacitances C_{n2+} and C_{n2-} between the PCB track on the secondary side and ground
- diode internal capacitance C_j [37]

It should be noticed, that the EMI generation mechanism description requires an accurate models of semiconductor devices, transformer and parasitic capacitances [38]. The methods of its parameters extraction is shown in Chapter 2.

In Fig. 4.11 the main coupling path – both common (green line) (brown line) and differential mode (magenta line) – are presented [39]. In the case when the flyback convert is fed from the diode rectifier the modes can change from differential to common and vice versa. In the next section influence of chosen components on the interference level and path is discussed.
The presented analysis has been done based on measurements in the few prototypes and simulation models. In the laboratory prototype investigation, voltages, some currents and interference can be measured. The influence of the components on EMI generation and propagation can be mainly investigated by simulation, thus the wideband simulation model of the converter was built including the complex model of major components and parasitics. The damping and attenuation elements like snubber or clamp were not included, in order to make the phenomena more visible. In Figs. 4.12 and 4.13 the spectra of transistor, diode and 50Ω LISN resistor are presented for continuous and

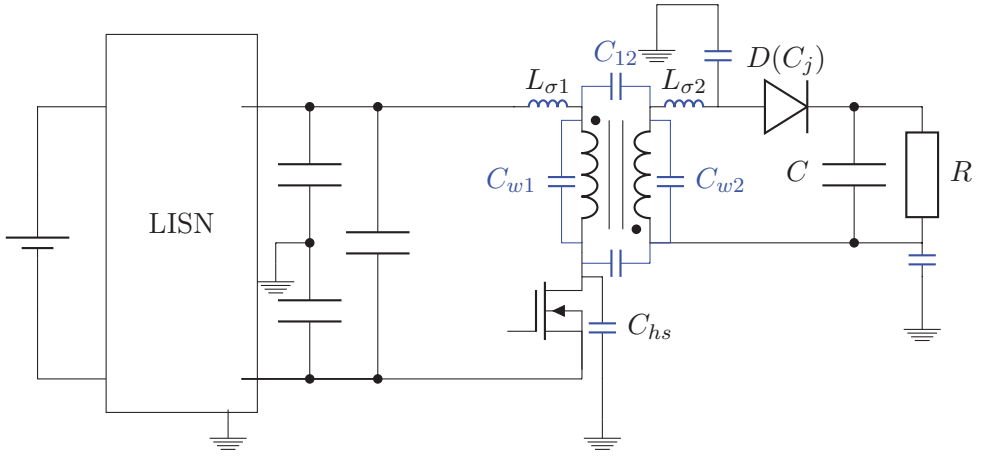

Fig. 4.10: Flyback converter - equivalent circuit with parasitic

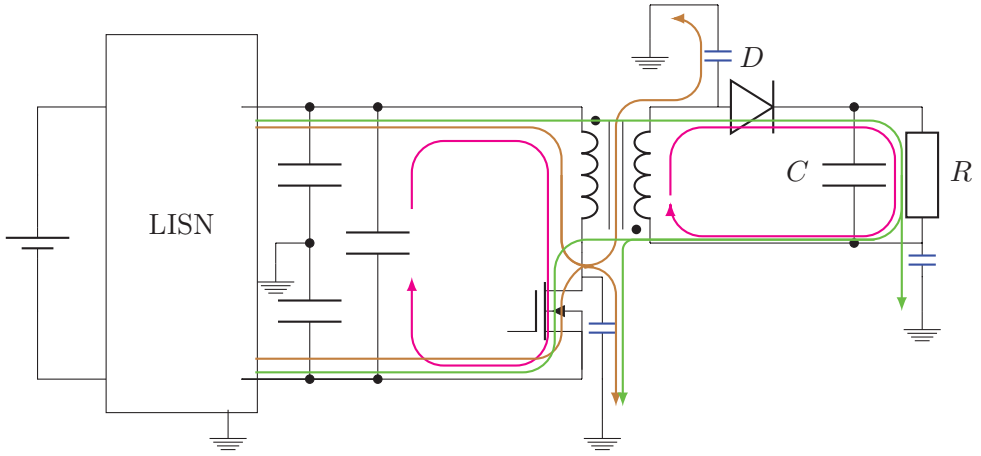

Fig. 4.11: Main propagation paths in flyback converter

discontinuous modes. The shape of both spectra are similar, there is only the difference caused by the oscillation in discontinuous mode during transistor turning off (visible in Fig. 4.13 for 1.8 MHz).

In the spectra the distinctive peaks appear:

- the basic harmonics (here for 37 kHZ)
- the sub-harmonics (in the range 80 - 400 kHz)
- oscillation in discontinuous mode during transistor turn off (for 1.8 MHz) (Eq. (4.61))
- ringing oscillation during transistor turn on (for 18.3 MHz)
- ringing oscillation during diode turn on (for 22.1 MHz) (Eq. (4.62))
- peaks link with transistor slew rate (for 21.7 MHz)

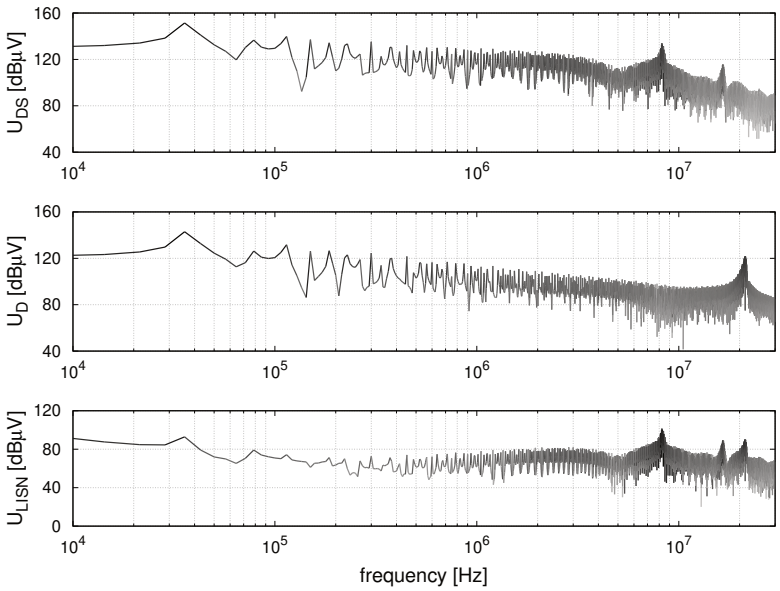

Fig. 4.12: Flyback converter voltages spectra in continuous mode

4.2.1 Transistor

The main interference source in the flyback converter is the fast switching transistor. In typical application, the MOSFET or other field effect transistors

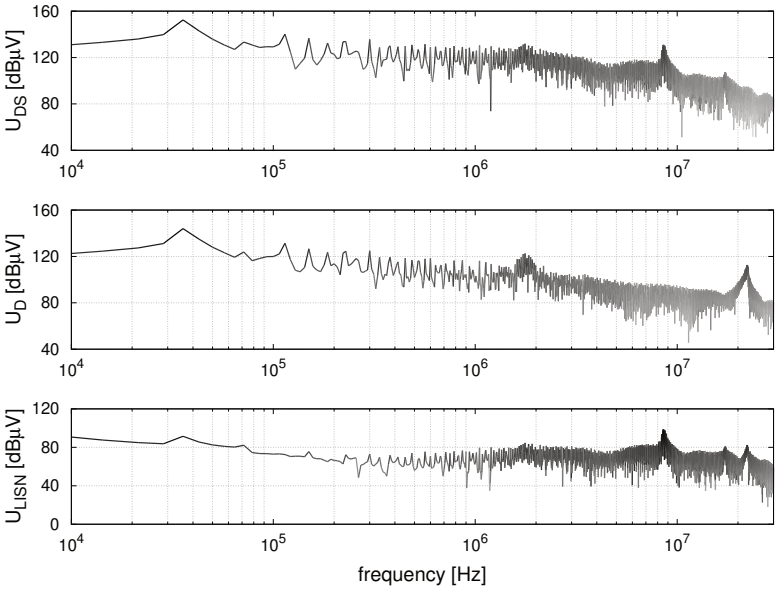

Fig. 4.13: Flyback converter voltages spectra in discontinuous mode

are used, but for high power the IGBT can be applied. During the commutation the current and the voltage change fast from operating level to near zero and vice versa. From EMI point of view, the transistor can be modeled as the two-state resistance parallel with nonlinear capacitance. The transistor internal capacitance – in the flyback converter – is the part of the resonant circuits and it is responsible for the resonant peak visible in spectra as the ringing peak after transistor turn on.

In Fig. 4.14 the spectra are presented where the internal transistor capacitance during commutation is two times greater in relation to Fig. 4.12. It can be noticed that ringing peak in the U_{ds} spectra is shifted left both in CCM and DCM. There is no influence on the others peaks. The C_{DS} capacitance dominates in interference generation but it is negligible in interference propagation. This is typical for a low power converter, where the transistor capacitance has similar value as internal capacitance of transformer C_{w1}. For middle and high power, this effect can be no visible, because the transformer capacitance is larger by several orders. The value of transistor capacitance during turning on

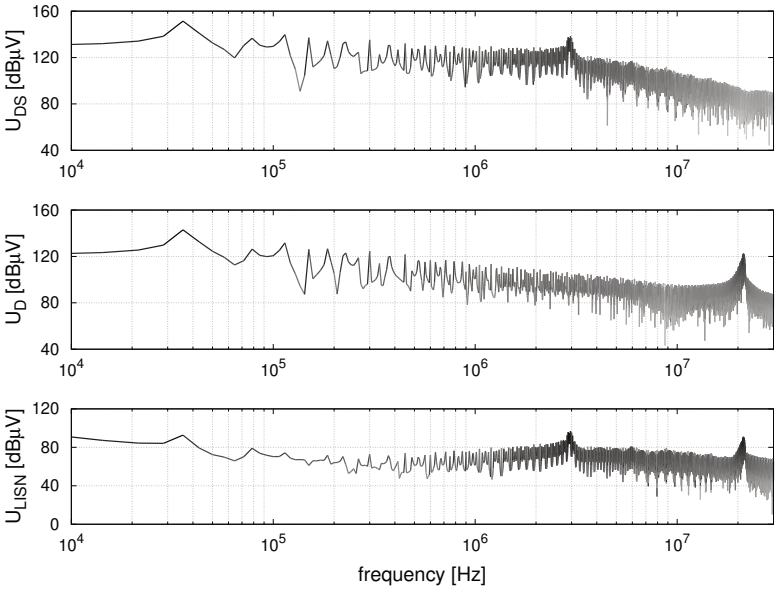

Fig. 4.14: Influence of MOSFET internal capacitance increase: $C_{DS} * 2$

$C_{DS} = C_{oss} - C_{rss}$ can be derived from the data-sheet as a function of drain – source voltage $U_{ds} = E + (U_o + U_d)\vartheta$, where E is the input voltage, Uo - output voltage and U_d - diode voltage.

The transistor is located on the PCB and typically affixed to the heat sink. The heat sink usually is grounded. This structure can be represented by the capacitance between drain node and the ground C_{pd}. This capacitance has great impact on propagation of the common mode interference [40, 41]. The drain node potential is changing fast during transistor commutation, thus the parasitic current flows to the ground and returns in both primary side main paths of the converter. In Fig. 4.15 the impact on the voltage spectra is presented, where C_{pd} has been increased 10 times. It may happen for a converter with different lengths of the PCB track, distances between the track and the ground or construction of the heat sink. The location of peaks has not changed, but the level of transistor ringing and adequate noise registered in the LISN increased.

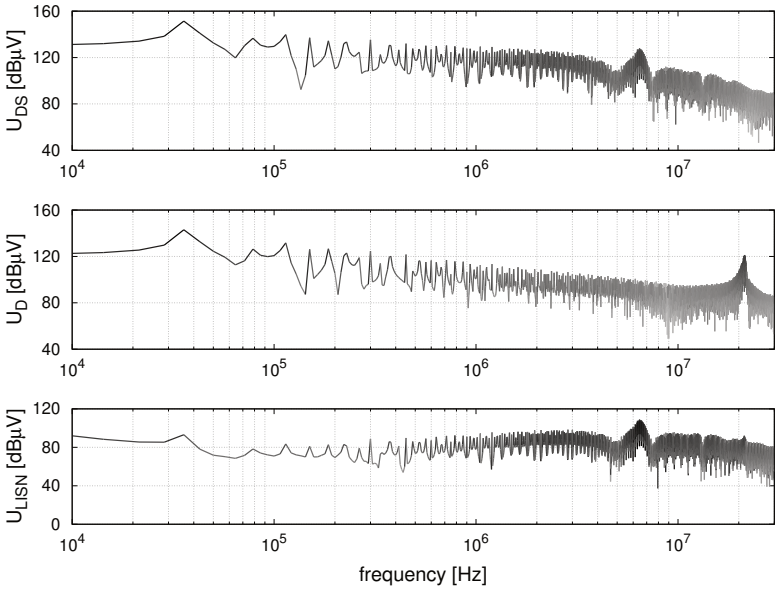

Fig. 4.15: Influence of dren - ground parasitic capacitance increase: C_{pd}*10

4.2.2 Diode

The diode located in the secondary side circuit starts to conduct current when transistor in the primary side is turned off. In the flyback converter fast diodes (eq. Schottky diode) should be used. During the commutation the voltage oscillation is generated. The frequency and amplitude of this oscillation depends on the components of resonant circuit that consists of the transformer parasitic (leakage inductance and windings capacitance) and internal diode capacitance C_d. Due to the use of a dominate role of the transformer, the wires and tracks parasitics can be neglected. For estimation of C_d the model based on the space charge layer capacitance can be used [37].

$$C_d = \frac{C_{d0}}{\left(1 + \frac{U_R}{\phi}\right)^{1/2}} \tag{4.60}$$

where:

ϕ – diffusion potential (for silicon diode $0.6 - 0.8\ V$),

U_R – reverse voltage (defined positive),

C_{d0} – capacitance at zero applied voltage (parameter from datasheet),

The internal diode capacitance C_d impacts mainly on the diode ringing frequency, which is visible in Fig. 4.16, where it is increased 10 times. The major difference is in the U_d spectra where the diode ringing peak shifts to the left from 22 to 2.6 MHz. It can be noticed that C_d does not affect on the interference level because of transformer filtering effect.

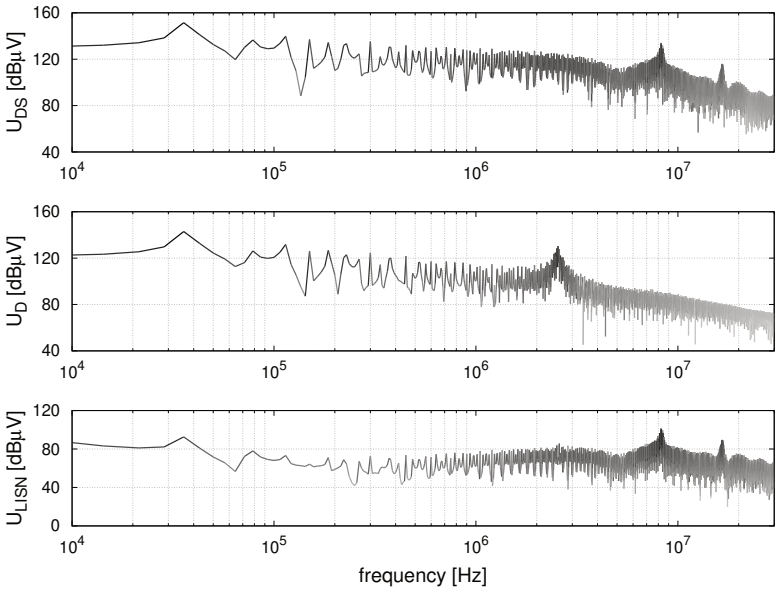

Fig. 4.16: Influence of internal diode capacitance increase: C_d*10

The parasitic capacitance C_{pc} between diode cathode node and the ground has minor but not negligible impact on the DM interference propagation. It consists a part of the propagation path of DM perturbation generated both for transistor and diode turning off. In Fig. 4.17 the value of C_{pc} is increased ten times as compared to Fig. 4.12. It can be noticed that the level of diode ringing peak registered in the LISN is increased although the level of this peak

in U_D spectra remains the same. The significance of C_{pc} depends on the PCB layout and transformer construction for specified application. Usually, for low power converters, it could be neglected. The C_{pc} does not effect on the diode ringing frequency.

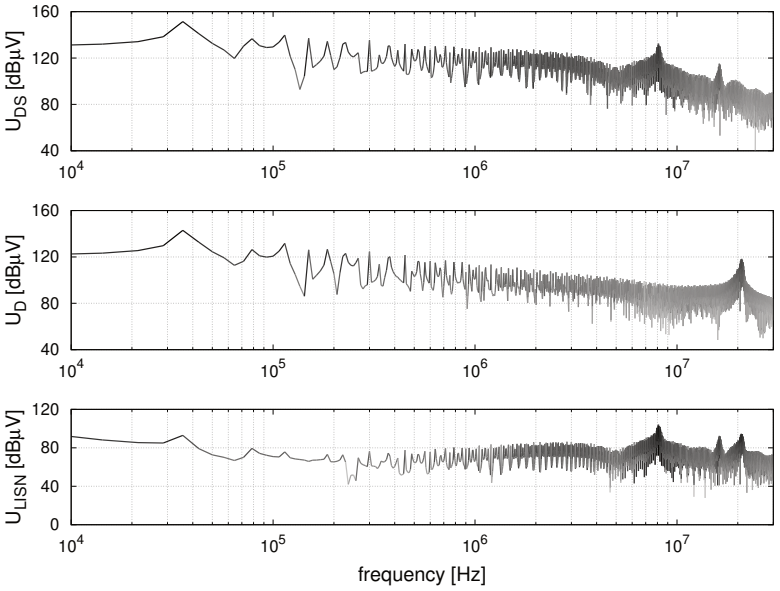

Fig. 4.17: Influence of cathode - ground parasitic capacitance increase: C_{pc}*10

4.2.3 Transformer

The air-gapped transformer (coupled inductors) in the flyback converter is used for storage and transfer of energy. As all physical devices – except the operation parameters – it has parasitic parts which impacts on interference generation and propagation. The leakage inductance L_σ derived from leakage flux results from imperfect magnetic coupling between windings. It depends on geometrical parameters of the transformer, materials and the spooling method. The L_σ has the great impact on interference generation as a part of resonant circuit during transistor and diode commutation. The interaction between L_σ, semiconductors internal capacitance and transformer capacitance is the origin

of voltage and current oscillation when semiconductors change their state [42]. In Fig. 4.18 it is shown what can happen, when L_σ increases ten times in comparison to Fig. 4.12. All characteristic ringing peaks shift to the left and their level increases. This phenomenon is visible for the whole power range of this kind of converter, but especially it could be dangerous for high power devices, where the great dimension transformer has relatively large leakage inductance.

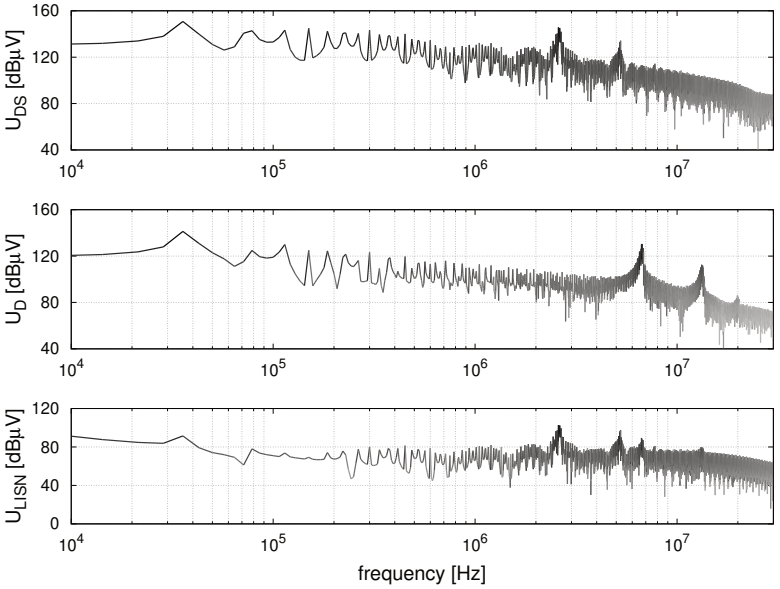

Fig. 4.18: Influence of transformer leakage inductance increase: L_σ*10

The capacitive behavior of the flyback transformer can be described using lumped capacitors representing winding capacitance and straight and cross inter-winding capacitance as it is shown in (Fig. 2.11). Additionally, the capacitance to the ground could be included. Both windings capacitance C_1 and C_2 take part in ringing oscillation together with leakage inductance L_σ [43]. The impact on the ringing frequency is not so strong as L_σ, because they are part of total capacitance in the resonant circuit including semiconductors internal capacitance and other parasitics (of course it strongly depends of the physical and geometrical properties and the nominal power of converter). In

Fig. 4.19 the characteristic spectra are shown, where winding capacitance C_1 increased tenfold. It can be noticed that the ringing peaks are shifted to the left slightly, compared to Fig. 4.18. The level of ringing peak increased insignificantly. The second peak (here for 10.4 MHz) in the U_{DS} spectra is damped as a result of the filter operation of C_1. The similar effect takes place for the second winding because of the C_2. These winding capacitance are the part of interference propagation paths, but their impact in the EMI registered in LISN is small.

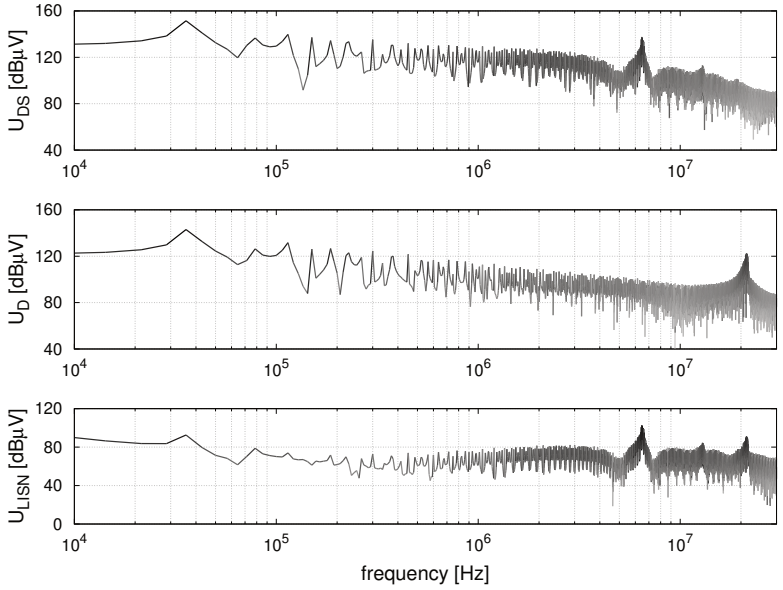

Fig. 4.19: Influence of transformer winding capacitance increase: C_1*10

The inter-winding capacitances in transformer (Fig. 2.11) have great impact on CM and DM generation and propagation. The interference current flows through these capacitances in both directions, thus they are part of all main resonant circuits. They participate in all generations of oscillations. In Fig. 4.20, example of an impact of C_{12} on voltage spectra is presented. The C_{12} value increased tenfold. The ringing frequencies moved to the left. Moreover, the dumping effect appears in the narrow range (here for 5 MHz). This phenomenon could be applied to attenuate the interference, by conscious design and choice

of transformer where the C_{12} has a significant value, for example by using the sandwich winding technique.

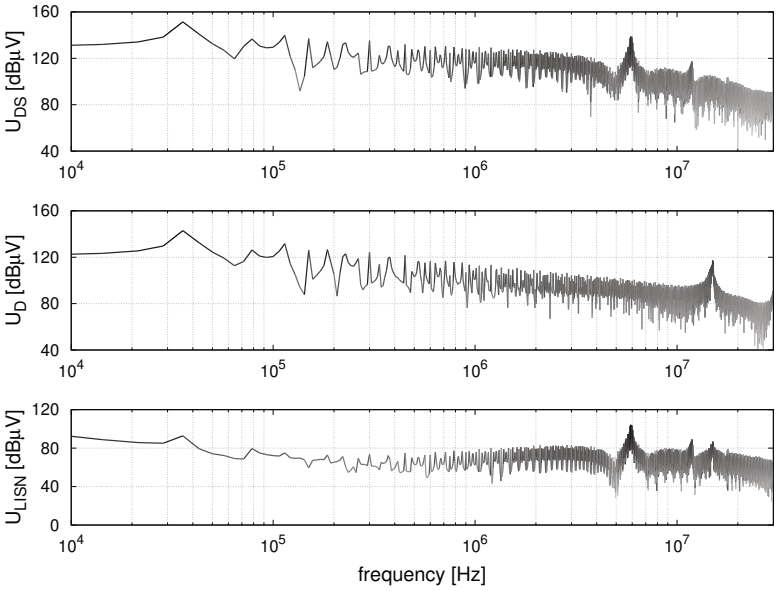

Fig. 4.20: Influence of transformer inter-winding capacitance increase: C_{12}*10

The close loop propagation path inside the converter could be created by adding the auxiliary Y-capacitor between winding [44]. The fast Y-type capacitor should be used in this application. There are few methods to connect the Y-capacitor, but in the author's opinion it depends on the geometrical structure of converter and transformer and it should be selected individually for the specific application.
In figure Fig. 4.21 the example of C_y location is presented, where the additionally capacitor connects the second winding beginning and the MOSFET source node. In this case C_y impacts on the level of diode ringing interference registered in $LISN$. In Fig. 4.22 the spectra of U_{LISN} in function of the $C_y \in (1pF \div 1\mu F)$ are depicted. It is visible that the diode ringing peak strongly decreases where C_y became greater than sum of transformer inter-winding capacitances $\sum C_{tr}$. Moreover, the slight decreasing of interference linked with transistor commutation is visible for $C_y = \sum C_{tr}$. In conclusion,

in order to find optimal value of C_y the knowledge about the internal transformer capacitance is necessary. It allows to create the additionally closed path for interference inside the converter.

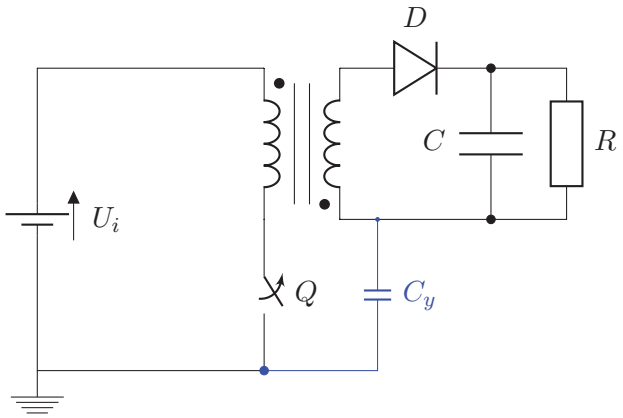

Fig. 4.21: Example of C_y placement

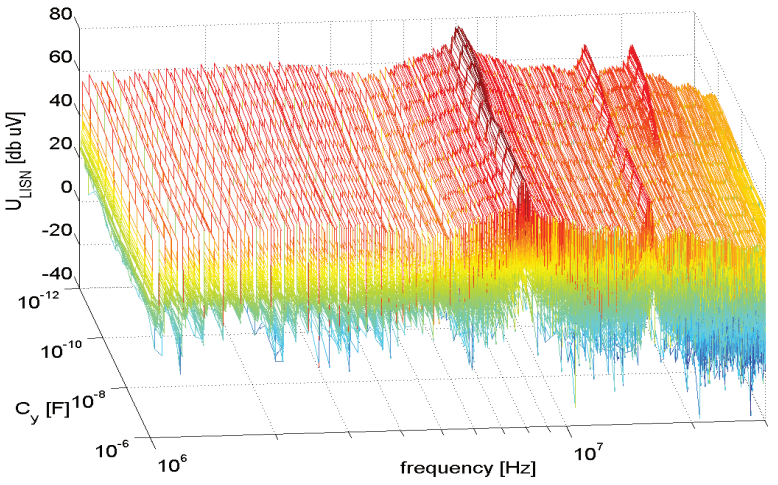

Fig. 4.22: Influence on U_{LISN} of C_y located as in Fig. 4.21

4.2.4 Simplified model for ringing frequency identification

One of the most effective method of EMI reduction is application of snubbers. It can be noticed that the design procedure requires precise evaluation of the ringing frequency generated during semiconductor switches commutation and the value of the transformer leakage inductance. The most popular and practical way is to measure these oscillations during laboratory tests – but it requires the working prototype. This knowledge in the early design stage enables less time-consuming design of the presented flyback converter. The simple model is described in details in [45] can be used for fast ringing frequency both for transistor and diode turn off. The model is defined for two state of converter and it includes:

- transformer leakage inductance L_σ
- primary winding lumped parasitic capacitance C_1
- secondary winding lumped parasitic capacitance C_2' referred to primary using the turns ratio ϑ
- parasitic capacitance C_{pd} between the MOSFET and heat sink, connected to the primary ground potential
- output filter capacitance C_{out}' referred to primary
- internal transistor capacitance C_{DS}
- internal diode capacitance C_D (Eq. (4.60))

The MOSFET turn off model is presented in Fig. 4.23 yields:

$$f_{rT} = \frac{1}{2\pi\sqrt{L_\sigma(C_{pd} + C_{DS} + C_1)}} \tag{4.61}$$

Respectively, for the diode turn-off (Fig. 4.24) ringing frequency one obtains

$$f_{Dr} = \frac{1}{2\pi\sqrt{L_\sigma(C_D' + C_2')}} \tag{4.62}$$

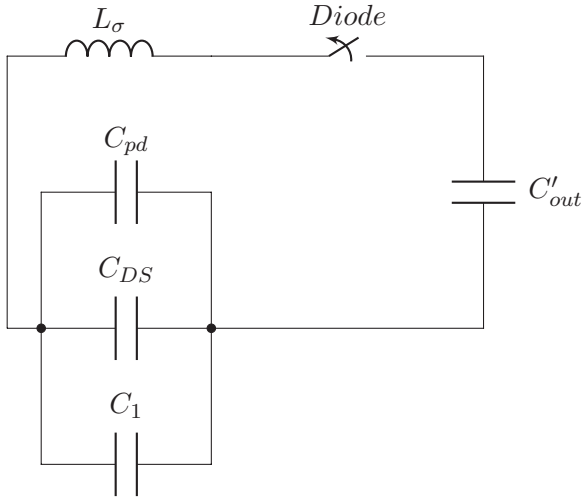

Fig. 4.23: Simplified flyback converter resonance circuit for MOSFET turn-off and diode turn-on

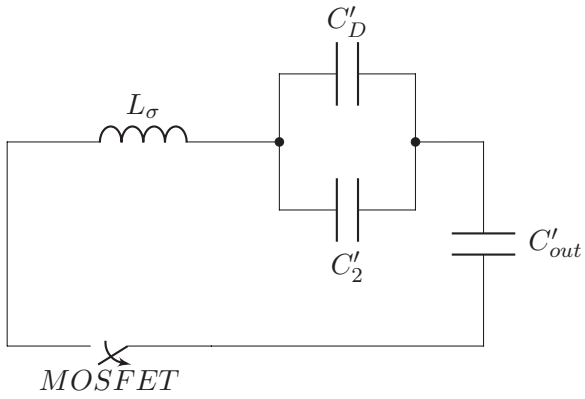

Fig. 4.24: Simplified flyback converter resonance circuit for diode turn-off and MOSFET turn-on

Chapter 5

Isolated converters

5.1 Introduction

The common feature of isolated converters is having the transformer, which is used for isolating and transferring energy between the input and the output circuit. The flyback converter is also isolated converter, but the transformer is also used to storage energy (separately describe in Chapter 4). The role of the transformer determines the mechanism of interference generation and propagation. In this chapter electromagnetic compatibility of isolated converters is described by example of the full bridge converter. From the EMC point of view, the phenomena for other isolated converters like forward, push-pull, half bridge or even LLC resonant converters has the same nature.

5.2 Full bride converter – basic operation

The full bridge converter contains the four power electronics switches (usually MOSFET or IGBT transistors $T_1 \div T_4$ connected with the reverse diodes). The converter is composed of the two legs of the inverter and rectifier linked by the transformer. The rectifier should be build with fast diodes as half or full wave topology [46]. For the bidirectional converter, the impulse full bridge can be used as rectifier-inverter in the secondary side of the transformer. In fig Fig. 5.1 the full bridge converter with the diode rectifier with center-tapped transformer is presented. Moreover, it is possible to build the non-isolated full

https://doi.org/10.2478/9783110623925-005

bridge converter without transformer where the average value of the output voltage can be controlled using the bipolar or unipolar strategy.
In DC-DC converter – shown in Fig. 5.1 – the switches are non-overlapping turned on in pairs T_1, T_4 and T_2, T_3. In typical application the transistors are control by a dedicated integrated circuit or a micro-controller, which generates the U_{GS} voltages. It is important to assure that control circuit does not cause undesirable connections in the converter, so the special technique – eg. boostrap with additional capacitors - should be used. The maximum duty cycle for each pair is equal to:

$$\gamma_{max} = 0.5 - \frac{t_d}{T} \tag{5.1}$$

where t_d is a dead time to avoid short circuit in leg and T is the operation period. Dead time depends on the type of transistors used and ranges from fractions of microsecond to dozens of microseconds. The role of the transformer is to transfer – not to storage – energy, thus the magnetizing inductance should be as small as possible, but large enough to limit the current.

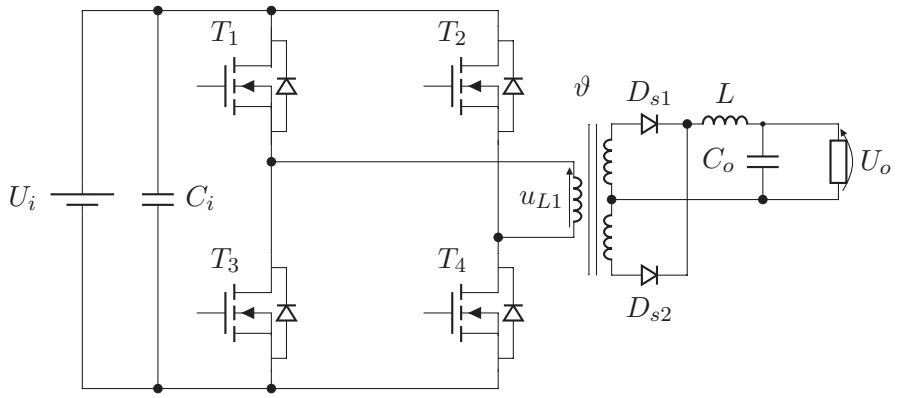

Fig. 5.1: Full bridge DC-DC converter - basic schema

5.2.1 Continuous mode

In the time interval $t \in (0, \gamma T)$ the switches T_1 and T_2 are turned on as it is presented in Fig. 5.2. Assuming the zero voltage drop across the switches, the

voltage on the primary transformer winding is:

$$u_{L1} = U_i = L_m \frac{\mathrm{d}i_{L1}}{\mathrm{d}t} \tag{5.2}$$

where: L_1 is magnetizing inductance from primary side winding. Transforming Eq. (5.2), the primary current is equal to:

$$i_{L1} = \frac{1}{L_1}\int_0^t u_{L1}\mathrm{d}t + i_{L1}(0) = \frac{U_i}{L_1} + i_{L1}(0) \tag{5.3}$$

where $i_{L1}(0)$ is the primary side current at $t = 0$. For continuous mode it has some non zero value, but for discontinuous mode equals zero. The ripple current depends on value of magnetizing inductance and operation frequency $f_s = 1/T$:

$$\Delta i_{L1} = i_{L1}(\gamma T) - i_{L1}(0) = \frac{U_i \gamma T}{L_1} = \frac{U_i \gamma}{f_s L_1} \tag{5.4}$$

Because $i_{L1(AV)} = 0$, the i_{L1} reaches minimal value at time $t = 0$ and it is equal to:

$$\Delta i_{L1}(0) = -\frac{\Delta i_{L1}}{2} = \frac{U_i \gamma}{2 f_s L_1} \tag{5.5}$$

and maximal at time $t = \gamma T$ as it is presented in Fig. 5.5:

$$\Delta i_{L1}(\gamma T) = \frac{\Delta i_{L1}}{2} = \frac{U_i \gamma}{2 f_s L_1} \tag{5.6}$$

The diode D_{s1} is turned on and the D_{s2} is off. The voltage across inductor – from the second Kirchhoff's low –is the difference between the second winding and output voltages.

$$\Delta u_L = U_i \vartheta - U_o = L \frac{\mathrm{d}i_o}{\mathrm{d}t} \tag{5.7}$$

Thus output current is equal:

$$i_o = \frac{1}{L}\int_0^t u_L \mathrm{d}t + i_{Lmin} = \frac{1}{L}\int_0^t (U_i\vartheta - U_o)\mathrm{d}t + i_{Lmin} = \frac{1}{L}(U_i\vartheta - U_o) + i_{Lmin} \tag{5.8}$$

where i_{Lmin} is the minimal output current value at $t = 0$.
The maximal inductor current i_{Lmax} is at time $t = \gamma T$

$$i_{Lmax} = \frac{1}{L}(U_i\vartheta - U_o)\gamma T + i_{Lmin} \tag{5.9}$$

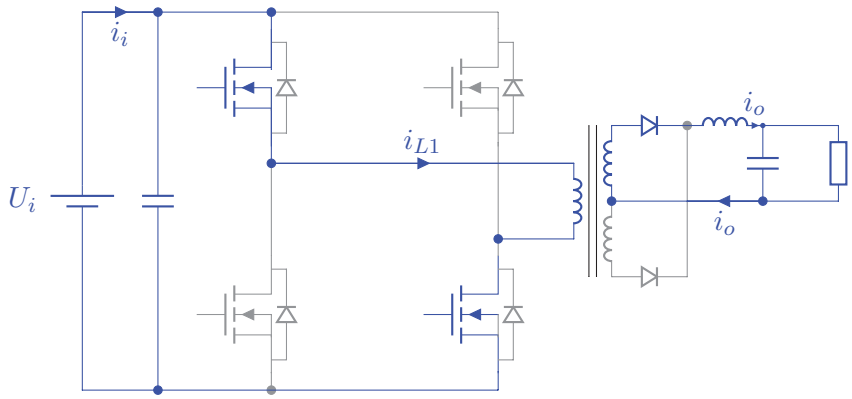

Fig. 5.2: Equivalent circiut of the full bridge DC-DC converter for $t \in (0, \gamma T)$

The current ripple Δi_L is the difference between minimal and maximal value of i_L:

$$\Delta i_L = i_{Lmax} - i_{Lmin} = \frac{1}{L}(U_i\vartheta - U_o)\gamma T \tag{5.10}$$

After time $t = \gamma T$ the switches T_1 and T_4 are turned off as it is shown in Fig. 5.3. The primary side current stops to flow, because all four switches are off. Both diodes in the secondary side are turned on, thus voltage across the inductor is equal $-U_o$. The output current i_L decreases linearly:

$$i_L = \frac{1}{L}\int_t^{\gamma T} u_L \mathrm{d}t + i_L(\gamma T) = -\frac{U_o}{L}(t - \gamma T) + i_L(\gamma T) \tag{5.11}$$

and the current ripple Δi_L is

$$\Delta i_L = \frac{U_o}{L}(\frac{T}{2} - \gamma T) \tag{5.12}$$

At time $t = T/2$ the switches T_2 and T_3 are turned on as it is shown in Fig. 5.4. The primary winding current starts to flow – analogously as it was for $t \in (0, \gamma T)$ – but in opposite direction:

$$i_{L1} = \frac{1}{L_1}\int_{T/2}^{t} u_{L1} \mathrm{d}t + i_{L1}(T/2) = \frac{U_i}{L_1}(t - \frac{T}{2}) + \frac{U_i\gamma}{2f_sL1} \tag{5.13}$$

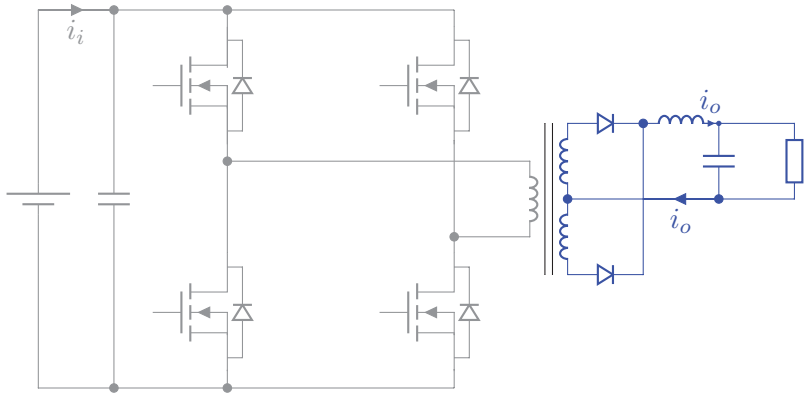

Fig. 5.3: Equivalent circiut of the full bridge DC-DC converter for $t \in (\gamma T, T/2)$

In the secondary side, the diode D_{s2} is on and the output current is similar as described by Eq. (5.8), but time is shifted by $T/2$. The current ripple Δi_L for times $t \in (0, \gamma T)$ and $t \in (\gamma T, T/2)$ should be equal, so referring to Eq. (5.10) and Eq. (5.12):

$$\frac{1}{L}(U_i\vartheta - U_o)\gamma T = \frac{U_o}{L}(\frac{T}{2} - \gamma T) \Leftrightarrow (U_i\vartheta - U_o)\gamma = U_o(\frac{T}{2} - \gamma), \tag{5.14}$$

the relationship between the input voltage U_i and the load voltage U_o for ideal components is given by:

$$\frac{U_o}{U_i} = 2\gamma\vartheta. \tag{5.15}$$

5.2.2 Boundary conduction mode

The converter is the boundary conduction mode, when i_L falls to zero only at time $t = k \cdot T/2$ (for k= 0,1,2,3 ...). Substituting for equations from the previous section ($i_{Lmin} = i_L(kT/2) = 0$), the current ripple $\Delta i_{L(b)}$ in boundary conduction mode is:

$$\Delta i_{L(b)} = \frac{U_o T(\frac{1}{2} - \gamma_{(b)})}{L_{(b)}} \tag{5.16}$$

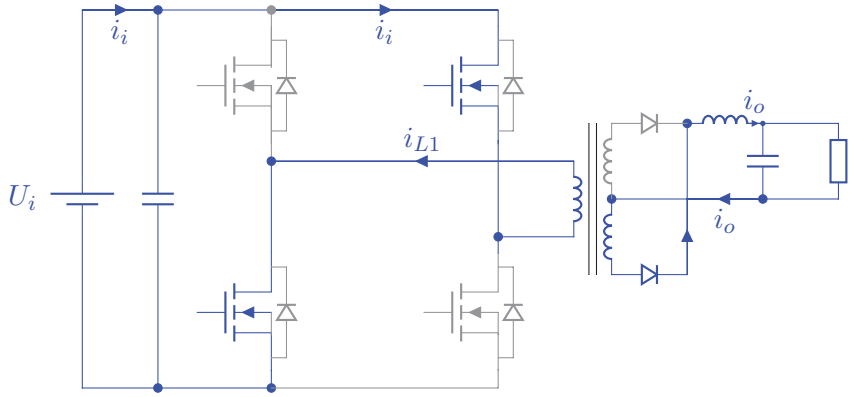

Fig. 5.4: Full bridge DC-DC converter - basic schema

Substituting Eq. (5.15) to Eq. (5.12) and Eq. (5.16), the average value of the output current is:

$$I_{o(b)} = \frac{\Delta i_{L(b)}}{2} = \frac{U_o(\frac{1}{2} - \gamma_{(b)})}{2 f_s L_{(b)}} = \frac{U_o}{R_{(b)}} \tag{5.17}$$

The load resistance $R_{(b)}$ at the boundary is equal to :

$$R_{(b)} = \frac{U_o}{I_{o(b)}} = \frac{2 f_s L_{(b)}}{1/2 - \gamma} \tag{5.18}$$

The minimal value for maintain the converter in the continuous conduction mode is given by:

$$L_{min} = \frac{U_o(1/2 - \gamma_{(b)})}{2 f_s I_{o(b)}} \tag{5.19}$$

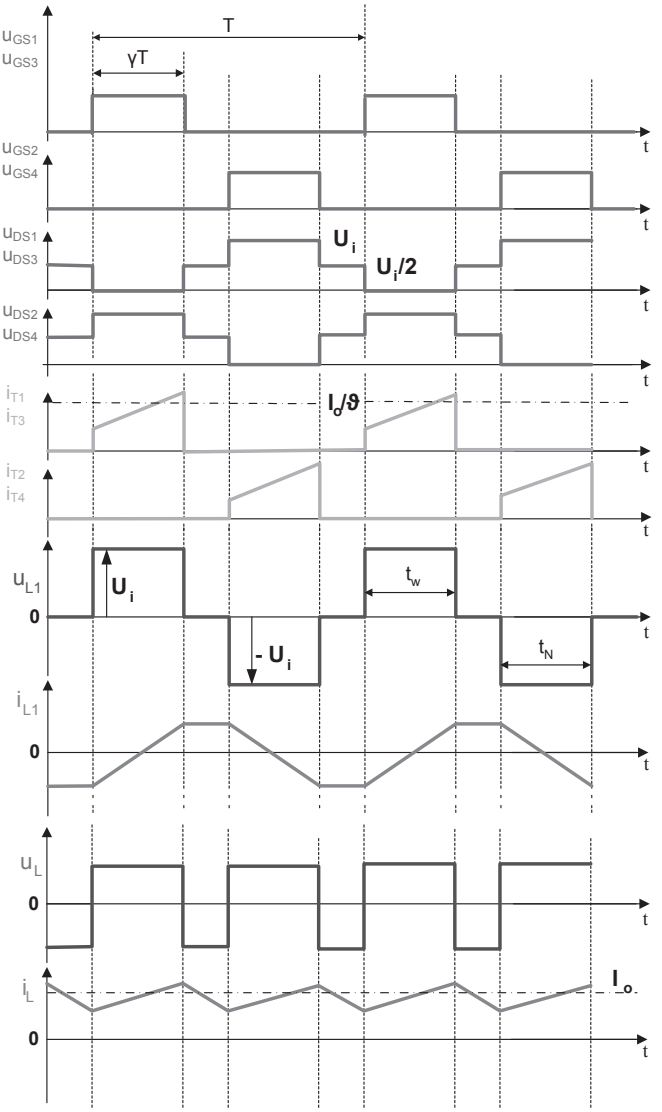

Fig. 5.5: Current and voltage waveforms for full bridge converter operates in continuous mode

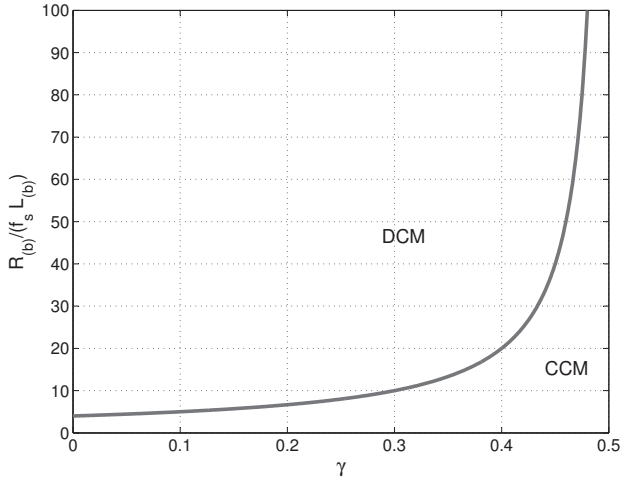

Fig. 5.6: Load resistance $R_{(b)}/(f_s L_{(b)})$ in function od duty cycle γ. Boundary between CCM and DCM

5.3 EMI propagation paths

In the full bridge DC-DC converter there are many sources of interference: four transistors switched in pairs because of occurrence of the dead time and the alternation switching of two rectifier diodes in the secondary side. The EMI has both CM and DM components, but usually CM dominate. The main sources are the fast switched transistors, but the greater impact on the interference properties and the propagation path has transformer, especially for high and middle power converter where the transformer parasitics have greater values than others ones.

In Fig. 5.7, the parasitic components that have the greatest impact on EMI are presented:

- the primary C_{w1} and secondary C_{w2}, C_{w3} windings capacitance, winding-to-winding capacitance C_{12}, C_{21},

- the magnetizing inductances L_m, primary and secondary leakage inductance L_σ

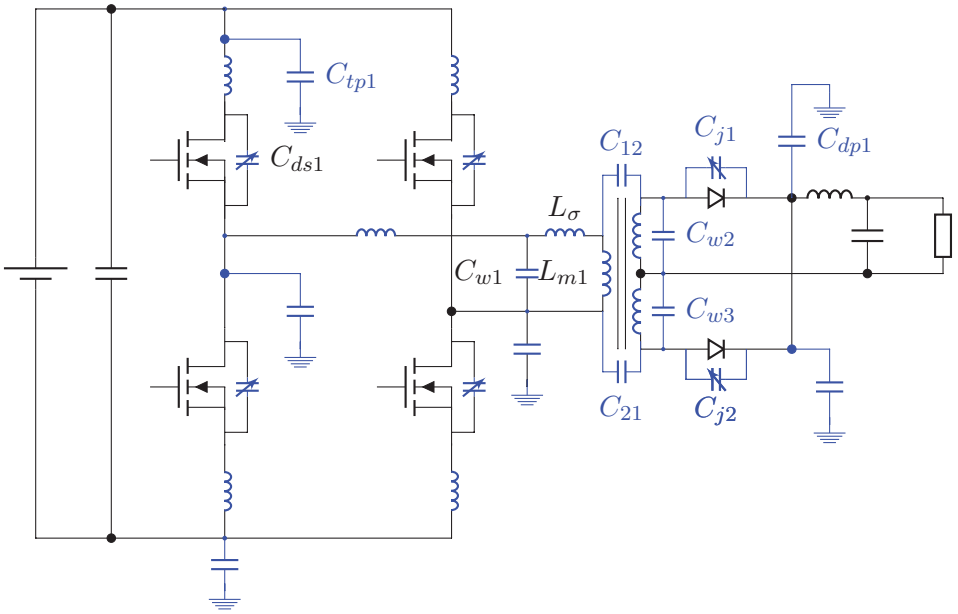

Fig. 5.7: Full bridge DC-DC converter - most significant elements in EMI generation and propagation

- parasitic capacitance to the ground near to transistors drain node C_{tp}, diodes cathode node C_{dp1}
- transistor internal capacitance (for low power converters)

The inductance of the PCB conducting tracks are negligible compared to transformer inductances. The differential mode interference, generated in converter, flows through all components in the time interval between transistors commutation, but it can be easily limited or almost all canceled by the input capacitors filters. It is preferable to use as the input filter at least two capacitors produced in the different technologies (see Section 2.2.2): first to provide a stable voltage level, second – fast capacitor - for filtering high frequency DM noise. The common mode interference is generated during transistor commutation. It is can be divided into two groups: internal and outgoing, especially in converters where transistors are alternately switched. The propagation paths

of the internal interference are closed inside the converter e.q. when the transistor T_1 is switch on, the potential of their drain fast changes and the part of noise flows to the ground through parasitic capacitance C_{tp1} and come back via parasitic capacitance connected to source node of transistor T_3 and next through its internal capacitance C_{ds3} (orange path in Fig. 5.8). This kind of interference cannot come out of the converter, but it can perturb the auxiliary circuits like control, drivers or sensors, what can cause the dysfunction of the whole converter.

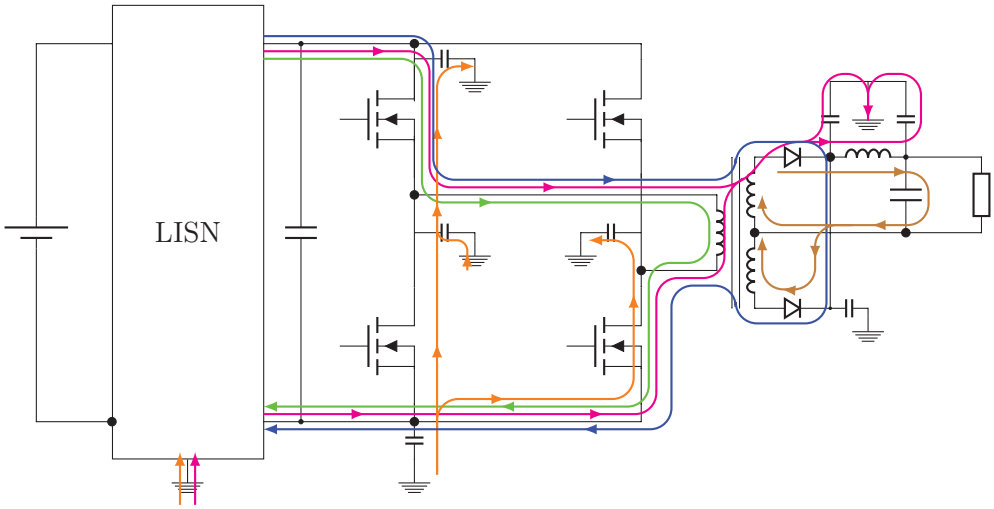

Fig. 5.8: Full bridge DC-DC converter - EMI propagation paths

The outgoing interference always flows through the parasitic capacitance to the ground and can be measured with LISN. In the middle and high power isolated converters, the transformer has the greatest impact on the level and oscillations frequency of EMI, because the values of its parasitic are much greater than the others components of converter. The main outgoing interference paths contain the transformer, thus the characteristic peaks in voltages spectra depends on its parasitic parameters. In Fig. 5.9 the spectra of voltages on transformer primary winding U_{L1}, secondary side diode U_D and interference registered in LISN U_{LISN} are presented. The analysis is based on the prototypes measurement and

simulation of wide band model build using components described in Chapter 2.

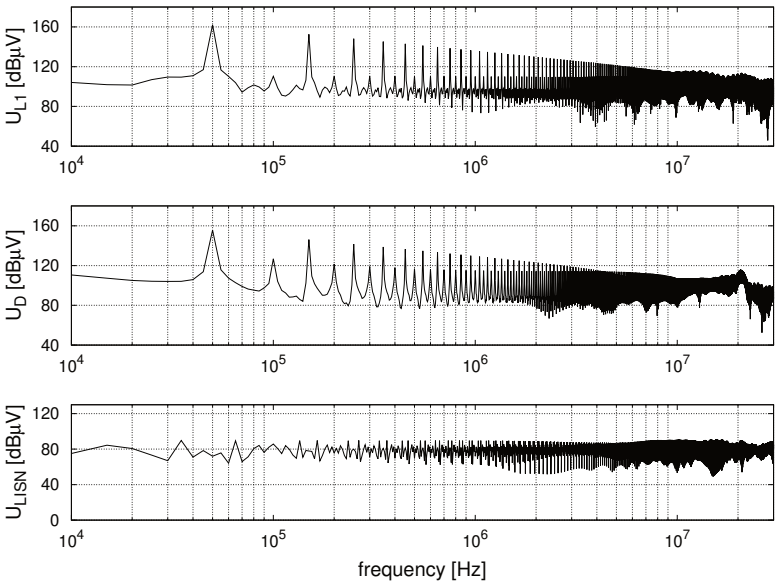

Fig. 5.9: Full bridge converter voltages spectra

In the spectra the distinctive peaks appear:

- the basic harmonic (here for 50 kHz)
- the over-harmonics (in the range 100 k - 2 MHz)
- ringing oscillation during diode turn on (for 21 MHz)
- peaks link with transistor slew rate (for 28 MHz)

The oscillation during transistor turn on and off are not visible in this particular case, because they are located in the frequency range above 30 MHz.

5.3.1 Transformer

The transformer is a very important component in the EMC analyses of isolated converters, where it is used to transfer energy from source to load. Its pa-

rameters depend on technology, technique of construction and used materials. The procedure of transformer design for SMPS is widely described in literature [47, 48, 1] or websides. The significant part of interference – generated by fast changing semiconductors devices state in both sides of the transformer – flows through the transformer. The resonant circuit contains the transformer magnetizing and leakage inductances and internal capacitances and also parasitic components of semiconductors and conducting track. Considering the inductances in the resonant circuit, the magnetizing inductance L_m has usually the greatest value and also has the most influence on the EMI level and propagation path. From the EMC point of view, the value of the L_m should be as small as possible, in order to shift the resonant peak to high frequency range. If the value of L_m is large, the undesirable peaks in EMI spectra appear. In Fig. 5.10 the voltages spectra are presented in case the value of C_{pL_m} is increased ten times as compared to Fig. 5.9.

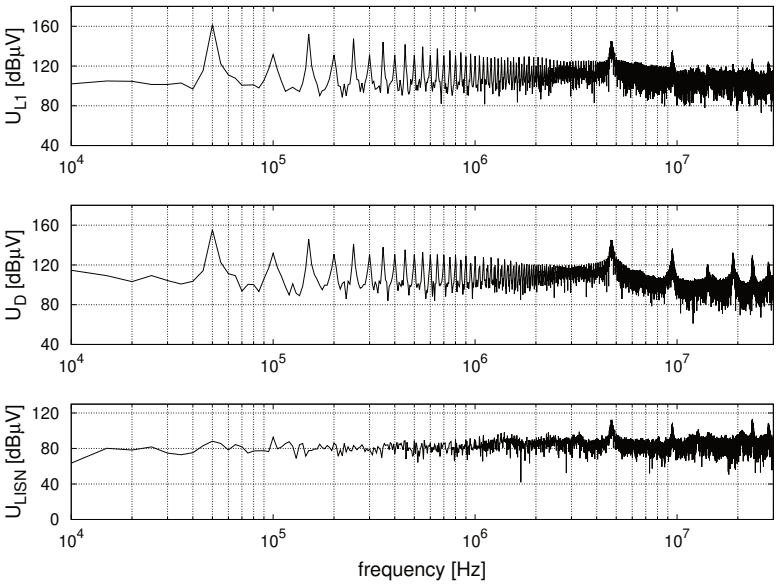

Fig. 5.10: Influence of transformer magnetizing inductance increase: $L_{m1} * 10$

The level of presented voltages increased significantly for frequency equals 4.7 MHz, 10.5 MHz and their harmonics. The limitation of this kind of interference

needs significant filtering treatment and it is preferable to avoid it in the early design stage, by the selection of the appropriately low magnetizing inductance L_m. The design process is the compromise between transformer properties, switching frequency, the EMI level and filtering capability. From power converting and the EMC point of view, the leakage inductance L_σ should be as small as possible. It is responsible for ringing and overvoltage, but this effect can be efficient by applying the RCD clamp. The RCD clamp dissipates the power, however it entails the undesirable power loss and reduces the efficiency. In Fig. 5.11 the voltages spectra are presented in case the value of L_σ is increased ten times as compared to Fig. 5.9. In this case, increasing the value of L_σ causes the gain of ringing, which is visible in diode voltage spectra U_d as meaningful peaks at 7.2 MHz and 10.6 MHz. The lower interference peak is propagated to LISN, but the higher is closed in the secondary side circuit loop. This effect occurs in this particular converter, but in general which part of ringing interference is propagated depends on individual properties of the circuit and filtering ability of transformer. In high power converters, the leakage inductance L_σ are the main parameters in ringing generation and its limitation is the best method of EMI reduction.

The transformer model consists of the lumped capacitors which represent its capacitive behavior, but in the reality, the electric field connected with interference flowing through the coils is distracted. The windings capacitance C_1 and C_2 are the part of the CM interference resonant circuit. They are responsible for the level and frequency of the EMI generated during semiconductors commutation. The C_1 and C_2, next to L_σ , take the part in generation of ringing. In Fig. 5.12 the voltages spectra are presented in case the value of C_2 is increased five times as compared to Fig. 5.9. It is visible, that C_2 is the part of few resonant circuits in both sides of converter and it interacts with transistors and diodes capacitance, magnetizing L_m and leakage $L_\sigma$inductances and copper tracks parasitics. The influence of winding capacitance is significant in high (here above 10 MHz) frequency range. The characteristic peak appears in diode voltage spectra and they are propagated out of the converter through the parasitic capacitance to the ground. In practice, the winding capacitances should be as small as possible and the PCB conducting tracks should be short to ensure geometrical proximity between the semiconductors and the transformer.

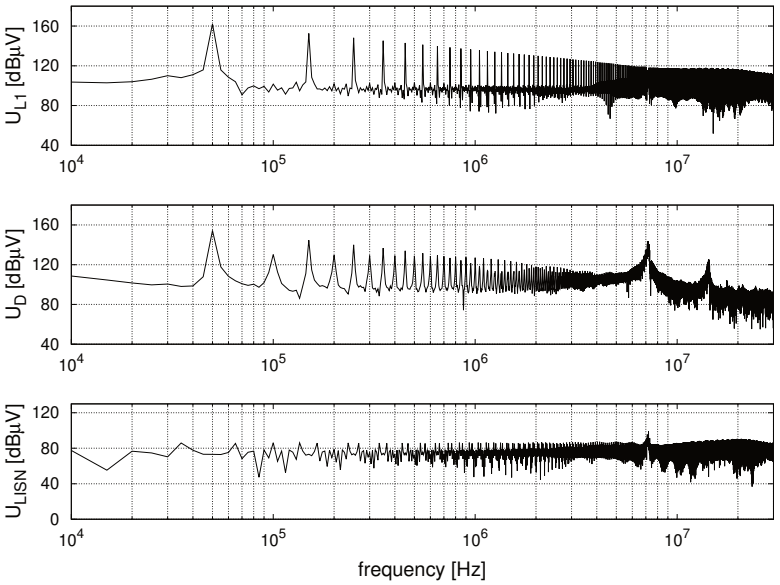

Fig. 5.11: Influence of transformer leakage inductance increase: $L_{\sigma 1} * 10$

The inter-winding capacitances C_{12} and C_{21} are the part of high frequency interference path in (in presented example the range above 15 MHz) and they have negligible impact on low frequency noise, even in the high power converter. However, they are responsible for ringing during diode turn on and transfer noise between two sides of transformer. They have influence on perturbation coming out of the converter and registered in LISN, but its impact depends on geometrical properties of primary side layout. If the level of outgoing interference is too great in the high frequency range, the close loop can be created by increasing the parasitic capacitance connected with transistors T_3 or T_4 source node. It can be preformed by changing the PCB track width. Moreover, the y-capacitors can be added between two sides of transformer in order to shape propagation path , but it location and value depend on individual properties of the PCB layout and transformer and the best solution is to examine the impact in the working prototype. In Fig. 5.13 the voltages spectra are presented in case the value of C_{12} is increased five times as compared to Fig. 5.9.

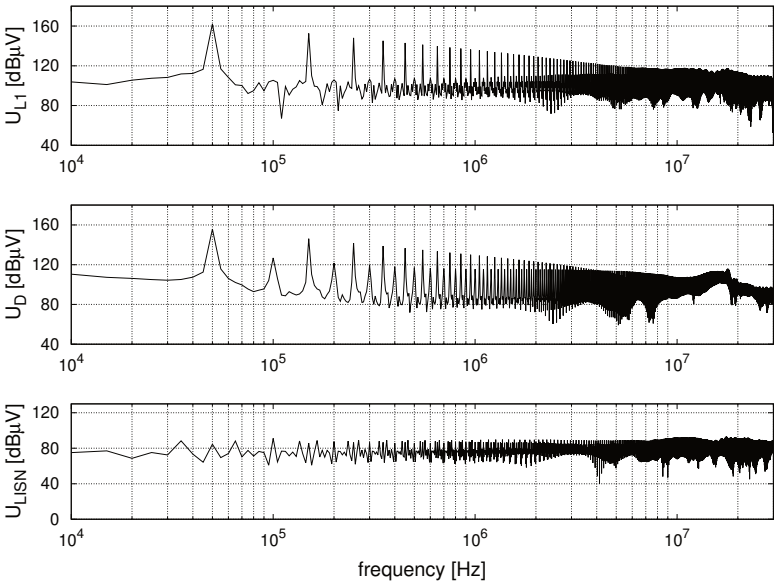

Fig. 5.12: Influence of transformer winding capacitance increase: $C_2 * 5$

5.3.2 Semiconductors

The voltage across the transistors U_{DS} is controlled by the control system and driver. The fast changing of U_{DS} is the source of high frequency noise. If the PCB layout is symmetrical – the parasitic capacitances to the ground or heat sink in each branch has similar values – the main part of CM noise is closed in the internal loop, moreover the CM noise is limited by the input filter. However, the U_{DS} impacts on outgoing interference generated by diodes in the secondary side of the converter, because the state of diodes is correlated with transistor state. The nonlinear internal capacitance of transistor is the part of resonant circuits, where the interference is generated, but its impact is negligible because – in the middle and high power converter – the value of C_{DS} is much smaller compared to other parasites and for lower power converter the resonant peaks are located very high in frequency range above the 30 MHz. In Fig. 5.14 the voltages spectra are presented in case the value of C_{DS} is increased ten times as compared to Fig. 5.9. In the primary side the interference peak appears (here in the frequency of range about 5MHz in U_{L1} spectra), but it

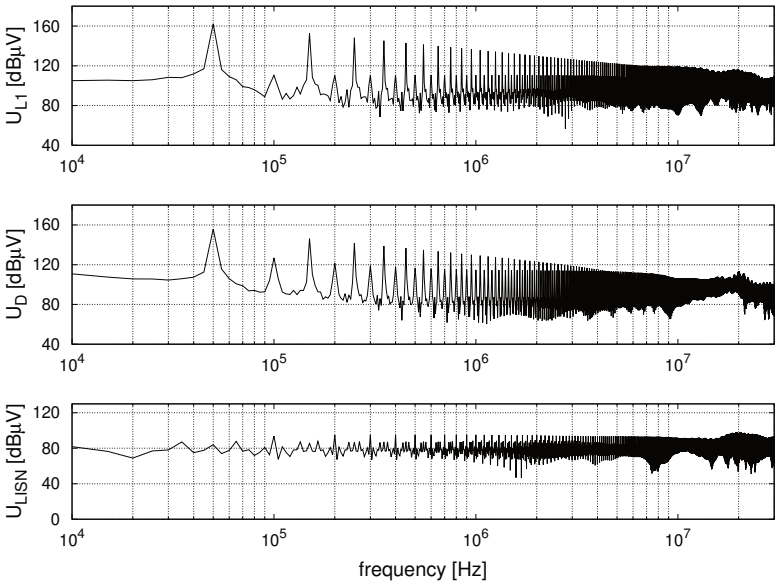

Fig. 5.13: Influence of transformer inter-winding capacitance increase: $C_{12} * 5$

is not propagated to the $LISN$. Furthermore, high level peak is visible in 24 MHz in all presented spectra, which is effect of interaction of parasitics and it is propagated to the $LISN$. In some cases – especially in the middle power converters – the resonant circuit containing the transistor, the inter-winding capacitance C_{12} or/and C_{21}, diode and PCB parasitic can be a source of high level interference, which should be suppress using the RCD damper which lead to undesirable power dissipation.

The diode turn off generates the ringing in the secondary side circuit, which is propagated through the transformer and parasitic to the primary side and $LISN$. The resonant circuit consists of the diode capacitance C_j, the transformer internal capacitance C_2, C_{12} and the magnetizing inductance L_m, the transistor capacitance C_{ds} and the PCB parasitics. Although, the non-linear capacitance of diode junction C_j is relatively small, it has the great impact of the interference generation, because it interacts with L_m. In Fig. 5.15 t he voltages spectra are presented in the case the value of C_j is increased only two times as compared to Fig. 5.9. Two characteristic high frequency peaks

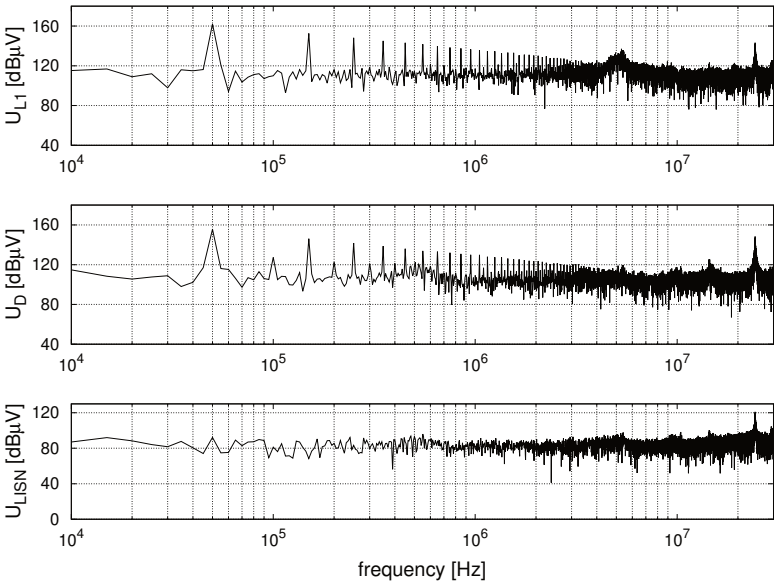

Fig. 5.14: Influence of transistor capacitance increase: $C_{ds} * 10$

are visible: first (here in 14.5 MHz) represents the ringing in the whole described resonant circuit, (here in 23 MHz) the second includes only secondary side components. It should be noted that lower frequency noise has an internal character. It is closed inside the converter and it is not propagated out to the LISN. The higher frequency noise goes out through the parasitic ground capacitances to the LISN. In order to avoid this situation, the conducted PCB tracks ground capacitance in the neighborhood of diode should be as small as possible. It can be obtained by shortening of the length of conducting tracks, its distant position over the ground or non-grounding heat-sink. The CM filter should also limit the level of interference, but proper track design is more effective and cheaper solution.

If the ground capacitance of conducted PCB tracks, in the neighborhood of diode, has to high value, it can be the origin of high frequency noise as it is shown in Fig. 5.16 where the ground capacitance of the PCB track connected to diode anode increased ten times compared to Fig. 5.9.

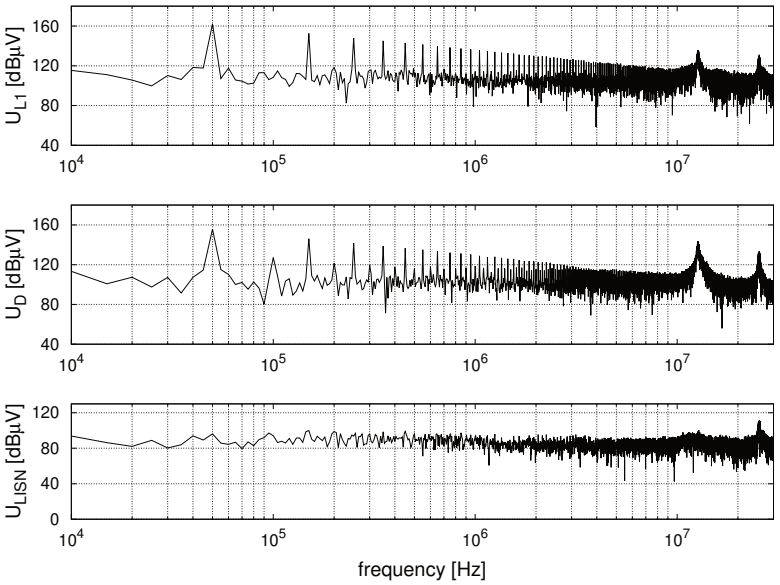

Fig. 5.15: Influence of diode capacitance increase: $C_j * 2$

The isolated converters have a transformer which impacts on character off interference. In the flyback converter the transformer is dedicated to storage energy, thus its influence is stronger that other converters (like half-, full-bridge, forward or push-pull) where the parasitic elements play an important role. For this reason, ringing frequency prediction in the early design step requires complex models which is a long time and work consuming process, so the better solution is to build the prototype where the oscillation can be measured directly.

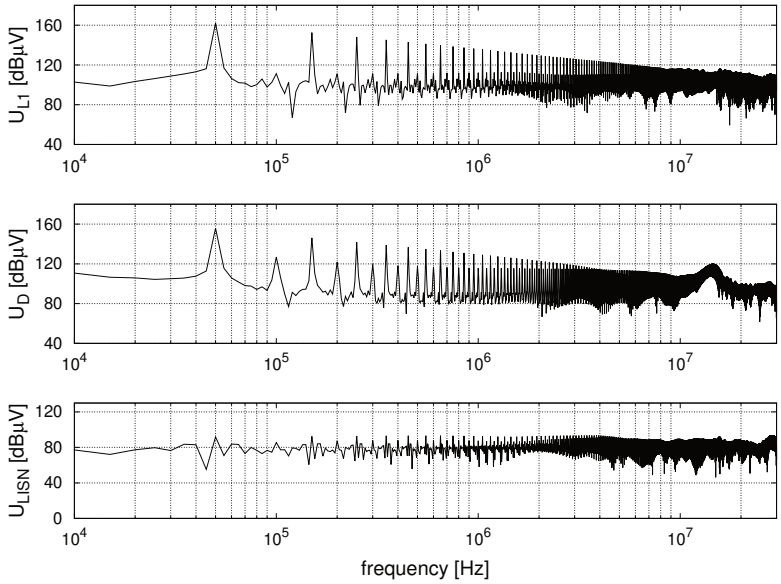

Fig. 5.16: Influence of parasitic capacitance between diode anode node and the ground increase: $C_{dp1} * 10$

Chapter 6

Summary

In modern Power Electronics converters the problem of EMI generation is important and can not be neglected. Furthermore, development of semiconductors technology causes the increasing of the switching frequency, in order to get greater efficiency and to use smaller passive components. Unfortunately, the increased frequency causes the increasing of the level of the interference especially in the high frequency range. The best way to limit the level of the interference is properly designing with the identification of the source of perturbation, creating internal loops or selection of appropriate components and their parameters. A well-designed circuit allows to limit the role of filters and attenuating elements, which is connected with the cost and efficiency of the converter. In this book, analysis of interference generation and propagation is presented on the example of three basic converters, but this knowledge can be easily extended to and type of converter. The information about the basic operation, the propagation paths and the influence of the most important components and parasitic – contained in this book – can be useful for design of the converters with low level of outgoing EMI.

https://doi.org/10.2478/9783110623925-006

List of Symbols

CCM continuous current conduction mode.

CM common mode noise.

C_{DS} MOSFET drain-source capacitance.

C_D diode internal capacitance.

C_{GD} MOSFET gate-drain capacitance.

C_{GS} MOSFET gate-source capacitance.

DCM discontinuous current conduction mode.

DM differential mode noise.

γ duty cycle.

ESL equivalent series inductance.

ESR equivalent series resistance.

I_{RM} maximal diode revers recovery current.

$LISN$ Line Impedance Stabilization Network.

L_σ leakage inductance.

Q_{Rr} diode revers recovery charge.

R_σ leakage resistance.

T operation period.

f operation frequency.

ϑ transformer turns ratio.

t_{Rr} diode recovery time.

U_{DS} dren-source voltage.

U_D diode anode - cathode voltage.

U_{GS} gate-source voltage.

Bibliography

[1] W. M. Flanagan, *Handbook of transformer design and applications*. McGraw-Hill New York, 1993, vol. 2.

[2] K. Pietrczak, "Why diode softness matters ?? understanding the switching characteristics of fast diodes and their impact on EMI and voltage stress." in *Telecommunications Energy Conference 'Smart Power and Efficiency' (INTELEC), Proceedings of 2013 35th International*, Oct 2013, pp. 1–5.

[3] X. Yuan, S. Walder, and N. Oswald, "EMI generation characteristics of sic and si diodes: Influence of reverse-recovery characteristics," *Power Electronics, IEEE Transactions on*, vol. 30, no. 3, pp. 1131–1136, March 2015.

[4] P. Musznicki, J.-L. Schanen, and P. Chrzan, "Design of hight voltage busbar: trade off between electrical field and stray inductance," *3rd International Workshop Compatibility in PowerElectronics CPE 2003*, 2003.

[5] J. Ben Hadj Slama, S. Hrigua, F. Costa, B. Revol, and C. Gautier, "Relevant parameters of spice3 MOSFET model for EMC analysis," in *Electromagnetic Compatibility, 2009. EMC 2009. IEEE International Symposium on*, 2009, pp. 319–323.

[6] M. Turzynski and W. Kulesza, "A simplified behavioral mosfet model based on parameters extraction for circuit simulations." *Power Electronics, IEEE Transactions on*, vol. PP, no. 99, pp. 1–1, 2015.

[7] W. Mi, "Extraction des paramétres et domaine de validité du modèle d'un composant de puissance." Ph.D. dissertation, INSA de Lyon, 01 2004.

[8] A. Massarini and M. K. Kazimierczuk, "Self-capacitance of inductors," *IEEE Transactions on Power Electronics*, vol. 12, no. 4, pp. 671–676, Jul 1997.

[9] K. Harada, A. Katsuki, and M. Fujiwara, "Use of esr for deterioration diagnosis of electrolytic capacitor," *IEEE Transactions on Power Electronics*, vol. 8, no. 4, pp. 355–361, Oct 1993.

[10] P. Musznicki, J.-L. Schanen, P. Granjon, and J. Łuszcz, "Impact of dielectric deterioration on the conducted emi emissions in the dc-dc boost converter," *Przeglad Elektrotechniczny*, vol. 2, 2011.

[11] Y. Yang, Z.-J. Wang, X. Cai, and Z. Wang, "Improved lumped parameter model for transformer fast transient simulations," *Electric Power Applications, IET*, vol. 5, no. 6, pp. 479–485, July 2011.

[12] J. Biela and J. Kolar, "Using transformer parasitics for resonant converters;a review of the calculation of the stray capacitance of transformers," *Industry Applications, IEEE Transactions on*, vol. 44, no. 1, pp. 223–233, Jan 2008.

[13] M. Xinkui and C. Wei, "More precise model for parasitic capacitances in high-frequency transformer," in *Power Electronics Specialists Conference, 2002. pesc 02. 2002 IEEE 33rd Annual*, vol. 2, 2002, pp. 1054–1057 vol.2.

[14] A. Baktash and A. Vahedi, "Calculation of parasitic elements in toroidal core transformers," *Plasma Science, IEEE Transactions on*, vol. 42, no. 6, pp. 1690–1696, June 2014.

[15] S. Saravi, A. Tahani, F. Zare, and R. Kordkheili, "The effect of different winding techniques on the stray capacitances of high frequency transformers used in flyback converters," in *Power and Energy Conference, 2008. PECon 2008. IEEE 2nd International*, Dec 2008, pp. 1475–1478.

[16] H.-Y. Lu, J. G. Zhu, and S. Hui, "Experimental determination of stray capacitances in high frequency transformers," *Power Electronics, IEEE Transactions on*, vol. 18, no. 5, pp. 1105–1112, Sept 2003.

[17] Z. Zhongyuan, L. Fangcheng, and L. Guishu, "A high-frequency circuit model of a potential transformer for the very fast transient simulation in

GIS," *Power Delivery, IEEE Transactions on*, vol. 23, no. 4, pp. 1995–1999, Oct 2008.

[18] S. Pramanik and L. Satish, "Estimation of series capacitance for a three-phase transformer winding from its measured frequency response," *Power Delivery, IEEE Transactions on*, vol. 28, no. 4, pp. 2437–2444, Oct 2013.

[19] N. Abeywickrama, Y. Serdyuk, and S. Gubanski, "High-frequency modeling of power transformers for use in frequency response analysis (FRA)," *Power Delivery, IEEE Transactions on*, vol. 23, no. 4, pp. 2042–2049, Oct 2008.

[20] Suwarno and F. Donald, "Frequency response analysis (FRA) for diagnosis of power transformers," in *Electrical Engineering/Electronics Computer Telecommunications and Information Technology (ECTI-CON), 2010 International Conference on*, May 2010, pp. 112–116.

[21] D. Aguglia, P. Viarouge, and C. Martins, "Frequency domain non-linear identification method for high voltage pulse transformers," in *Electrical Machines (ICEM), 2012 XXth International Conference on*, Sept 2012, pp. 1977–1983.

[22] P. Musznicki, P. J. Chrzan, M. Rucinski, and M. Kolincio, "Adaptive estimation of the transformer stray capacitances for dc-dc converter modelling," *IET Power Electronics*, vol. 9, no. 15, pp. 2865–2870, 2016.

[23] A. Schellmanns, J.-P. Keradec, J.-L. Schanen, and K. Berrouche, "Representing electrical behaviour of transformers by lumped element circuits: a global physical approach," in *Industry Applications Conference, 1999. Thirty-Fourth IAS Annual Meeting. Conference Record of the 1999 IEEE*, vol. 3, 1999, pp. 2100–2107 vol.3.

[24] C. R. Paul, *Introduction to Electromagnetic Compatibility.* New York: Wiley-Intersciences, 1992.

[25] A. E. Ruehli, "Inductance calculations in a complex integrated circuit environment," *IBM Journal of Research and Development*, vol. 16, no. 5, pp. 470–481, Sep. 1972.

[26] J. L. Schanen, E. Clavel, and J. Roudet, "Modeling of low inductive busbar connections," *IEEE Industry Applications Magazine*, vol. 2, no. 5, pp. 39–43, Sept 1996.

[27] E. Bogatin, "Design rules for microstrip capacitance," *Components, Hybrids, and Manufacturing Technology, IEEE Transactions on*, vol. 11, no. 3, pp. 253–259, 1988.

[28] J. C. Crebier, J. Roudet, and J. L. Schanen, "Problems using lisn in emi characterization of power electronic converters," in *30th Annual IEEE Power Electronics Specialists Conference. Record. (Cat. No.99CH36321)*, vol. 1, Aug 1999, pp. 307–312 vol.1.

[29] S. Wang, F. C. Lee, and W. G. Odendaal, "Characterization, evaluation, and design of noise separator for conducted emi noise diagnosis," *IEEE Transactions on Power Electronics*, vol. 20, no. 4, pp. 974–982, July 2005.

[30] R. Miftakhutdinov, "Compensating dc/dc converters with ceramic output capacitors," *Texas Instruments Incorporated*, 2005.

[31] L. Jourdan, J. L. Schanen, J. Roudet, M. Bensaied, and K. Segueni, "Design methodology for non insulated dc-dc converter: application to 42v-14v "powernet"," in *2002 IEEE 33rd Annual IEEE Power Electronics Specialists Conference. Proceedings (Cat. No.02CH37289)*, vol. 4, 2002, pp. 1679–1684.

[32] D. Stepins, "Conducted emi of switching frequency modulated boost converter," *Electrical, Control and Communication Engineering*, vol. 3, no. 1, pp. 12–18, 2013.

[33] L. Popova, R. Juntunen, T. Musikka, M. Lohtander, P. Silventoinen, O. Pyrhonen, and J. Pyrhonen, "Stray inductance estimation with detailed model of the IGBT module," in *Power Electronics and Applications (EPE), 2013 15th European Conference on*, Sept 2013, pp. 1–8.

[34] M. Pong, C. M. Lee, and X. Wu, "EMI due to electric field coupling on PCB," in *Power Electronics Specialists Conference, 1998. PESC 98 Record. 29th Annual IEEE*, vol. 2, May 1998, pp. 1125–1130 vol.2.

[35] J. Picard, "Under the hood of flyback SMPS designs," *Texas Instruments Power Supply Design Seminar*, 2010.

[36] M. Mohammadi, E. Adib, and H. Farzanehfard, "Lossless passive snubber for double ended flyback converter with passive clamp circuit," *Power Electronics, IET*, vol. 7, no. 2, pp. 245–250, February 2014.

[37] S. A. Maas, *Nonlinear microwave and RF circuits*. Artech House, 2003.

[38] P. Meng, J. Zhang, H. Chen, Z. Qian, and Y. Shen, "Characterizing noise source and coupling path in flyback converter for common-mode noise prediction," in *2011 Twenty-Sixth Annual IEEE Applied Power Electronics Conference and Exposition (APEC)*, March 2011, pp. 1704–1709.

[39] J. Liu, Y. Wang, D. Jiang, and Q. Cao, "Fast prediction for conducted emi in flyback converters," in *2015 IEEE International Conference on Computational Electromagnetics*, Feb 2015, pp. 247–249.

[40] M. Yazdani, H. Farzanehfard, and J. Faiz, "Conducted EMI modeling and reduction in a flyback switched mode power supply," in *Power Electronics, Drive Systems and Technologies Conference (PEDSTC), 2011 2nd*, Feb 2011, pp. 620–624.

[41] J. Lou, Q. Sun, W. You, Y. Shu, A. Bhobe, and J. Yu, "Analytical calculation of conducted emi in flyback converters," in *2016 Asia-Pacific International Symposium on Electromagnetic Compatibility (APEMC)*, vol. 01, May 2016, pp. 395–397.

[42] K. R. A. Britto, R. Dhanasekaran, R. Vimala, and B. Saranya, "Modeling of conducted emi in flyback switching power converters," in *2011 International Conference On Recent Advancements In Electrical, Electronics And Control Engineering*, Dec 2011, pp. 377–383.

[43] L. Longtao, W. Lixin, L. Chao, and S. Chao, "A simulation of conducted EMI in flyback converters," in *Power Electronics and Motion Control Conference (IPEMC), 2012 7th International*, vol. 3, June 2012, pp. 1794–1798.

[44] M. M. Jha, K. B. Naik, and S. P. Das, "Estimation of optimum value of y-capacitor for reducing emi in switch mode power supplies," *Electrical*

Power Quality and Utilisation. Journal, vol. Vol. 15, iss. 2, pp. 47–50, 2009.

[45] M. Rucinski, P. Musznicki, and P. J. Chrzan, "Electromagnetic interference frequencies prediction model of flyback converter for snubber design," *IET Power Electronics*, vol. 8, no. 6, pp. 994–999, 2015.

[46] M. K. Kazimierczuk, *Pulse-width modulated DC-DC power converters*. John Wiley & Sons, 2015.

[47] L. H. Dixon, *Magnetics Design Handbook*. Unitrode Products from Texas Instruments, 2001.

[48] C. W. T. McLyman, *Transformer and inductor design handbook*. CRC press, 2016.

Chapter 7

Appendix

Partial element equivalent circuit (PEEC)

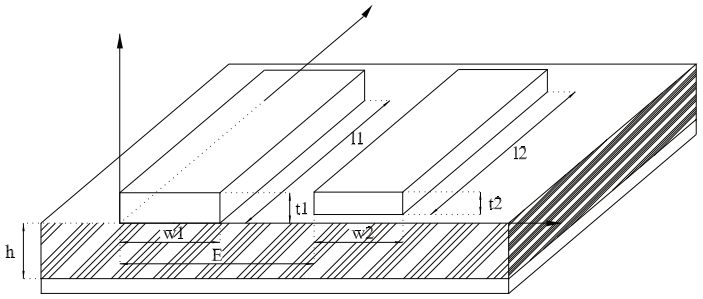

The geometrical description of 2 conductors for inductance calculation

$$M_{p12} = \frac{1}{w_1 t_1 w_2 t_2} \sum_{h=1}^{4} \sum_{i=4}^{4} \sum_{j=4}^{4} (-1)^{h+i+j+1} f\left(q_{h-1}, p_{i-1} o_{j-1}\right)$$

https://doi.org/10.2478/9783110623925-007

$$q(E,w_1,w_2)=\begin{pmatrix} E-w_1 \\ E+w_2-w_1 \\ E+w_2 \\ E \end{pmatrix},$$

$$r(P,t_1,t_2)=\begin{pmatrix} E-t_1 \\ E+t_2-t_1 \\ E+t_2 \\ E \end{pmatrix},$$

$$o(l_1,l_2,l_3)=\begin{pmatrix} l_3-l_1 \\ l_3+l_2-l_1 \\ l_3+l_2 \\ l_3 \end{pmatrix}$$

$$f(x,y,z)=(y^2\tfrac{z^2}{4}-\tfrac{y^4}{24}-\tfrac{z^4}{24})x-\ln(\tfrac{x^2+\sqrt{x^2+y^2+z^2}}{\sqrt{y^2+z^2}})+(y^2\tfrac{x^2}{4}-\tfrac{y^4}{24}-\tfrac{x^4}{24})z-$$

$$\ln(\tfrac{z^2+\sqrt{z^2+y^2+z^2}}{\sqrt{y^2+x^2}})+(x^2\tfrac{z^2}{4}-\tfrac{x^4}{24}-\tfrac{z^4}{24})y-\ln(\tfrac{y^2+\sqrt{x^2+y^2+z^2}}{\sqrt{y^2+x^2}})+$$

$$+\left[\tfrac{1}{60}(x^4+y^4+z^4+3x^2y^2+3z^2y^2+3x^2z^2)+\sqrt{x^2+y^2+z^2}\right]$$

$$+\tfrac{(-1)xyz^3}{6}arctg(\tfrac{xy}{z\sqrt{x^2+y^2+z^2}})+\tfrac{(-1)xzy^3}{6}arctg(\tfrac{xz}{y\sqrt{x^2+y^2+z^2}})+$$

$$+\tfrac{(-1)zyx^3}{6}arctg(\tfrac{zy}{x\sqrt{x^2+y^2+z^2}})$$

List of Figures